Title:

Hamster PIWI proteins bind to piRNAs with stage-specific size variations during oocyte maturation

Kyoko Ishino[1], Hidetoshi Hasuwa[1], Jun Yoshimura[2], Yuka W. Iwasaki[1,7], Hidenori Nishihara[3], Naomi M. Seki[1,4], Takamasa Hirano[1,5], Marie Tsuchiya[1], Hinako Ishizaki[5], Harumi Masuda[1], Tae Kuramoto[3], Kuniaki Saito[1,5], Yasubumi Sakakibara[6], Atsushi Toyoda[5], Takehiko Itoh[3], Mikiko C. Siomi[4], Shinichi Morishita[2], and Haruhiko Siomi,[1,+]

1. Department of Molecular Biology, Keio University School of Medicine, Tokyo 160-8582, Japan
2. Department of Computational Biology and Medical Sciences, Graduate School of Frontier Sciences, The University of Tokyo, Tokyo 113-0032, Japan
3. School of Life Science and Technology, Tokyo Institute of Technology, Kanagawa 226-8501, Japan
4. Graduate School of Science, The University of Tokyo, Tokyo 113-0032, Japan
5. National Institute of Genetics, Mishima 411-8540, Japan
6. Department of Biosciences and Informatics, Keio University, Yokohama 223-8522, Japan
7. Japan Science and Technology Agency (JST), Precursory Research for Embryonic Science and Technology (PRESTO), Saitama, Japan.

+Correspondence: awa403@keio.jp

Abstract

In animal gonads, transposable elements (TEs) are actively repressed to preserve genome integrity through the Piwi-interacting RNA (piRNA) pathway. In mice, piRNAs are most abundantly expressed in male germ cells, and form effector complexes with three distinct PIWI proteins. The depletion of individual *Piwi* genes causes male-specific sterility owing to severe defects in spermatogenesis with no discernible phenotype in female mice.

Unlike mice, most other mammals have four PIWI genes, some of which are expressed in the ovary. Here, purification of PIWI complexes from oocytes of the golden hamster revealed that the size of the piRNAs loaded onto PIWIL1 changed during oocyte maturation. In contrast, PIWIL3, an ovary-specific PIWI in most mammals, associates with short piRNAs only in metaphase II oocytes, which coincides with intense phosphorylation of the protein. An improved high-quality genome assembly and annotation revealed that PIWIL1- and PIWIL3-associated piRNAs appear to share the 5′-ends of common piRNA precursors and are mostly derived from unannotated sequences with a diminished contribution from TE-derived sequences, most of which correspond to endogenous retroviruses (ERVs). Although binding sites for the transcription factor A-Myb are identified in the transcription start site regions of the testis piRNA clusters, the piRNA clusters in the ovary show no well-defined binding motifs in their upstream regions. These results show that hamster piRNA clusters are transcribed by different transcriptional factors in the ovary and testis, resulting in the generation of sex-specific piRNAs. Our findings show the complex and dynamic nature of biogenesis of piRNAs in hamster oocytes, and together with the new genome sequence generated, serve as the foundation for developing useful models to study the piRNA pathway in mammalian oocytes.

Highlights

- The size of PIWIL1-associated piRNAs changes during oocyte maturation

- Phosphorylation of PIWIL3 in MII oocytes coincides with its association with small 19-nt piRNAs

- Improved high-quality genome assembly and annotation identifies young endogenous retroviruses as major targets of piRNAs in hamster oocytes

- PIWIL1- and PIWIL3-associated piRNAs share the 5′-ends of the common piRNA precursors in oocytes

Introduction

Transposition of mobile DNA elements can cause severe damage by disrupting either the structural or regulatory regions on the host genome (Chuong et al., 2017; Han and Boeke, 2005; Hancks and Kazazian, 2016). To avoid such detrimental effects, many animals have a conserved adaptive immune system known as the piRNA pathway in gonads (Iwasaki et al., 2015; Ozata et al., 2019; Pillai and Chuma, 2012). piRNAs form effector complexes with PIWI proteins, a germline-specific class of Argonaute proteins, to guide recognition through complementary base-pairing, leading to silencing their target transposable elements (TEs) mainly in two ways: post-transcriptional silencing by PIWI-mediated cleavage of target transcripts in the cytoplasm and transcriptional silencing by PIWI-mediated chromatin modifications on target loci. Mutations in genes involved in the pathway can lead to sterility.

Although the mechanisms for generating piRNAs appear to largely differ among animals, the defined characteristics of piRNAs include a predominant length of 26–32 nucleotides (nt), a strong bias for uracil (U) at the 5′-ends (1U-bias), 2-O-methylation of the 3′-ends, and clustering of reads to distinct genomic locations (Iwasaki et al., 2015; Ozata et al., 2019). The characterization of the piRNA populations in *Drosophila* and mouse has led to two models for the biogenesis mechanisms: the ping-pong cycle (Brennecke et al., 2007; Gunawardane et al., 2007) and phased (Han et al., 2015; Mohn et al., 2015), which are intimately connected. Long single-stranded precursors, often more than 10 kb in size, are derived from discrete genomic loci that are now referred to as piRNA clusters or piRNA genes (Aravin et al., 2006; Brennecke et al., 2007; Girard et al., 2006; Lau et al., 2006; Vagin et al., 2006). Two major clusters exist to serve as genomic piRNA source loci: intergenic and genic clusters. Intergenic piRNA clusters are often located in the heterochromatic regions and comprise various types of TEs that tend to be young and potentially active, suggesting that intergenic piRNA clusters provide the host with acquired and heritable memory systems to repress TEs (Brennecke et al., 2007; Khurana et al., 2011). Genic piRNAs mainly arise from 3′ untranslated regions (UTRs) of the protein-coding genes (Robine et al., 2009; Saito et al., 2009). The function of the genic piRNAs is not well understood, but some genic piRNAs

show significant complementarity to protein-coding genes (Saito et al., 2009; Gonzalez et al., 2015).

piRNA precursors are cleaved by either endonuclease Zucchini/mitoPLD or by the Slicer activity of PIWIs with pre-existing piRNAs to produce 5′ monophosphorylated piRNA intermediates that are loaded onto PIWI proteins (Brennecke et al., 2007; Gainetdinov et al., 2018; Gunawardane et al., 2007; Han et al., 2015; Ipsaro et al., 2012; Mohn et al., 2015; Nishimasu et al., 2012). PIWI-piRNA complexes then initiate piRNA production that is formed by an amplification loop termed the ping-pong cycle in which reciprocal cleavage of TE and cluster transcripts by PIWI proteins generates new piRNA 5′-ends and amplifies piRNA populations while destroying TE mRNAs in the cytoplasm. The ping-pong cycle produces two classes of piRNAs overlapped by precisely 10 nt at their 5′-ends: one class shows a strong preference for U at their 5′-ends (1U) and the second class shows a preference for adenine at nucleotide 10 (10A). The ping-pong cycle is then accompanied by the phased production of piRNAs downstream of the cleavage site, which further creates a sequence diversity of piRNAs. The 3′-ends of piRNAs are determined either by direct cleavage of Zucchini/mitoPLD (mouse *Zucchini* homolog) or PIWIs or by trimming piRNA intermediates by resecting enzymes (Nibbler in *Drosophila*, Trimmer in silkworm, and PNLDC1 in mouse) (Ding et al., 2017; Hayashi et al., 2016; Izumi et al., 2016; Nishida et al., 2018; Nishimura et al., 2018). piRNA biogenesis is then concluded with 2-O-methylation of the 3′-ends by HENMT1 methylase, which has been hypothesized to stabilize mature piRNAs (Gainetdinov et al., 2018; Horwich et al., 2007; Kirino and Mourelatos, 2007; Saito et al., 2007). The extent of 3′-end cleaving/trimming and consequently piRNA length is determined by the footprint of the PIWI protein, possibly explaining the different size profiles of piRNAs associated with distinct PIWI proteins. Structural studies have shown that the 5′- and 3′-ends of the guide small RNAs, including piRNAs, are recognized by the MID-PIWI and PAZ domains of Argonaute/PIWI proteins, respectively (Matsumoto et al., 2016; Wang et al., 2008; Yamaguchi et al., 2020).

Mammalian PIWI-piRNA pathways have been studied mainly in mice (Pillai and Chuma, 2012). Similar to *Drosophila*, mice express three PIWI proteins, MIWI (PIWIL1), MILI (PIWIL2), and MIWI2 (PIWIL4) in the testis, with varying spatiotemporal expression patterns during spermatogenesis. The non-redundant role of

Piwi genes in the mouse testis is demonstrated by the fact that depletion of individual *Piwi* genes causes male-specific sterility owing to severe defects in sperm formation (Aravin et al., 2007; Aravin et al., 2008; Carmell et al., 2007; Deng and Lin, 2002; Ernst et al., 2017; Kuramochi-Miyagawa et al., 2008; Pillai and Chuma, 2012; Thomson and Lin, 2009). Each PIWI protein associates with distinct piRNA populations; fetal prepachytene piRNAs and pachytene piRNAs. Prepachytene piRNAs are formed from TE- and other repeat-derived sequences. In contrast, pachytene piRNAs have a higher proportion of unannotated sequences with the diminished contribution of TE sequences, though they still function in TE silencing by guiding MILI and MIWI to cleave TE transcripts (De Fazio et al., 2011; Reuter et al., 2011). A specific transcriptional factor, A-MYB, binds the promoter regions of pachytene piRNA clusters as well as core piRNA biogenesis factors, including MIWI, and initiates their transcription (Li et al., 2013). Some pachytene piRNA clusters are divergently transcribed from bidirectional A-Myb-binding promoters (Li et al., 2013).

Although PIWI genes in fly and zebrafish are expressed in both testes and ovaries, mouse *Piwi* genes are expressed only weakly, if not at all, in the ovary, and depletion of these *Piwi* genes does not affect the female germline. Thus, these findings led to the assumption that the piRNA pathway does not play a role in mammalian oogenesis. Unlike mice, many other mammals possess four distinct PIWI genes (*Piwil1–4*), suggesting that piRNA-mediated silencing may differ between mice and mammals with four PIWI genes (Hirano et al., 2014; Sasaki et al., 2003). However, except for mice, little is known about mammalian piRNA pathways, particularly their roles in ovaries. Although recent studies have reported the presence of piRNA-like molecules in mammalian female germ cells, including humans (Kabayama et al., 2017; Roovers et al., 2015; Williams et al., 2015; Yang et al., 2019), it is not yet known whether they play a role in the ovary because of the difficulty of technical and/or ethical application of genetic analysis. Although mice and rats belong to the *Muridae* family of rodents, both of which lack *Piwil3*, the golden Syrian hamster (golden hamster, *Mesocricetus auratus*) belongs to the *Cricetidae* family and has four PIWI genes. Golden hamsters have been used as an experimental rodent model for studying human diseases, particularly for cancer development and many different infectious diseases including COVID-19, because they

display many features that resemble the physiology and pharmacological responses of humans (Hirose and Ogura, 2019; Sia et al., 2020). In addition, methods for manipulating gene expression, including the CRISPR/Cas9 system, have been recently employed in golden hamsters (Fan et al., 2014; Hirose et al., 2020). Herein, we analyzed PIWI-associated piRNAs in oocytes and early embryos of golden hamsters, in the hope of applying genetic analysis to the piRNA pathway in the ovary. Our analyses revealed that the size of PIWIL1-associated piRNAs changes during oocyte maturation and that PIWIL3 binds short piRNAs only at the metaphase II (MII) stage of the oocyte, which coincides with phosphorylation of the protein. With an improved high-quality genome assembly and annotation of golden hamster, we showed that PIWIL1- and PIWIL3-associated piRNAs appear to share their 5′-ends. Their contents are similar to those observed with pachytene piRNAs in the mouse testis, but their targets in oocytes are mostly endogenous retroviruses. We further identified ovarian piRNA clusters, and motif search for the transcription start site regions of the piRNA clusters revealed no distinct binding motifs in their upstream regions, although A-Myb-binding motifs were enriched in the upstream regions of the testis piRNA clusters. Our study provides a basis for understanding the roles of the piRNA pathway in mammalian oocytes.

Results

PIWI genes are expressed in the oocyte of the golden hamster

To examine the expression of PIWI genes in golden hamster gonads, we performed RNA-sequencing (RNA-seq) analysis using hamster ovary, oocyte, and testis samples and analyzed the expression level of PIWI genes by calculating transcripts per kilobase million mapped (TPM) (Figure 1A). The estimated expression levels of *Piwil1* and *Piwil2* were relatively high in the testis (TPM = 24.24 and TPM = 14.07, respectively). *Piwil1* was also expressed in the ovary (TPM = 4.63), while *PiwiL2* is not detected in the whole ovary and appeared to be only weakly expressed in the oocyte. *Piwil4* appeared to be expressed only in the testis, consistent with previous transcriptome analysis in human oocytes (Yang et al., 2019). Interestingly, *Piwil3* was highly expressed in the oocyte (TPM = 14.60). In sharp contrast, the expression of *Piwil3* could not be detected in the testis. These results are consistent with previous analyses of bovine and human PIWIL3

(Roovers et al., 2015; Yang et al., 2019). To analyze the expression levels of known PIWI-piRNA pathway factors other than PIWI genes, we also calculated the TPM values of the predicted homologous genes using RNA-seq data (Figure S1A). Most of the known PIWI-piRNA pathway factor homologs, including *Mov10l1*, *Mael*, *MVH* (mouse *Vasa* homolog), *MitoPLD*, *Gtsf1*, *Henmt1*, and Tudor domain families (Iwasaki et al., 2015), were expressed in both testes and oocytes, suggesting that both testes and oocytes of hamsters have similar biogenesis pathways to produce piRNAs.

To confirm the expression of PIWIs in the ovary, we isolated their cDNAs from the ovary. Open reading frames (ORFs) of sequenced *Piwil1* and *Piwil2* cDNAs correspond well with the respective annotated gene products deposited in the Broad Institute database (MesAur1.0, Broad Institute data) (Figure S1B). However, to our surprise, during the cloning of the *Piwil3* cDNA, we found that the large extension of the amino-terminal portion of the ORF contains 14 repeats of nucleotide sequences encoding the amino acid sequences QLQSPGAGPPRSGA (Figure 1B). To further confirm the expression of PIWIs in the ovary at the protein level, we produced specific monoclonal antibodies against PIWIL3 (Figure S1C). We also found that a monoclonal antibody that recognizes marmoset PIWIL1 (Hirano et al., 2014) cross-reacts with hamster PIWIL1 specifically among hamster PIWI proteins (Figure S1C). Thus, we focused our analysis on PIWIL1 and PIWIL3. Immunostaining with the antibodies produced showed that both PIWIL1 and PIWIL3 were expressed in the cytoplasm of growing oocytes in the ovary (Figure 1C). Western blotting with anti-PIWIL1 antibody showed a discrete band at 90 kDa in the ovary, metaphase II (MII) oocytes, and 2-cell embryos (Figure 1D). Western blotting with anti-PIWIL3 antibody revealed a discrete band at 130 kDa in the ovary and 2-cell embryos, which is consistent with the calculated molecular weight of the protein with the large amino-terminal extension (Figure 1B and 1D). Intriguingly, the size of the protein largely shifted by approximately 40 kDa in MII oocytes (Figure 1D).

PIWIL3 protein is highly phosphorylated in metaphase II oocytes

This large increase of the PIWIL3 protein in size, together with the broad and fuzzy nature of the band on the gel (Figure 1D), prompted us to test whether this size shift could be due to modification of the protein with phosphorylation. Treatment of MII oocytes with calf intestinal alkaline phosphatase (CIP), an enzyme known to dephosphorylate proteins

(Siomi et al., 2002), caused a discrete band to migrate to the estimated molecular weight of 130 kDa, demonstrating that PIWIL3 is heavily phosphorylated in MII oocytes (Figure 1E). These results show that PIWIL1 and PIWIL3 are expressed in growing oocytes in the ovary as well as in early embryos and that PIWIL3 is modified with phosphorylation specifically at the MII stage of oocytes. Since the mouse genome lacks *Piwil3* and thus the characterization of PIWIL3 protein has been delayed, our findings indicate that *Piwil3* may have specific functions in female gonads.

The size of piRNAs loaded onto PIWIL1 changes during oocyte maturation

To isolate PIWIL1- and PIWIL3-associated small RNAs from oocytes, we immunopurified the associated complexes from MII oocytes with specific monoclonal antibodies produced. We then isolated RNAs, ^{32}P-labeled them, and analyzed them using a denaturing polyacrylamide gel (Figure 2A). Intriguingly, PIWIL1 was associated with two populations of small RNAs: one with 29–30 nt and the other with 22–23 nt in MII oocytes. We then immunopurified PIWIL1-associated complexes from whole ovaries (including growing oocytes) and 2-cell embryos. The sizes of PIWIL1-associated piRNAs in whole ovaries and 2-cell embryos were 29–30 nt and 22–23 nt, respectively (Figure 2B). The resistance of PIWIL1-associated piRNAs in MII oocytes to periodate oxidation (NaIO4) and β-elimination reactions show that they are modified at the 3′ terminal nucleotide with a 2′-O-methyl marker (Figure S2A). We also isolated PIWIL1-associated small RNAs from whole testes and found that small RNAs (29–30 nt) were loaded onto PIWIL1 in the testis (Figure S2B). These results show that piRNAs loaded onto PIWIL1 change their sizes during oocyte maturation, from the size equivalent to that observed in the testis to a mixture of long and short populations, and short piRNAs (22–23-nt). To our knowledge, this is the first study to show that the size of piRNAs loaded onto a distinct PIWI protein changes during germline development.

Phosphorylated PIWIL3 appears associated with short piRNAs only in MII oocytes

In sharp contrast, PIWIL3 was found to bind to a class of small RNAs with 19 nt (Figure 2A), which is consistent with the recent finding that human PIWIL3 associates with small RNAs (~20 nt) in human oocytes (Yang et al., 2019). 19–20 nt RNAs in oocytes almost completely disappeared after β-elimination reactions, indicating that PIWIL3-associated piRNAs lack 2′-O-methylation at their 3′ terminal (Figure S2C). We failed to detect small

RNAs associated with PIWIL3 in whole ovaries and 2-cell embryos (Figure 2C). With the caveat that this could be because of technical reasons for immunoprecipitation with the antibodies and/or the buffer conditions used, our findings suggest that PIWIL3 may bind piRNAs with 19 nt exclusively in MII oocytes but be freed from piRNAs as 'empty' PIWIL3 at the early stages of oocyte maturation and in early embryos. PIWIL3 is heavily phosphorylated only in MII oocytes, raising the possibility that phosphorylation of the protein may be required for the association with a class of short piRNAs. To test this, we performed immunoprecipitation with an anti-PIWIL3 antibody using MII oocyte lysate that had been treated with CIP and examined whether the CIP treatment affected the association of piRNAs with PIWIL3. Indeed, PIWIL3 treated with CIP was free from piRNAs (Figure 2D). This shows that phosphorylation of the protein is required for PIWIL3 probably either to get loaded with piRNAs or hold them or both.

Generating the hamster genome assembled by resequencing the whole genome to accurately map piRNAs

Although the draft genome of the golden hamster has been sequenced (the MesAur1.0 genome), we soon came to realize that we needed much more accurate genome sequence data to further characterize these PIWI-associated piRNAs on the genome mainly because the MesAur1.0 genome sequence contains a large number of gaps (N) (17.58% of the genome; 420 Mb of the 2.4 Gb) and remains fragmented. Because TEs and other repeats in the genome are the main targets of piRNAs in many animals, the lack of accurate sequences of TEs and other repeats is a serious problem when mapping piRNAs on the genome. Accurate detection of TEs requires both full collection/classification of TE consensus sequences and high-quality genome assembly. Thus, we re-sequenced the golden hamster genome.

Details of the hamster genome assembly are shown in the Methods section. The final genome assembly is summarized in Table 1. The nucleotide difference between the DNA Zoo MesAur1.0_HiC assembly and our assembly was 0.140%. We assessed the completeness of the genome assemblies using the BUSCO tool (Waterhouse et al., 2018) and found that our golden hamster genome assembly included 3,991 complete genes (97.2%) and 37 fragmented genes among 4,104 single-copy genes. Our new golden hamster genome allowed us to resolve several issues that had remained ambiguous. For

example, although putative ancestral karyotypes of rodents in the *Muridae* and *Cricetidae* families have been partly reconstructed by traditional chromosome painting (Romanenko et al., 2012), we compared our nearly complete genome with the mouse (*Mus musculus*) and rat (*Rattus norvegicus*) reference genomes (Methods) and identified conserved synteny blocks between the golden hamster, mouse, and rat genomes (Figure 3A). We inferred ancestral karyotypes by integrating synteny blocks shared between two or three species according to maximum parsimony, to minimize the amount of chromosomal rearrangement (Methods) and obtained a high-resolution ancestral karyotype of *Muridae* using the golden hamster genome as the outgroup as well as a precise ancestral *Cricetidae* karyotype (Figure 3B). Although our ancestral *Cricetidae* and *Muridae* karyotypes were consistent with most previous inference (Romanenko et al, 2012), we resolved some problems: for example, it was unclear whether mouse chromosomes 3 and 4 possessed synteny blocks from a common ancestral karyotype, and our analysis demonstrated the existence of a proto-chromosome in the ancestral *Cricetidae* karyotype (brown blocks in Figure 3B). We also confirmed previous speculation that mouse chromosomes 5 and 16 obtained blocks from a common *Muridae* proto-chromosome (light orange in Figure 3B), and that chromosomes 10, 15, and 17 obtained blocks from a common *Cricetidae* proto-chromosome (maroon blocks in Figure 3B). Finally, we identified two groups of mouse chromosomes (6, 8) and (8, 13) having large blocks from common *Muridae* proto-chromosomes.

Using our genome assembly, we compared the hamster genomic locus containing the *Piwil3* gene with syntenic regions of the mouse and rat genomes. The *Piwil3* gene is flanked by *Wscd2* and *Sgsm1* in the hamster genome (Figure S3A). The order of the two genes is conserved in the syntenic regions of the mouse and rat genomes. We then extracted the genomic regions between these genes from our hamster genome and the reference genomes of mouse (mm10) and rat (rn6), compared the syntenic regions using dot plots (Figure S3B), and observed the absence of the *Piwil3* gene. The validity of the hamster genomic region with *Piwil3* was confirmed by checking each base in the region was covered by an ample number of long reads (Figure S3C). In addition, we performed a similarity search with blastn and ssearch36 using the protein-coding sequence (CDS) of hamster *Piwil3* as a query and found no hits in the corresponding regions of the mouse and rat genome. The PIWIL3 gene is conserved in most mammals,

including humans, suggesting that *Piwil3* might have been deleted after speciation in mice and rats.

With the new golden hamster genome sequence generated, we also conducted a *de novo* repeat characterization and identified 177 consensus sequences of repetitive elements at the subfamily level, including 3 SINEs, 12 LINEs, 156 long terminal repeat (LTR) retrotransposons, and 2 DNA transposons. RepeatMasker analysis using our custom repeat library (RepeatMasker rodent library with newly identified 177 consensus sequences) revealed that SINEs, LINEs, LTR retrotransposons, and DNA transposons occupy 9.2%, 16.9%, 12.1%, and 1.3% of the hamster genome, respectively. The contents of TEs are equivalent to those found in mice and rats, but the fractions of SINE and LINE are, respectively, higher and slightly lower in the hamster than those observed in mice and rats (Table 2). The contents of the MesAur1.0 genome (MesAur1.0_HiC) were similarly analyzed. In contrast to our assembly, a much lower proportion of young TEs were detected even using our custom repeat library (Figure S4A, Table S4). This is mostly because of the high frequency of gaps (Ns) in the MesAur1.0_HiC assembly (Table 1), which resulted in apparently less similarity between TEs and their consensus sequences.

The custom library substantially improved the detection ability of recently active TEs, as represented by a higher proportion of young elements, for example, those with low (< 5.0) Kimura two-parameter (K2P) divergence from the consensus (Figure 4A). Hamster-specific subfamilies of B1 SINE were recently active, and 36,000 copies of young full-length B1s are present in the assembly. We identified three groups of the LINE-1 (L1) family, two of which were recently highly active (L1-4_MAu and L1-5_MAu), and the genome harbors at least 1,000 young full-length copies (Figure 4B). The most active LTR retrotransposons belong to the ERV2/ERVK superfamily, including IAP (for ERV classification, see Kojima 2018; Vargiu et al., 2016). We identified 20 families of ERV2 that contain an internal portion between LTRs, and 11 of them possess a clear reverse transcriptase domain. There are over 13,000 LTR sequences and 1,600 internal portions of the recently active elements in the genome. Among them, we found three recently expanded families: IAP1E_MAu, ERV2-5_MAu, and ERV2-7_MAu, which accounted for 29.9%, 14.7%, and 26.8% of the very young (<2.0 K2P divergence) LTR retrotransposons, respectively (Figure 4C). It is likely that not only IAP but also

other ERV2/ERVK elements are currently active in the hamster genome. Together, these results show that our effort to re-sequence the golden hamster genome significantly improved annotations, especially for recently active TEs, which are potential piRNA targets.

Characterization of piRNAs loaded onto PIWIL1 or PIWIL3

To characterize piRNAs loaded onto PIWIL1 or PIWIL3 in oocytes, we performed small RNA sequencing using piRNA samples immunopurified with an anti-PIWIL1 or an anti-PIWIL3 antibody from oocytes. For PIWIL1-associated piRNAs, we also sequenced piRNA samples immunopurified with an anti-PIWIL1 antibody from testes. Replicates were highly correlated with each other ($R^2 > 0.9$) (data not shown); therefore, we merged the reads. First, we performed a length distribution analysis of the obtained reads (Figure 5A-E). We observed peak signals at the size range of 29–30 nt in the testes and ovaries, 29 nt and 23 nt in MII oocytes, and 23 nt in 2-cell embryos of PIWIL1-associated piRNAs and 19 nt in MII oocytes of PIWIL3-associated piRNAs, confirming that the length of PIWIL1- and PIWIL3-associated piRNAs sequenced is consistent with that observed on the gels. Then we divided into two groups using the length of PIWIL1-associated piRNAs in MII oocyte; Oocyte long piRNAs (L1 OoL-piRNAs) and Oocyte short piRNAs (L1 OoS-piRNAs) for further analysis. Sequencing also revealed that the piRNA populations in all samples showed a strong 1U bias, a conserved characteristic for piRNAs (Figure 5A–E).

We then mapped piRNAs to the new hamster genome (hamster.sequel.draft-20200302.arrow.fasta). Among the PIWI-associated piRNA reads, 50.0~67.4% of the reads were uniquely mapped to the genome and 6.2~43.3% were mapped multiple times (Figure 6A, upper panel). Then, we annotated each piRNA read to analyze the genomic region from which the piRNA reads were generated. Approximately 79.05~89.84% of the reads mapped to unannotated intergenic regions, and only 7.07~13.19% originated from TEs (Figure 6A, lower panel). This profile is similar to that of pachytene piRNAs associated with mouse MIWI, in which ~70% is derived from intergenic regions and ~24% from TEs (Reuter et al., 2011).

The characteristics of PIWIL1-piRNAs were virtually indistinguishable between the testis and ovary. To determine whether this was due to the common piRNA sequences, we calculated reads per million mapped reads (RPM) for each piRNA sequence and compared the correlation between testis and ovary samples. The RPM of piRNAs greatly varied between the testis and ovary samples ($R^2 = 2.08e-06$). In addition, when we checked the top ten piRNA sequences with the most abundant read counts, none of the sequences were common between the testis and ovary (data not shown). These results show that testis and ovary PIWIL1-piRNAs possess distinct sequences (Figure 6B).

We found that most piRNAs in hamster female gonads were derived from LTR retrotransposons, including endogenous retroviruses (ERVs), compared to PIWIL1-piRNAs in the hamster testis, which corresponded to both LINEs and LTR retrotransposons (Figure S5). This observation is consistent with the fact that the main targets of the piRNA pathway in mouse testes are L1 and IAP elements. In the mouse genome, L1 is the most active TE family, as represented by an increasing accumulation of their young copies (Figure S4B). There are also young LTR retrotransposons in mice, among which IAP and MERVL (ERV3/ERVL) families are highly active, while ERV2/ERVK families, except IAPs, showed much lower proportions among the young elements (Figure S4C). Interestingly, most LTR retrotransposons from which piRNAs in hamster female gonads were derived were evolutionally younger judged by the K2P divergence (Figure 4C). This suggests that hamster oocyte piRNAs were generated from the higher activity of recent transposition. In contrast, testis PIWIL1-piRNAs target both LINEs and LTR retrotransposons. Together with the diversity in PIWI-associated piRNA sequences of the oocyte and testis (Figure 6B), this supports the notion that PIWI-piRNA target TEs are different for male and female gonads.

Relationships among PIWIL1- and PIWIL3-bound piRNAs in hamster oocytes

Figure 2 and 5 show that piRNAs loaded onto PIWIL1 in MII oocytes consist of two distinct populations, short piRNAs (L1 OoS-piRNAs) and long piRNAs (L1 OoL-piRNAs). Shorter piRNAs (18–20 nt) were loaded onto PIWIL3 in MII oocytes. These findings prompted us to test whether these piRNAs are derived from the same genomic loci and whether L1 OoS-piRNAs and/or PIWIL3-associated piRNAs are processed

products of L1 OoL-piRNAs by cleaving and/or trimming their 3′-ends. To this end, we asked whether the genomic positions of the 5′- or 3′-ends of the L1 OoL-piRNAs differ from those of L1 OoS-piRNAs or PIWIL3-piRNAs and calculated the probabilities of the 5′- or 3′-ends of L1 OoL-piRNAs coinciding with the 5′- or 3′-ends of L1 OoS-piRNAs or PIWIL3-piRNAs (Gainetdinov et al., 2018). In MII oocytes, L1 OoL-piRNAs were much more likely to share 5′-ends with L1 OoS-piRNAs and PIWIL3-piRNAs (Oo PIWIL3) than with 3′-ends (0.65 for 5′-ends versus 0.03 for 3′-ends and 0.54 for 5′-ends versus 0.02 for 3′-ends, respectively; Figure 7A). These results suggest that approximately half of these three piRNA populations share the same 5′ cleaved piRNA precursors, thereby sharing the same piRNA clusters as piRNA sources. Thus the size differences among these piRNAs account for their 3′-end formation of these populations that may be determined by the footprint of piRNA-binding PIWI proteins, probably because of either the structures of partner PIWI proteins (in particular, the distance between MID-PIWI and PAZ domains) or conformational changes in the partner proteins (see Discussion).

The finding that piRNA populations in oocytes share the same 5′ cleaved piRNA precursors suggests little ping-pong amplification among them. We calculated the ping-pong signature of each piRNA and found that they had little or no ping-pong signatures (Figure 7B). This result indicates that most of the piRNAs expressed in oocytes are not involved in the ping-pong cycle. Recently, a novel class of small RNAs with 21–23 nt, termed short PIWI-interacting RNAs (spiRNAs), was identified in mouse oocytes (Kabayama et al., 2017). They are produced by the ping-pong cycle driven by the MILI slicer activity, and thus, small piRNAs found in hamster oocytes are distinct from spiRNAs.

piRNA clusters in the oocytes are distinct from those observed in the testis

We found that more than half of PIWIL1- and PIWIL3-associated piRNAs are likely to share 5′-ends of precursor transcripts, suggesting that the primary source of piRNAs is also shared among them. To test the possibility that PIWIL1- and PIWIL3-associated piRNAs share piRNA clusters from which they are derived, we next focused on the identification of piRNA clusters in hamster testes, ovaries, MII oocytes, and 2-cell embryos. We identified piRNA clusters using proTRAC (version 2.4.3) under the

following conditions as described (Yang et al., 2019) with some modifications: (1) more than 75% of the reads were appropriate to the length of each piRNA; (2) more than 75% of the reads exhibited the 1 U or 10 A preference; (3) more than 75% of reads were derived from the main strand; and (4) -pimin option with 21, 28, and 18 for oocyte PIWIL1-piRNAs and PIWIL3-piRNAs, respectively. We identified 101, 89, 74, 55, and 61 piRNA clusters in testis PIWIL1-piRNAs, ovary PIWIL1-piRNAs, MII oocyte PIWIL1-piRNAs, 2-cell PIWIL1-piRNAs, and oocyte PIWIL3-piRNAs, respectively. In the testis, both unidirectional clusters, in which piRNAs map to only one strand, and bidirectional clusters, in which the polarity of piRNA production switches between plus and minus strands, were identified, although unidirectional clusters were dominant (Figure 8A and Figure S7A). We found that the majority of the piRNA clusters identified in female gonads were unidirectional (Figure 8B and Figure S6A).

Interestingly, approximately 90% of the piRNA clusters corresponding to PIWIL1-associated piRNAs in testis, ovary, and MII oocytes were sex-specific, and only eight piRNA clusters were identified commonly in both male and female gonads (Figure 8C). These results support the idea that transcription of the primary source of piRNA (piRNA clusters) plays a key role in the production of sex-specific piRNAs (Figure 6B and 8C). We next examined overlaps among ovaries, MII oocytes, and 2-cell embryo PIWIL1 piRNA clusters and found that they shared 31 clusters (Figure 8D). PIWIL1-piRNAs in 2-cell embryos shared approximately 85% of the source clusters with those in MII oocytes, while they shared approximately 60% of the source clusters with those in the ovary, which suggests that the genomic regions where piRNAs are derived are altered during oocyte maturation. PIWIL3-associated piRNAs shared 77% of the clusters with PIWIL1-associated piRNAs in MII oocytes. These results are consistent with the findings that PIWIL1- and PIWIL3-associated piRNA populations are likely to share the same 5′ cleaved piRNA precursors (Figure 7A). Finally, we found that piRNAs loaded onto PIWIL3 in MII oocytes shared a large number of piRNA clusters with piRNAs loaded onto PIWIL1 in 2-cell embryos, suggesting that they may have common targets (Figure 8E).

Given that the transcription of piRNA clusters greatly differs in male and female gonads, we analyzed the motif sites surrounding the potential transcription start

sites of the testis and ovary piRNA clusters. We first extracted sequences surrounding the transcriptional start sites of unidirectional and bidirectional piRNA clusters, predicted from small RNA-seq and RNA-seq mapping data. We used these sequences and performed motif searches using MEME v.5.1.0, which can discover motifs enriched in the given dataset. The results of the MEME analysis show that the A-Myb binding site is significantly represented in the bidirectional piRNA clusters in the testis transcriptional start site surrounding regions (Figure S6B), where it was under-represented in the ovary transcriptional start site surrounding regions (data not shown). Moreover, we calculated the expression level of A-Myb family homolog genes in hamster testis, ovary, and oocyte using RNA-seq data, and found that A-Myb was especially highly expressed in the testis (TPM = 66.33), whereas it was hardly expressed in the ovary and oocyte (TPM = 2.02 in the ovary and was not detected in MII oocytes, respectively) (Figure S6C), consistent with previous findings that in mice, A-Myb is expressed only in the testis, but not in the female gonads (Li et al., 2013). It has been previously shown that A-Myb regulates transcription of piRNA clusters in mice and roosters (Li et al., 2013). These results suggest that piRNA clusters in hamster testes may also be regulated by the transcription factor A-Myb.

In contrast, we failed to detect clear binding consensus sequences for oocyte-expressing transcriptional factors in the upstream regions of unidirectional piRNA clusters in oocytes. Although we also identified some bidirectional clusters in oocytes (Figure S7A), clear binding consensus sequences for oocyte-expressing transcriptional factors between regions of piRNA clusters could not be detected. This could be due to a lack of information on the exact 5′-ends of the piRNA precursors. Alternatively, the transcription of piRNA clusters in oocytes may differ from the testis piRNA clusters in their modes in which, for example, multiple transcriptional factors, but not a few master transcriptional factors such as A-Myb, may drive the transcription of their loci.

Discussion

In this study, we generated a new golden hamster genome, which revealed the presence of young and possibly transposition-competent TEs in the genome. This also allowed us to characterize piRNAs in golden hamster oocytes. Intriguingly, the size of PIWIL1-

associated piRNAs changes during oocyte maturation. In sharp contrast, PIWIL3 binds to piRNAs only in MII oocytes, and the size of loaded piRNAs is shorter (19 nt).

PIWI proteins and piRNAs in hamster oocytes and early embryos

The change in the size of PIWIL1-associated piRNAs during oocyte maturation may necessitate unloading of the 3′-ends of the long piRNAs from PIWIL1 to shorten the long PIWIL1-associated piRNAs to short 22–23 nt either by trimming or by direct cleavage to determine their new 3′-ends. Alternatively, PIWIL1-associated short piRNAs may not be the processed products of loaded long piRNAs, but they may be produced by a mechanism similar to that produced by long piRNAs and then loaded onto either newly produced PIWIL1 or PIWIL1, which has unloaded piRNAs. Because it is thought that the size of small guide RNAs is determined by the footprint of small RNA-binding Argonaute/PIWI proteins (Wang et al., 2008), the change in the size of PIWIL1-associated piRNAs implies a change in the structure of the protein that accommodates short piRNAs. The question is how the change in the structure of PIWIL1 is induced to either unload long piRNAs or reload short piRNAs or to conclude the production of short piRNAs, but not long piRNAs, from intermediates, of which the 5′-ends are likely anchored within the MID-PIWI domain of PIWIL1. It is known that the release of the 3′-end of the guide small RNA from the PAZ domain of some bacterial Argonaute proteins occurs during target recognition, which is accompanied by conformational changes in the PAZ domain (Kaya et al., 2016; Sheng et al., 2014). A recent study has also shown that disengagement of the small RNA 3′-end from the PAZ domain occurs during the mammalian Argonaute activity cycle (Baronti et al., 2020). Thus, it is tempting to speculate that conformational changes in PIWIL1, either upon target recognition of long piRNA-loaded PIWIL1 or by hitherto unknown mechanisms, may occur to conclude the production of short piRNAs. In other words, PIWIL1 could switch between states of structural rearrangements to produce two types of piRNAs. In this context, it is interesting that short piRNAs are loaded onto PIWIL3 when the protein is heavily phosphorylated. Indeed, we demonstrated that phosphorylation is required for PIWIL3 to associate with piRNAs. It is known that the loading of small guide RNAs onto Argonaute proteins appears to be affected by phosphorylation, although the underlying mechanisms are poorly understood (Treiber et al., 2019). Phosphorylation could induce changes in the structure of PIWIL3

so that the protein is loaded with processed intermediates of piRNA precursors and the footprint of the protein determines the size of loaded piRNAs. Alternatively, but not mutually exclusive, PIWIL3 may need to be phosphorylated to stably hold piRNAs. Our findings suggest that hamster PIWI proteins in the oocyte can alternate between states (allostery). It will be interesting to model the structural changes in the PIWI protein using published data on structures of PIWI proteins and other Argonaute proteins.

We found that PIWIL3 binds piRNAs only in MII oocytes but appears to be free from piRNAs at other stages of oocyte maturation. There are precedents for piRNA-independent functions of PIWI proteins. Mouse PIWIL1 (MIWI) was found to bind spermatogenic mRNAs directly, without using piRNAs as guides, to form mRNP complexes that stabilize mRNAs essential for spermatogenesis (Vourekas et al., 2012). Recent studies have also shown that human PIWIL1 (HIWI) functions as an oncoprotein via piRNA-independent mechanisms (Li et al., 2020; Shi et al., 2020). Although Argonaute/Piwi proteins tend to be destabilized when small RNAs are not loaded onto them (Elkayam et al., 2012; Haase et al., 2010; Kobayashi et al., 2019; Smibert et al., 2013), these studies suggest that PIWI proteins may be stable in some conditions in the absence of piRNAs to play a role in some cellular functions.

piRNA-target TEs in the hamster oocyte

In mouse testes, the main target TEs in the piRNA pathway are those of LINE1 and IAP family members. Two distinct piRNA populations are present in mouse testes: pre-pachytene piRNAs are enriched in TE-derived sequences (approximately 80% of the total) (Aravin et al., 2008) and pachytene piRNAs have a higher proportion of unannotated sequences, with diminished contribution from TE-derived sequences (approximately 25%) (Aravin et al., 2006; Girard et al., 2006). These piRNAs guide PIWI proteins to target LINE1 and IAP elements and repress them either by cleaving their transcripts in the cytoplasm or by modifying their chromatin loci in the nucleus (Iwasaki et al., 2015; Ozata et al., 2019). Recent studies also support a model in which TE-derived piRNAs serve as a guide to selectively target young L1 families for *de novo* DNA methylation (Molaro et al., 2014) or H3K9me3 modification (Pezic et al., 2014) in fetal testes. However, the Slicer activity of both MIWI and MILI is still required to maintain

TE silencing in the mouse testis after birth, suggesting that continuous cleavage of TE transcripts by the Slicer activity is essential for repressing TEs in mouse testes (Reuter et al., 2011; De Fazio et al., 2011). We found that the contents of PIWIL1- and PIWIL3-associated piRNAs in hamster oocytes are similar to those observed in mouse pachytene piRNAs. However, the major target TEs in the piRNA pathway in hamster oocytes appear as endogenous retroviruses (ERVs), including ERV2 families. Indeed, our results are concordant with the fact that 41.5% of recently active LTR retrotransposons are accounted for by ERV2 families such as ERV2-7_MAu and ERV2-5_MAu. The differences in piRNA targets between testes and oocytes suggest the possibility that the activity of IAP and these ERV2 elements might be distinctively controlled and their young copies in the genome might have jumped in different types of germline cells. Recent studies have shown that ERVs, which constitute a large portion (8~10%) of mammalian genomes (Mandal and Kazazian, 2008), have a significant impact on shaping transcriptomes and DNA methylation patterns (methylomes) in mammalian oocytes in a species-specific manner (Brind'Amour et al., 2018; Franke et al., 2017). These oocyte transcriptomes and methylomes in mammals are defined by a balance between activation and repression of ERVs. Thus, the piRNA pathway is likely to contribute to the formation of species-specific transcriptomes and methylomes in oocytes. Indeed, it was recently shown that unmethylated IAP promoters in *Miwi*-deficient mouse testes rewire the transcriptome by driving the expression of neighboring genes (Vasiliauskaite et al., 2018). This also implies that spermatogonial dysfunction, observed in *PIWI*-deficient mice, may not simply be due to deregulation of TEs but due to transcriptional rewriting. It will be interesting to see if the lack of PIWIL1 or PIWIL3 leads to dysfunctions in hamster oocytes.

piRNA clusters in hamster oocytes and early embryos

We found that nearly 80% of piRNA clusters corresponding to PIWIL1-associated piRNAs in testis, ovary, and MII oocytes of hamsters were sex-specific. This is in agreement with previous studies with total small RNA-seq of ovaries, indicating that piRNAs in human and bovine ovaries mostly share common piRNA clusters with piRNAs in testes (Roovers et al., 2015; Williams et al., 2015). However, a recent study showed that only about 30% of human oocyte piRNA clusters overlapped with the human testis-

piRNA clusters, proving that testes and oocytes differentially express piRNA clusters (Yang et al., 2019). Our study, together with that of human oocyte piRNAs, suggest a model in which the expression of oocyte and testis piRNA clusters have different functions with distinct targets. Transcriptional factors that regulate their expression are also distinct, though further analysis, including ATAC-seq to define transcription start sites of piRNA precursors, will be needed to identify the transcriptional factors responsible for piRNA clusters in hamster oocytes. In addition, we demonstrated that nearly half of the two populations of PIWIL1-associated piRNAs in oocytes share common clusters and that nearly half of PIWIL3-associated piRNAs in MII oocytes map to clusters from which PIWIL1-associated piRNAs are derived. These results suggest the possibility that a considerable portion of oocyte piRNA cluster transcripts are processed by a common biogenesis pathway but are loaded onto distinct PIWI proteins.

In summary, we have demonstrated that piRNAs are abundantly expressed in hamster oocytes and their size changes during oocyte maturation. Given the recent development of methods to produce genome-edited hamsters (Fan et al., 2014; Hirose et al., 2020), our findings have set the stage for understanding the role that the piRNA pathway plays in mammalian oocytes. Our newly assembled golden hamster genome will also greatly promote the use of golden hamster as a model to understand human disease.

Materials and methods

Animals and tissue collection

Ovaries were collected from 4-week-old golden hamsters that were obtained from the Sankyo Labo Service Corporation, Inc. MII oocytes were collected from 8-week-old golden hamsters that were injected with 40 U of equine chorionic gonadotropin (Serotropin; ASUKA Pharmaceutical Co., Ltd., Tokyo, Japan) at estrus. Two-cells were collected from 8-week-old golden hamsters that were injected with equine chorionic gonadotropin at estrus and mated with adult male hamsters.

5′ RACE

Total RNA for *PIWIL3* 5′ RACE was extracted from the ovaries of 8-week-old golden hamsters using ISOGEN (Nippon Gene) and RNeasy (Qiagen). 5′ RACE was performed

using the SMARTer RACE 5/3 kit (Takara Bio) according to the manufacturer's instructions. The PCR-amplified PIWIL3 5′ RACE fragments were cloned into the pRACE vector and sequenced.

Construction of golden hamster PIWI expression vector

To construct the golden hamster PIWI gene expression vectors, PIWI genes were amplified by PCR using gene specific primers and 3-week-old hamster testis and ovary cDNA. The PCR products were digested with *SpeI* and *NotI*, and then cloned into pEF4-3xFlag vector.

Generation of anti-Hamster PIWIL3 monoclonal antibodies

Anti-PIWI monoclonal antibodies were produced as described previously (Ishizuka et al. 2002; Nishida et al. 2007) with some modifications. Monoclonal mouse antibodies against hamster PIWIL3 were generated by injecting mice with glutathione S-transferase (GST)-Hamster PIWIL3 (20–260 amino acids from the N-terminal where contains repeat region) and then fusing lymph node and spleen cells with the myeloma cell line P3U1 by GenomONE™-CF EX Sendai virus (HVJ) Envelope Cell Fusion Kit (Cosmo Bio) to produce hybridomas. Polyclonal antibodies were selected using ELISA, immunostaining, western blotting, and immunoprecipitation. The hybridoma clone 3E12 used in this study is available for all these applications.

Western blotting

Western blot analysis was performed as described previously (Miyoshi et al. 2010). One-tenth of protein from ovaries, proteins from 15 oocytes and 2-cell embryos, and one-tenth of protein from the testes were subjected to SDS-PAGE. Culture supernatants of anti-marmoset PIWIL1 (MARWI) (1A5-A7) hybridoma cells (Hirano et al. 2014) and anti-hamster PIWIL3 (3E12) hybridoma cells (1:500) and mouse monoclonal anti-β-tubulin (1:5000, DSHB, E7) were used.

Immunofluorescence

The ovaries from 8-week-old wild type female golden hamsters were embedded without fixation for frozen sections. Freezing blocks were sliced to 8 μL and treated with an anti-

PIWIL1 monoclonal antibody (1A5) or anti-PIWIL3 monoclonal antibody (3E12). An Alexa488-conjugated anti-mouse IgG (Molecular Probes) was used as the secondary antibody. Fluorescence was observed with an IX72 fluorescence microscope (Olympus).

Immunoprecipitation

Immunoprecipitation details have been described previously (Saito et al. 2009). Briefly, the ovaries were homogenized using TissueLyser II (QIAGEN) and oocytes and 2-cell embryos in which the zona pellucida were eliminated using polyvinyl acetate with acetic tyrode solution and homogenized by pipetting in binding buffer (30 mM HEPES, pH 7.3, 150 mM potassium acetate, 2 mM magnesium acetate, 5 mM dithiothreitol (DTT), 1% Nonidet P-40 (Calbiochem, 492016), 2 mg/mL Leupeptin (Sigma, L9783), 2 mg/mL Pepstatin (Sigma, P5718), and 0.5% Aprotinin (Sigma, A6279)). PIWIL1 and PIWIL3 proteins were immunopurified using anti-MARWI (1A5) and anti-Hamster PIWIL3 (3E12) immobilized on Dynabeads protein G (Life Technologies, 10004D) and anti-Mouse IgG (IBL, 17314) were used as non-immune, negative controls. The reaction mixtures were incubated at 4°C overnight and the beads were rinsed three times with binding buffer.

β-elimination

Periodate oxidation and β-elimination were performed as described previously (Hirano et al. 2014; Kirino and Mourelatos 2007; Ohara et al. 2007; Saito et al. 2007; Simon et al. 2011). A 100 μL mixture consisting of purified RNAs and 10 mM NaIO4 (Wako, 199-02401) was incubated at 4°C for 40 min in the dark. The oxidized RNAs were then incubated with 1 M Lys-HCl at 45°C for 90 min to achieve β-elimination.

^{32}P-labeling

The 5′-end of the RNAs were labeled with [gamma-^{32}P] ATP (Perkin Elmer) and T4 polynucleotide kinase (ATP: 5-dephosphopolynucleotide 5'-phosphotransferase, EC 2.7.1.78). The labeled RNAs were cleaned using Micro Bio-Spin™ column 30 (Bio-Rad) and ethanol precipitation. The precipitated RNAs were subjected to SDS-PAGE with 15% urea.

Summary of genome sequence and assembly of the golden hamster

Raw PacBio reads (Table S1) were assembled into contigs using the FALCON genome assembler, which is widely used for processing long reads (Chin et al., 2016). To correct assembly errors in the FALCON contigs, we applied the Racon module (Vaser et al., 2017) three times. To obtain a chromosome-scale genome assembly, we aligned all contigs to the 22 golden hamster chromosomes (MesAur1.0_HiC, DNA Zoo) (Figure S7). We attempted to fill 3,797 gaps in the reference chromosomes using the FALCON contigs and error-corrected reads. We generated error-corrected reads using the FALCON assembler, which aligned PacBio raw reads to each other, obtained the consensus sequence of aligned reads using multiple alignments, and then output the consensus sequences as error-corrected reads. To fill unsettled gaps, we aligned error-corrected reads to the gaps using the minimap2 program (Li, 2018) and manually inspected the results to determine whether the gaps were spanned by more than one error-corrected read (Table S2). Finally, we polished the draft assembly using the PacBio raw reads and Arrow program.

PacBio read assembly

We used the FALCON genome assembler version 2018.08.08-21.41-py2.7-ucs4-beta (Chin et al. 2016) with default parameter settings to assemble PacBio reads. To correct errors in the assembly, we applied the RACON module (version 1.4.10; Vaser et al. 2017) three times with default parameter settings.

Genome assembly alignment

We aligned all contigs in the assemblies to the golden hamster reference assembly (DNA Zoo release MesAur1.0_HiC.fasta.gz) using MUMmer 4.0.0beta2 software (Marçais et al. 2018) with the nucmer program, and the following parameters: mum min cluster = 100, max gap = 300. We also used the minimap2 version 2.13 (Li, 2018) with default parameter settings.

Effects of the Arrow program on the draft genome

We polished the draft genome using the Arrow program (version 2.3.3; https://github.com/PacificBiosciences/GenomicConsensus) with default parameter settings. We used the QUAST 5.0.2 tool (Gurevich et al. 2013) to calculate mismatch and

indel ratios for our golden hamster genome with respect to the DNA Zoo Hi-C genome, both before and after genome polishing (Table S3).

Gene lift over from N2 to VC2010

We lifted gene structures and other genome annotations from the golden hamster reference assembly (MesAur1.0 release 100) to our golden hamster assembly. Such cross-assembly mapping typically requires an annotation file in a standard format (e.g., GFF3; https://github.com/The-Sequence-Ontology/Specifications/blob/master/gff3.md), chain alignment (Kent et al. 2003), and a program capable of mapping annotations based on chain alignment (e.g., liftOver) (Speir et al. 2016). The reference genome sequence was downloaded (ftp://ftp.ensembl.org/pub/release-100/fasta/mesocricetus_auratus/dna/Mesocricetus_auratus.MesAur1.0.dna.toplevel.fa.gz) as were the annotations of canonical golden hamster genes (ftp://ftp.ensembl.org/pub/release-100/gff3/mesocricetus_auratus/Mesocricetus_auratus.MesAur1.0.100.gff3.gz). Both the genome sequence and its annotations were obtained from the Ensembl database (release-100). To chain-align our golden hamster assembly (as the query) to the reference assembly (as the target), we used methods almost identical to those described by the University of California Santa Cruz (UCSC) for same-species genomic chain alignment (http://genomewiki.ucsc.edu/index.php/DoSameSpeciesLiftOver.pl). The liftOver protocol required several utility programs from UCSC, some of which were downloaded as precompiled binaries (http://hgdownload.cse.ucsc.edu/admin/exe/linux.x86_64). To map genome annotations, we used liftOver with the parameter -gff -minMatch = 0.90.

Comparative genome analysis

We compared our golden hamster genome with the mouse reference genome (*Mus musculus* GRCm38.p6 release-100 in the Ensembl database; ftp://ftp.ensembl.org/pub/release-100/fasta/mus_musculus/dna/) and the rat reference genome (*Rattus norvegicus* Rnor_6.0 release-100 in the Ensembl database; ftp://ftp.ensembl.org/pub/release-100/fasta/rattus_norvegicus/dna/) using the Murasaki program (ver. 1.6.8) with a seed pattern weight of 76 and a length of 110 (Popendorf et al. 2010).

Chromosomal evolution in Rodentia

First, we identified synteny blocks that were shared between two or three species, that is, hamster, mouse, and/or rat (details provided in Figure S8). Next, we inferred ancestral karyotypes of Muridae and *Cricetidae* (Figure 3B) by integrating synteny blocks according to maximum parsimony, minimizing the total number of chromosomal rearrangements such as chromosome fusions, chromosome fissions, and translocations. We excluded inversions from chromosomal rearrangements, which were markedly more prevalent than the other rearrangements. We compared our nearly complete golden hamster genome with the mouse (*Mus musculus*) sand rat (*Rattus norvegicus*) reference genomes. Figure 4A shows conserved synteny blocks between the golden hamster, mouse, and rat genomes. We inferred ancestral karyotypes by integrating synteny blocks shared between two or three species according to maximum parsimony to minimize the amount of chromosomal rearrangement. We obtained a high-resolution ancestral karyotype of Muridae, including mice and rats, using the golden hamster genome as the outgroup as well as a species ancestral *Cricetidae* karyotype (Figure 3B).

Characterization of TEs in the hamster genome

We first used the RepeatModeler ver. 2.0 (Flynn et al, 2020) coupled with LTR_retriever ver. 2.8 (Ou and Jiang, 2018) for *de novo* identification of repetitive elements in the hamster genome. Among the initial repeat candidates obtained, 282 elements, covering ~37% of the genome in total, were used for subsequent in-depth characterization. In the accurate identification process, we conducted a BLASTN search and collected 80–100 sequences along with the 6-kbp flanking sequences of each element. The sequences were aligned with MAFFT ver 7.427 (Katoh and Standley, 2013) followed by manual curation, and a refined consensus sequence was constructed to be used for the next round of blastn search. This process was repeated for three rounds at maximum until the consensus sequence reached the 5' and 3' termini. We finally constructed 177 consensus sequences at the subfamily level and classified them based on the sequence structure and a comparison with known elements using CENSOR (Jurka et al. 2005) and RepeatMasker ver. 4.1.0. We finally constructed a custom repeat library by adding 177 novel consensus sequences to the original rodent repeat library. RepeatMasker analysis was conducted for genome annotation using the cross-match engine with the sensitive mode (-s). Young (*i.e.*, recently active) complete TEs were selected based on the <5.0 K2P divergence from the

consensus sequence and the full-length insertions, although ignoring the lack of sequence homology in up to 50 bp of the 5-terminal of LINEs and 3 bp at the edge of other TEs.

Small RNA-seq library preparation

PIWIL1 and PIWIL3-associated piRNAs were prepared as described previously (Hirano et al. 2014). PIWI family associated small RNAs were extracted from immunopurified proteins using ISOGEN (Nippon Gene, 311-02501). Libraries were prepared using NEBNext Small RNA Library Sample Prep Set (New England BioLabs (NEB), E7330) with slight modifications. Small RNAs obtained and purified using SPRIselect (Beckman Coulter, B23317) underwent 3 ligation at 16°C for 18 h, then free 3 adaptors were degraded using 5 deadenylase (NEB, M0331) and RecJf (NEB, M0264). The 3′-ligated RNAs underwent 5 adaptor ligation at 25°C for 1 h. The RNAs were reverse-transcribed using SuperScriptIII (Life Technologies, 18080-044) and were PCR-amplified using Q5 Hot Start High-Fidelity DNA Polymerase (NEB, M0493) with 18 cycles.

Small RNA sequencing and data processing

PIWIL1 and PIWIL3-associated small RNAs were sequenced using MiSeq (Illumina) with three replicates from different samples. A total of 32,478,862 reads were obtained and processed as described previously (Iwasaki et al. 2017). The adaptors were trimmed from the reads using Cutadapt version 2.10 (Martin 2011). The replicates were highly correlated ($R^2 \geqq 0.9$), so the reads were merged. Each read was mapped to the reference genome (hamster.sequel.draft-20200302.arrow.fasta) using Bowtie version 1.2.3 (Langmead et al. 2009) with the -v 0 option, which extracts the small RNA reads that were perfectly mapped. Genome mapped reads were selected by size using Seqkit (Shen et al. 2016). The PIWIL1-piRNAs were divided into two groups: Oocyte Short (OoS) group, which included 21–27 nt RNAs, and Oocyte Long (OoL) group with 28–31 nt RNAs. PIWIL3-piRNAs with 18–20 nt were selected for further analysis.

RNA-seq data processing

The RNA-seq library in oocytes was prepared using the SMART-Seq® Stranded Kit (TaKaRa, 634442). Total RNAs obtained using NucleoSpin® RNA Plus XS (TaKaRa, 740990) from approximately 100 oocytes were fragmented at 85℃ for 6 min. Sheared

RNAs were processed under the "Low input category." PCR1 was performed with 5 cycles, followed by PCR2 with 13 cycles, and the final cleanup was performed once. RNA-seq libraries in the ovary and testis were prepared using the TruSeq Stranded mRNA Sample Prep kit. The libraries were sequenced using HiSeq2000 (Illumina) and the obtained reads were combined, resulting in a total of 79,152,300 pair-end reads for hamster testis and 81,979,150 pair-end reads for hamster ovary, respectively. Reads with trimming adaptors and quality filtering were mapped to the hamster reference genome (hamster.sequel.draft-20200302.arrow.fasta) using hisat2 version 2.2.0 (Kim et al. 2015) with the strandness option (--strandness FR). To calculate transcripts per kilobase million mapped (TPM) as expression levels of genes, we used StringTie version 2.1.3 (Pertea et al. 2015).

Sequence logo

Sequence logos were generated using the motifStack R package (http://www.bioconductor.org/packages/release/bioc/html/motifStack.html). Small RNA sequences were aligned at the 5′-end, and nucleotide bias was calculated per position.

Annotation of reads

Annotation of genome mapped reads was determined as described previously (Iwasaki et al., 2017) with some modifications. We examined the overlap between read-mapped genomic regions and feature track data. Each feature data was obtained from RpeatMasker (Smit et al. http://www.repeatmasker.org/) for transposons, repeats, tRNAs, rRNAs and snoRNAs, miRDeep2 version 2.0.1.2 (Friedländer et al. 2012) for miRNAs and UCSC LiftOff pipeline for protein-coding genes. Reads were assigned to a feature when the length of its overlap was longer than 90% of the small RNA. The priority of the feature assignment was defined to avoid any conflict of the assignment. For this study, the priority was in the following order: transposon, repeat, miRNA, rRNA, tRNA, snRNA, snoRNA, and protein-coding genes (exons and introns). Any unassigned regions were regarded as unannotated regions.

piRNA target TE prediction

Prediction of PIWI-piRNA targets derived from TE regions was determined as described previously (Hirano et al. 2014; Iwasaki et al. 2017) with some modifications. First, we

eliminated piRNA reads that mapped to tRNAs or rRNAs. The extracted reads were aligned to consensus sequences of transposons (Rodentia custom library), allowing two mismatches. The alignment was performed using Bowtie because of the large number of obtained sequences.

piRNA cluster prediction

Prediction of piRNA clusters was performed using proTRAC version 2.4.3 (Rosenkranz et al. 2012) under the following conditions as described previously (Yang et al., 2019): (1) more than 75% of the reads that were appropriate to the length of each piRNA; (2) more than 75% of the reads exhibited the 1 U or 10 A preference; (3) more than 75% of reads were derived from the main strand; and (4) -pimin option with 21, 28, and 18 for oocyte PIWIL1-piRNAs and PIWIL3-piRNAs, respectively.

Motif search at the transcriptional start site of piRNA clusters.

We analyzed the motif sites surrounding the transcription start sites of the testis and ovary piRNA clusters. We first extracted sequences surrounding transcriptional start sites of unidirectional and bidirectional piRNA clusters predicted from small RNA-seq and RNA-seq mapping data. For the detection of bidirectional piRNA clusters, we first determined the number of reads per base in the cluster based on the results of RNA-seq with TopHat version 2.1.1 (Kim et al., 2013). We next detected the direction of each base site and a region in which the same direction was contiguous by more than 200 bp was identified. If (+) or (-) occupies more than 75% of the cluster, the cluster is designated as the direction. If the number of reads was less than five, the direction was the same as the previous base site. The region between the switch of transcriptional direction was extracted along with 200bp upstream and downstream regions, as transcriptional start site of bidirectional clusters. The bidirectional cluster with multiple switching regions identified using these criteria was omitted. For the detection of unidirectional piRNA clusters, we extracted 300 bp upstream and 200 bp downstream of genomic regions where piRNA clusters overlapped with the transcript regions detected from Cufflinks version 2.2.1 (Trapnell et al., 2010). The direction of the sequence strands was the same as in the transcripts. We then used these sequences and performed motif searches using MEME version.5.1.0 (Bailey et al., 2009). Tomtom version 5.1.1 (Bailey et al., 2009) was used for motif comparison.

Visualization of sequenced reads

To visualize the read density obtained from smRNA-seq snd RNA-seq, we created a BigWig file by using HOMER version 4.11 (Heinz et al. 2010) and displayed the Integrative Genomics Viewer (IGV) version 2.4.1. (Robinson et al., 2011). The normalized expression level of each sample was calculated using reads per million reads (RPM).

Accession number

The accession number for the deep-sequencing datasets reported in this paper is PRJDB10770 in DDBJ.

Acknowledgments

We thank all members of the Siomi laboratory, especially Drs. Hirotsugu Ishizu and Akihiko Sakashita, for the discussions and comments on this study. We are also grateful to Yukiteru Ono for assisting the bioinformatics. S. Morishita thanks Drs. Erez Lieberman-Aiden and Olga Dudchenko for making the chromosome-scale DNA-ZOO hamster genome publicly available, Koko Saito and Dr. Chie Owa for PacBio Sequel sequencing, and Dr. Yoichiro Nakatani for stimulating discussion on chromosomal evolution in Rodentia. K.I. was supported by a Grant-in-Aid for JSPS Fellows (18J22025) from the Japan Society for the Promotion of Science (JSPS) and is the Keio University Doctoral Student Grant-in-Aid Program 2018 and 2019. This study was supported by Grants-in-Aid for Scientific Research on Innovative Areas (16H06279) (PAGS) to K.I., J.Y., Y.S., A.T., T.I., and S.M. from JSPS. Y.W.I. was supported by funding from JSPS KAKENHI Grant Numbers 19H05268 and 18H02421. S. Morishita was supported by the Japan Agency for Medical Research and Development (AMED) GRIFIN program. H. Siomi was supported by a Grant-in-Aid for Scientific Research (S) (25221003) from JSPS and is a recipient of funding for the Project for Elucidating and Controlling Mechanisms of Aging and Longevity (1005442) from AMED and the 'Program of totipotency: from decoding to designing' from JSPS (19H05753).

Author Contributions

KI and HH designed and performed most of the experiments with YWI, HM, TH, NMS, MT, KS, and MCS. JY, HI, YS, AT, TI, and SM participated in the *de novo* genome assembly of the golden hamster, and JY, YS, and SM in the chromosomal evolution in Rodentia. HN and TK detected transposable elements. HS conceived the study, and KI, SM, and HS wrote the paper with input from the other authors.

Conflict of interest

The authors declare that they have no conflict of interest.

Figure legends

Figure 1. PIWIs are expressed in hamster oocytes

(A) Expression patterns of PIWI families in male and female hamsters. Transcriptome data were obtained from Illumina HiSeq2000. The x-axis suggests the normalized expression level (TPM).

(B) Protein homology of PIWIL3 in hamster and human. Approximately 74.6% of the PAZ domain and 83.3% of the PIWI domain in hamster PIWIL3 are conserved in human PIWIL3. The large extension of the amino-terminal portion of the ORF, which contains 14 repeats of nucleotide sequences encoding the amino acid sequences QLQSPGAGPPRSGA is presented in hamster PIWIL3.

(C) PIWIL1 (upper panel) and PIWIL3 (lower panel) levels from an ovary. Immunostaining with PIWIL1 and PIWIL3 are shown: (green) PIWIL1 and PIWIL3; (blue) Hoechst. The signal in the zona pellucida at upper panel is the autofluorescence of anti-PIWIL1 antibody.

(D) Western blotting was performed from hamster whole ovaries, MII oocytes, and 2-cell embryos with anti-PIWIL3, anti-PIWIL1, and anti-β-TUBULIN antibodies. The size of the PIWIL3 protein largely shifted by approximately 40 kDa in MII oocytes. The anti-MARWI (PIWIL1) antibody (1A5) and anti-PIWIL3 antibody (3E12) detected a single band in each sample except for MII oocytes.

(E) Western blotting was performed from hamster MII oocytes with (+) or without (-) CIP treatment. A discrete band migrated to the estimated molecular weight of 130 kDa in the CIP-treated sample, demonstrating that PIWIL3 is heavily phosphorylated in MII oocytes.

Figure 2. The different populations of piRNAs associate with each of the PIWI proteins at different developmental stages

(A) Isolated RNAs from PIWIL1 and PIWIL3 immunoprecipitates in MII oocytes were ^{32}P-labeled and separated by a denaturing polyacrylamide gel. PIWIL1 and PIWIL3 proteins associate with ~28~31-nt and ~18~20-nt-long piRNAs, respectively.

(B) Western blotting and ^{32}P-labeling were performed from PIWIL1 immunoprecipitates in hamster whole ovaries, MII oocytes, and 2-cell embryos. Upper panel: Western blotting ; lower panel: ^{32}P-labeling.

(C) The same experiments with (B) were performed from PIWIL3 immunoprecipitates.

(D) Phosphorylation of the protein is required for PIWIL3 probably either to get loaded with piRNAs or hold them or both. PIWIL3 immunoprecipitates were treated with (+) or without (-) CIP. Upper panel: Western blotting; lower panel: ^{32}P -labeling of RNAs, which were purified from each PIWIL3 immunoprecipitate.

Figure 3. Chromosomal evolution in Rodentia

(A) Each line represents a reciprocally best-matching pair of positions in our hamster genome (middle) and the mouse (top) or rat (bottom) reference genome. In each line, the colored part represents the hamster chromosome, and the color palette displayed at the bottom shows the color-coding. Neighboring lines indicate synteny blocks conserved between two species.

(B) Schematic showing the ancestral karyotypes of *Cricetidae* and *Muridae* inferred from conserved synteny blocks using maximum parsimony. The top two karyotypes are identical and represent the ancestral *Cricetidae* karyotype; the middle two show the ancestral *Muridae* karyotype. Each box represents a conserved synteny block among the three species; the colored part indicates the hamster chromosome as per Figure A. Small synteny blocks are enlarged. Lines from one proto-chromosome to the descendant chromosomes indicate rearrangements (fusion, fission, or translocation). To simplify the graph, we omitted lines between the identical chromosomes within the same columns. Brown blocks show the existence of a proto-chromosome in the ancestral *Cricetidae* karyotype. We confirmed the previous speculation that mouse chromosomes 5 and 16 obtained blocks from a common *Muridae* proto-chromosome (light-orange), and that chromosomes 10, 15, and 17 obtained blocks from a common *Cricetidat*e proto-chromosome (maroon blocks). We also identified two groups of mouse chromosomes (6, 8) and (8, 13) having large blocks from common *Muridae* proto-chromosomes.

Figure 4. Identification of active transposable elements in the hamster genome

(A) Age distribution of the hamster TEs compared between the original and customized repeat libraries. The proportion of TEs is shown for 0.5 bins of Kimura 2-parameter (K2P) distance (CpG-corrected) from each consensus sequence.

(B) A Maximum-likelihood tree of the L1 ORF2 subfamilies and their age distribution (0.5 bins of K2P distance). The TE amount is the length occupied in Mbp.

(C) Amount of recently-active LTR retrotransposons compared among representative IAP and other ERV2 families.

Figure 5. Characterization of PIWI-associated piRNAs in hamster male and female gonads

Size distribution and nucleotide bias in PIWIL1-associated piRNAs in hamster (A) testis, (B) ovary, (C) MII oocyte, (D) 2-cell embryo, and (E) PIWIL3-associated piRNAs in hamster MII oocytes. Left panel: size distribution; peaks of size distribution are shown at 29–30 nt in testis and ovary PIWIL1-piRNAs, 29–30 nt and 23–24 nt in MII oocyte PIWIL1-piRNAs, 22–23 nt in 2-cell embryo PIWIL1-piRNAs and 19 nt in MII oocyte PIWIL3-piRNAs, respectively. The right panel shows nucleotide bias. All piRNA populations have a strong uridine (U) bias at their 5′-end.

Figure 6. Characterization of genome mapped PIWI-associated piRNA reads in hamster male and female gonads

(A) Genome mapping ratio and annotation of PIWIL1- and PIWIL3-associated piRNA reads in hamster testis, ovary, MII oocyte, and 2-cell embryo. The upper panel exhibits the genome mapped ratio of each PIWI-associated piRNA reads: (gray) unique mapped reads; (black) multiple mapped reads; (white) unmapped reads. Lower panel exhibits the results of annotation of genome mapped reads: (red) transposon; (orange) repeat; (yellow) protein-coding gene, including exon and intron; (purple) miRNA; (blue) tRNA; (skyblue) rRNA; (green) other ncRNA, including snoRNA and snRNA.

(B) Comparison between testis and ovary PIWIL1-associated piRNAs. Pearson correlation coefficient was calculated using R. Each dot exhibits the specific piRNA reads.

Figure 7. PIWIL1- and PIWIL3-associated piRNA populations are likely to share the same 5′ cleaved piRNA precursors

(A) Probability of distances between the 5′- or 3′-ends of OoL PIWIL1 (longer)- and OoS PIWIL1- or PIWIL3 (shorter)- piRNAs (Oo PIWIL3). The numbers indicate the total frequency of the 5′- or 3′-ends of shorter piRNAs residing before, after, or coinciding with the 5′- or 3′-ends of the longer piRNAs. This indicates that piRNA populations are likely to share the same 5′ cleaved piRNA precursors, but the 3′-end formation of these

populations may be determined by the footprint of piRNA-binding PIWI proteins probably because of either structure.

(B) A heat map showing the probability that the first base of the PIWI-associated piRNA reads mapped to the antisense strand overlap the 10th base of the reads, which mapped to the sense strand. This result shows that they do not have any ping-pong signals with each other.

Figure 8. piRNA clusters in hamster male and female gonads

(A) Example of male-specific piRNA cluster in hamster. Distributions of uniquely mapped piRNAs and RNA-seq reads located in piRNA clusters are shown.

(B) Example of female-specific piRNA cluster in hamster. Distributions of uniquely mapped piRNAs and RNA-seq reads located in piRNA clusters are shown.

(C) The Venn diagram shows the amount of overlap among PIWIL1-piRNA clusters, which are consistent with 28~30 nt piRNAs in hamster testis, ovary, and MII oocyte.

(D) The Venn diagram shows the amount of overlap among PIWIL1-piRNA clusters in hamster ovary, MII oocyte and 2-cell embryo.

(E) The Venn diagram shows the amount of overlap among PIWIL1-piRNA clusters in hamster 2-cell embryo and PIWIL3-piRNA clusters in hamster MII oocyte.

Table 1. The statistics of the genome assemblies

Table 2. Proportion (%) of transposable elements in rodents

Supplemental Figures:

Figure S1. Related to Figure 1.

(A) Expression levels of homolog genes in hamster testis, ovary, and MII oocyte, which is known to correspond to the PIWI-piRNA pathway in mouse and *Drosophila.* Expression levels are normalized by transcripts per kilobase million mapped (TPM).

(B) A phylogenetic tree of PIWI genes in hamster, human, mouse, and *Drosophila*. Their evolutionary distances were calculated using the maximum likelihood method.

(C) Western blotting was performed on 293T cells, which were transfected with *Piwil1* and *Piwil3* genes, respectively. The results show that anti-MARWI (marmoset PIWIL1) and hamster PIWIL3 antibodies specifically recognize their targets.

Figure S2. Related to Figure 2.

(A) PIWIL1-piRNAs were subjected to periodate oxidation and β-elimination treatment. Synthetic RNAs with or without 2′-*O*-methyl modification were used as controls (upper panel). The unchanged PIWIL1-piRNA signals indicate that the 3′-termini of PIWIL1-piRNAs is 2′-*O*-methylated, as the characteristic of piRNAs (lower panel).

(B) Western blotting (left panel) and ^{32}P labeling (right panel) were performed from PIWIL1 immunoprecipitates in hamster testis and ovary. Non-immune means negative control, using an anti-mouse IgG antibody.

(C) Composition of small RNAs in the hamster oocytes before and after NaIO4 oxidization. The average result of three biological replicates is shown.

Figure S3. Related to Figure 3.

(A) The synteny of the *Piwil3* gene. The synteny of *Wscd2* and *Sgsm1* genes was conserved between hamsters, mice, and rats. Otherwise, a synteny block of *Piwil3*, *Sgsm1*, and *Tmem1* was conserved between hamsters and humans.

(B) From our hamster genome and the reference genomes of mouse (mm10) and rat (rn6), we retrieved and compared the three genomic regions between *Wscd2* and *Sgsm1*. The *Piwil3* encoding region is present in the focal region of the hamster genome but is absent in the mouse and rat genomes. The *Piwil3* region is deleted in the mouse genome and is replaced with another sequencing in the rat genome.

(C) We aligned to PacBio long reads to the assembled contig with *Piwil3* (the red-colored region). In the lower portion, the respective blue and red colored lines show the alignments of reads in the plus and minus strands. We observed that each base position was covered by an ample number (ten or more) of long reads, and the read coverage was nearly even, thereby confirming the accuracy of the assembled contig.

Figure S4. Related to Figure 4.

Age distribution of TEs in another hamster assembly (DNA ZOO MesAur1.0_HiC) and mouse genome. The proportion of TEs is shown for 0.5 bins of K2P distance (CpG-corrected) from each consensus sequence.

(A) TEs in the MesAur1.0_HiC assembly was analyzed with the original (top) and customized (bottom) repeat libraries.
(B) TEs in the mouse genome was analyzed using the mouse repeat library. The color code is the same as in (A).
(C) Representative young LTR retrotransposons in the mouse genome.

Figure S5. Related to Figure 6.

Heat maps show strand bias of transposon-derived piRNAs corresponding to each PIWIs in hamster testis, ovary, MII oocyte and 2-cell embryo. Transposons are grouped into LINEs, SINEs, LTRs, and DNA transposons. Color intensities indicate the degree of strand bias: (blue) sense; (yellow) antisense; (white) unbiased. The frequencies of piRNAs mapped to each TE subfamily over the total TE-mapped piRNAs are shown in the bar graph.

Figure S6. Related to Figure 8.

(A) The number of predicted piRNA clusters in hamster testis, ovary, MII oocyte and 2-cell embryo. The black bar shows the unidirectional piRNA clusters and white shows the bidirectional piRNA clutsters, respectively.
(B) A motif search was performed for each unidirectional and bidirectional piRNA cluster in the hamster testis using MEME. The results suggest that the A-Myb binding site is significantly represented in the bidirectional piRNA clusters in testis transcriptional start site surrounding regions.
(C) Expression levels of transcription factor candidates detected using MEME. The expression pattern of the A-Myb gene in male and female hamsters. RNA-seq data were obtained using Illumina HiSeq2000. The x-axis suggests the normalized expression level (TPM).

Figure S7. Contigs aligned to the reference assembly.

The 22 panels show the alignments of our assembled contigs to the 22 Hi-C scaffolds of the DNA Zoo Hi-C assembly. Thick red and blue lines show alignments of contigs in the plus and minus strands, respectively. Labels beside each contig line indicate the contig identifier.

Figure S8. Map of conserved synteny between the hamster, mouse, and rat genomes.
(A) Each chromosome in the hamster (top), mouse (middle), and rat (bottom) genomes are associated with a two-column box. The left and right columns show chromosomes in the genomes of mouse and rat (top row), hamster and rat (middle row), and hamster and rat (bottom row), respectively. The same color-coding of chromosomes shown in the color pallet at the bottom was used for the three species.
(B) The upper portion is identical to Figure 1B. To facilitate the identification of synteny blocks, dot plots of the hamster (x-axis) and mouse (y-axis) genomes (bottom left), and the hamster (x-axis) and rat (y-axis) genomes (bottom right) are shown.
(C) Left panel, color-coded lines showing reciprocally best-matching pairs of positions in the hamster (middle) and mouse (top) or rat chromosomes (bottom) for each of the 22 hamster chromosomes. Right panel: synteny blocks between the hamster genome on the x-axis and the mouse (red) and rat (green) genomes on the y-axis.

Table S1. Related to Table 1.
Statistics of raw and "polished" long genome sequencing reads from the golden hamster sample using the PacBio Sequel system.

Table S2. Related to Table 1.
Series of connected contigs and error-corrected reads. For each chromosomal position, the first and penultimate columns list primary contigs obtained using the FALCON genome assembler (yellow), error-corrected reads (light blue), and remaining gaps (white). The fourth and fifth columns show the start and end positions for each contig, respectively.

Table S3. Related to Table 1.
Mismatch and indel ratios of our golden hamster genome assembly before and after polishing using PacBio long reads.

Table S4. Related to Table 2.
Proportion (%) of transposable elements in the MesAur1.0_HiC assembly.

References

Aravin, A., Gaidatzis, D., Pfeffer, S., Lagos-Quintana, M., Landgraf, P., Iovino, N., Morris, P., Brownstein, M.J., Kuramochi-Miyagawa, S., Nakano, T., *et al.* (2006). A novel class of small RNAs bind to MILI protein in mouse testes. Nature *442*, 203-207.

Aravin, A.A., Sachidanandam, R., Bourc'his, D., Schaefer, C., Pezic, D., Toth, K.F., Bestor, T., and Hannon, G.J. (2008). A piRNA pathway primed by individual transposons is linked to de novo DNA methylation in mice. Mol Cell *31*, 785-799.

Aravin, A.A., Sachidanandam, R., Girard, A., Fejes-Toth, K., and Hannon, G.J. (2007). Developmentally regulated piRNA clusters implicate MILI in transposon control. Science *316*, 744-747.

Bailey, T.L., Boden, M., Buske, F.A., Frith, M., Grant, C.E., Clementi, L., Ren, J., Li, W.W., and Noble, W.S. (2009). MEME SUITE: tools for motif discovery and searching. Nucleic Acids Res *37*, W202-208.

Baronti, L., Guzzetti, I., Ebrahimi, P., Friebe Sandoz, S., Steiner, E., Schlagnitweit, J., Fromm, B., Silva, L., Fontana, C., Chen, A.A., *et al.* (2020). Base-pair conformational switch modulates miR-34a targeting of Sirt1 mRNA. Nature *583*, 139-144.

Brennecke, J., Aravin, A.A., Stark, A., Dus, M., Kellis, M., Sachidanandam, R., and Hannon, G.J. (2007). Discrete small RNA-generating loci as master regulators of transposon activity in Drosophila. Cell *128*, 1089-1103.

Brind'Amour, J., Kobayashi, H., Richard Albert, J., Shirane, K., Sakashita, A., Kamio, A., Bogutz, A., Koike, T., Karimi, M.M., Lefebvre, L., *et al.* (2018). LTR retrotransposons transcribed in oocytes drive species-specific and heritable changes in DNA methylation. Nat Commun *9*, 3331.

Carmell, M.A., Girard, A., van de Kant, H.J., Bourc'his, D., Bestor, T.H., de Rooij, D.G., and Hannon, G.J. (2007). MIWI2 is essential for spermatogenesis and repression of transposons in the mouse male germline. Dev Cell *12*, 503-514.

Chin, C.S., Peluso, P., Sedlazeck, F.J., Nattestad, M., Concepcion, G.T., Clum, A., Dunn, C., O'Malley, R., Figueroa-Balderas, R., Morales-Cruz, A., *et al.* (2016). Phased diploid genome assembly with single-molecule real-time sequencing. Nat Methods *13*, 1050-1054.

Chuong, E.B., Elde, N.C., and Feschotte, C. (2017). Regulatory activities of transposable elements: from conflicts to benefits. Nat Rev Genet *18*, 71-86.

De Fazio, S., Bartonicek, N., Di Giacomo, M., Abreu-Goodger, C., Sankar, A., Funaya, C., Antony, C., Moreira, P.N., Enright, A.J., and O'Carroll, D. (2011). The endonuclease activity of Mili fuels piRNA amplification that silences LINE1 elements. Nature *480*, 259-263.

Deng, W. & Lin, H. (2002). Miwi, a murine homolog of piwi, encodes a cytoplasmic protein essential for spermatogenesis. Dev. Cell *2,* 819–830.

Ding D, Liu J, Dong K, Midic U, Hess RA, Xie H, Demireva EY, Chen C. (2017). PNLDC1 is essential for piRNA 3' end trimming and transposon silencing during spermatogenesis in mice. Nat Commun. *8*, 819

Elkayam, E., Kuhn, C.D., Tocilj, A., Haase, A.D., Greene, E.M., Hannon, G.J., and Joshua-Tor, L. (2012). The structure of human argonaute-2 in complex with miR-20a. Cell *150*, 100-110.

Ernst, C., Odom, D.T., and Kutter, C. (2017). The emergence of piRNAs against transposon invasion to preserve mammalian genome integrity. Nat Commun *8*, 1411.

Fan, Z., Li, W., Lee, S.R., Meng, Q., Shi, B., Bunch, T.D., White, K.L., Kong, I.K., and Wang, Z. (2014). Efficient gene targeting in golden Syrian hamsters by the CRISPR/Cas9 system. PLoS One *9*, e109755.

Flynn, J.M., Hubley, R., Goubert, C., Rosen, J., Clark, A.G., Feschotte, C., and Smit, A.F. (2020). RepeatModeler2 for automated genomic discovery of transposable element families. Proc Natl Acad Sci U S A *117*, 9451-9457.

Franke, V., Ganesh, S., Karlic, R., Malik, R., Pasulka, J., Horvat, F., Kuzman, M., Fulka, H., Cernohorska, M., Urbanova, J.*, et al.* (2017). Long terminal repeats power evolution of genes and gene expression programs in mammalian oocytes and zygotes. Genome Res *27*, 1384-1394.

Friedländer, M.R., Mackowiak, S.D., Li, N., Chen, W., and Rajewsky, N. (2012). miRDeep2 accurately identifies known and hundreds of novel microRNA genes in seven animal clades. Nucleic Acids Res *40*, 37-52.

Gainetdinov, I., Colpan, C., Arif, A., Cecchini, K., and Zamore, P.D. (2018). A Single Mechanism of Biogenesis, Initiated and Directed by PIWI Proteins, Explains piRNA Production in Most Animals. Mol Cell *71*, 775-790.e775.

Girard, A., Sachidanandam, R., Hannon, G.J., and Carmell, M.A. (2006). A germline-specific class of small RNAs binds mammalian Piwi proteins. Nature *442*, 199-202.

Gonzalez, J., Qi, H., Liu, N., and Lin, H. (2015). Piwi is a key rgulator of both somatic and germline stem cells in the *Drosophila* testis. Cell Rep 12, 150-161.

Gunawardane, L.S., Saito, K., Nishida, K.M., Miyoshi, K., Kawamura, Y., Nagami, T., Siomi, H., and Siomi, M.C. (2007). A slicer-mediated mechanism for repeat-associated siRNA 5' end formation in Drosophila. Science *315*, 1587-1590.

Gurevich, A., Saveliev, V., Vyahhi, N., and Tesler, G. (2013). QUAST: quality assessment tool for genome assemblies. Bioinformatics *29*, 1072-1075.

Haase, A. D., Fenoglio, S., Muerdter, F., Guzzardo, P. M., Czech, B., Pappin, D. J., Chen, C., Gordon, A., and Hannon, G. J. (2010). Probing the initiation and effector phases of the somatic piRNA pathway in *Drosophila*. Genes Dev *24*, 2499-2504.

Han, B.W., Wang, W., Li, C., Weng, Z., and Zamore, P.D. (2015). Noncoding RNA. piRNA-guided transposon cleavage initiates Zucchini-dependent, phased piRNA production. Science *348*, 817-821.

Han, J.S., and Boeke, J.D. (2005). LINE-1 retrotransposons: modulators of quantity and quality of mammalian gene expression? Bioessays *27*, 775-784.

Hancks, D.C., and Kazazian, H.H., Jr. (2016). Roles for retrotransposon insertions in human disease. Mob DNA *7*, 9.

Hayashi, R., Schnabl, J., Handler, D., Mohn, F., Ameres, S.L., and Brennecke, J. (2016). Genetic and mechanistic diversity of piRNA 3'-end formation. Nature *539*, 588-592.

Heinz, S., Benner, C., Spann, N., Bertolino, E., Lin, Y.C., Laslo, P., Cheng, J.X., Murre, C., Singh, H., and Glass, C.K. (2010). Simple combinations of lineage-determining transcription factors prime cis-regulatory elements required for macrophage and B cell identities. Mol Cell *38*, 576-589.

Hirano, T., Iwasaki, Y.W., Lin, Z.Y., Imamura, M., Seki, N.M., Sasaki, E., Saito, K., Okano, H., Siomi, M.C., and Siomi, H. (2014). Small RNA profiling and characterization of piRNA clusters in the adult testes of the common marmoset, a model primate. Rna *20*, 1223-1237.

Hirose, M., Honda, A., Fulka, H., Tamura-Nakano, M., Matoba, S., Tomishima, T., Mochida, K., Hasegawa, A., Nagashima, K., Inoue, K.*, et al.* (2020). Acrosin is essential for sperm penetration through the zona pellucida in hamsters. Proc Natl Acad Sci U S A *117*, 2513-2518.

Hirose, M., and Ogura, A. (2019). The golden (Syrian) hamster as a model for the study of reproductive biology: Past, present, and future. Reprod Med Biol *18*, 34-39.

Horwich, M.D., Li, C., Matranga, C., Vagin, V., Farley, G., Wang, P., and Zamore, P.D. (2007). The Drosophila RNA methyltransferase, DmHen1, modifies germline piRNAs and single-stranded siRNAs in RISC. Curr Biol *17*, 1265-1272.

Ipsaro, J.J., Haase, A.D., Knott, S.R., Joshua-Tor, L., and Hannon, G.J. (2012). The structural biochemistry of Zucchini implicates it as a nuclease in piRNA biogenesis. Nature *491*, 279-283.

Ishizuka, A., Siomi, M.C., and Siomi, H. (2002). A Drosophila fragile X protein interacts with components of RNAi and ribosomal proteins. Genes Dev *16*, 2497-2508.

Iwasaki, Y.W., Ishino, K., and Siomi, H. (2017). Deep sequencing and high-throughput analysis of PIWI-associated small RNAs. Methods *126*, 66-75.

Iwasaki, Y.W., Siomi, M.C., and Siomi, H. (2015). PIWI-Interacting RNA: Its Biogenesis and Functions. Annu Rev Biochem *84*, 405-433.

Izumi, N., Shoji, K., Sakaguchi, Y., Honda, S., Kirino, Y., Suzuki, T., Katsuma, S., and Tomari, Y. (2016). Identification and Functional Analysis of the Pre-piRNA 3' Trimmer in Silkworms. Cell *164*, 962-973.

Jurka, J., Kapitonov, V.V., Pavlicek, A., Klonowski, P., Kohany, O., and Walichiewicz, J. (2005). Repbase Update, a database of eukaryotic repetitive elements. Cytogenet Genome Res *110*, 462-467.

Kabayama, Y., Toh, H., Katanaya, A., Sakurai, T., Chuma, S., Kuramochi-Miyagawa, S., Saga, Y., Nakano, T., and Sasaki, H. (2017). Roles of MIWI, MILI and PLD6 in small RNA regulation in mouse growing oocytes. Nucleic Acids Res *45*, 5387-5398.

Katoh, K., and Standley, D.M. (2013). MAFFT multiple sequence alignment software version 7: improvements in performance and usability. Mol Biol Evol *30*, 772-780.

Kaya, E., Doxzen, K.W., Knoll, K.R., Wilson, R.C., Strutt, S.C., Kranzusch, P.J., and Doudna, J.A. (2016). A bacterial Argonaute with noncanonical guide RNA specificity. Proc Natl Acad Sci U S A *113*, 4057-4062.

Kent, W.J., Baertsch, R., Hinrichs, A., Miller, W., and Haussler, D. (2003). Evolution's cauldron: duplication, deletion, and rearrangement in the mouse and human genomes. Proc Natl Acad Sci U S A *100*, 11484-11489.

Khurana, J.S., Wang, J., Xu, J., Koppetsch, B.S., Thomson, T.C., Nowosielska, A., Li, C., Zamore, P.D., Weng, Z., and Theurkauf, W.E. (2011). Adaptation to P element transposon invasion in Drosophila melanogaster. Cell *147*, 1551-1563.

Kim, D., Langmead, B., and Salzberg, S.L. (2015). HISAT: a fast spliced aligner with low memory requirements. Nat Methods *12*, 357-360.

Kim, D., Pertea, G., Trapnell, C., Pimentel, H., Kelley, R., and Salzberg, S.L. (2013). TopHat2: accurate alignment of transcriptomes in the presence of insertions, deletions and gene fusions. Genome Biol *14*, R36.

Kirino, Y., and Mourelatos, Z. (2007). The mouse homolog of HEN1 is a potential methylase for Piwi-interacting RNAs. Rna *13*, 1397-1401.

Kobayashi, H., Shoji, K., Kiyokawa, K., Negishi, L., and Tomari, Y. (2019). Iruka Eliminates Dysfunctional Argonaute by Selective Ubiquitination of Its Empty State. Mol Cell *73*, 119-129.e5.

Kojima, K.K. (2018). Human transposable elements in Repbase: genomic footprints from fish to humans. Mob DNA *9*, 2.

Kuramochi-Miyagawa, S., Watanabe, T., Gotoh, K., Takamatsu, K., Chuma, S., Kojima-Kita, K., Shiromoto, Y., Asada, N., Toyoda, A., Fujiyama, A.*, et al.* (2010). MVH in piRNA processing and gene silencing of retrotransposons. Genes Dev *24*, 887-892.

Kuramochi-Miyagawa, S., Watanabe, T., Gotoh, K., Totoki, Y., Toyoda, A., Ikawa, M., Asada, N., Kojima, K., Yamaguchi, Y., Ijiri, T.W.*, et al.* (2008). DNA methylation of retrotransposon genes is regulated by Piwi family members MILI and MIWI2 in murine fetal testes. Genes Dev *22*, 908-917.

Langmead, B., Trapnell, C., Pop, M., and Salzberg, S.L. (2009). Ultrafast and memory-efficient alignment of short DNA sequences to the human genome. Genome Biol *10*, R25.

Lau, N.C., Seto, A.G., Kim, J., Kuramochi-Miyagawa, S., Nakano, T., Bartel, D.P., and Kingston, R.E. (2006). Characterization of the piRNA complex from rat testes. Science *313*, 363-367.

Li, F., Yuan, P., Rao, M., Jin, C.H., Tang, W., Rong, Y.F., Hu, Y.P., Zhang, F., Wei, T., Yin, Q.*, et al.* (2020). piRNA-independent function of PIWIL1 as a co-activator for anaphase promoting complex/cyclosome to drive pancreatic cancer metastasis. Nat Cell Biol *22*, 425-438.

Li, H. (2018). Minimap2: pairwise alignment for nucleotide sequences. Bioinformatics *34*, 3094-3100.

Li, X.Z., Roy, C.K., Dong, X., Bolcun-Filas, E., Wang, J., Han, B.W., Xu, J., Moore, M.J., Schimenti, J.C., Weng, Z.*, et al.* (2013). An ancient transcription factor initiates the burst of piRNA production during early meiosis in mouse testes. Mol Cell *50*, 67-81.

Mandal, P.K., and Kazazian, H.H., Jr. (2008). SnapShot: Vertebrate transposons. Cell *135*, 192-192.e191.

Marçais, G., Delcher, A.L., Phillippy, A.M., Coston, R., Salzberg, S.L., and Zimin, A. (2018). MUMmer4: A fast and versatile genome alignment system. PLoS Comput Biol *14*, e1005944.

Martin, M. (2011). <200-1885-3-PB.pdf>. EMBnet Journal *17*, 2.

Matsumoto, N., Nishimasu, H., Sakakibara, K., Nishida, K.M., Hirano, T., Ishitani, R., Siomi, H., Siomi, M.C., and Nureki, O. (2016). Crystal Structure of Silkworm PIWI-Clade Argonaute Siwi Bound to piRNA. Cell *167*, 484-497.e489.

Miyoshi, K., Miyoshi, T., Hartig, J.V., Siomi, H., and Siomi, M.C. (2010). Molecular mechanisms that funnel RNA precursors into endogenous small-interfering RNA and microRNA biogenesis pathways in Drosophila. Rna *16*, 506-515.

Mohn, F., Handler, D., and Brennecke, J. (2015). Noncoding RNA. piRNA-guided slicing specifies transcripts for Zucchini-dependent, phased piRNA biogenesis. Science *348*, 812-817.

Molaro, A., Falciatori, I., Hodges, E., Aravin, A.A., Marran, K., Rafii, S., McCombie, W.R., Smith, A.D., and Hannon, G.J. (2014). Two waves of de novo methylation during mouse germ cell development. Genes Dev *28*, 1544-1549.

Nishida, K.M., Saito, K., Mori, T., Kawamura, Y., Nagami-Okada, T., Inagaki, S., Siomi, H., and Siomi, M.C. (2007). Gene silencing mechanisms mediated by Aubergine piRNA complexes in Drosophila male gonad. Rna *13*, 1911-1922.

Nishida, K.M., Sakakibara, K., Iwasaki, Y.W., Yamada, H., Murakami, R., Murota, Y., Kawamura, T., Kodama, T., Siomi, H., and Siomi, M.C. (2018). Hierarchical roles of mitochondrial Papi and Zucchini in Bombyx germline piRNA biogenesis. Nature *555*, 260-264.

Nishimasu, H., Ishizu, H., Saito, K., Fukuhara, S., Kamatani, M.K., Bonnefond, L., Matsumoto, N., Nishizawa, T., Nakanaga, K., Aoki, J., *et al.* (2012). Structure and function of Zucchini endoribonuclease in piRNA biogenesis. Nature *491*, 284-287.

Nishimura T, Nagamori I, Nakatani T, Izumi N, Tomari Y, Kuramochi-Miyagawa S, Nakano T. (2018). PNLDC1, mouse pre-piRNA Trimmer, is required for meiotic and post-meiotic male germ cell development. EMBO Rep. *19*, e44957

Ohara, T., Sakaguchi, Y., Suzuki, T., Ueda, H., Miyauchi, K., and Suzuki, T. (2007). The 3' termini of mouse Piwi-interacting RNAs are 2'-O-methylated. Nat Struct Mol Biol *14*, 349-350.

Ou, S., and Jiang, N. (2018). LTR_retriever: A Highly Accurate and Sensitive Program for Identification of Long Terminal Repeat Retrotransposons. Plant Physiol *176*, 1410-1422.

Ozata, D.M., Gainetdinov, I., Zoch, A., O'Carroll, D., and Zamore, P.D. (2019). PIWI-interacting RNAs: small RNAs with big functions. Nat Rev Genet *20*, 89-108.

Pertea, M., Pertea, G.M., Antonescu, C.M., Chang, T.C., Mendell, J.T., and Salzberg, S.L. (2015). StringTie enables improved reconstruction of a transcriptome from RNA-seq reads. Nat Biotechnol *33*, 290-295.

Pezic, D., Manakov, S.A., Sachidanandam, R., and Aravin, A.A. (2014). piRNA pathway targets active LINE1 elements to establish the repressive H3K9me3 mark in germ cells. Genes Dev *28*, 1410-1428.

Pillai, R.S., and Chuma, S. (2012). piRNAs and their involvement in male germline development in mice. Dev Growth Differ *54*, 78-92.

Popendorf, K., Tsuyoshi, H., Osana, Y., and Sakakibara, Y. (2010). Murasaki: a fast, parallelizable algorithm to find anchors from multiple genomes. PLoS One *5*, e12651.

Reuter, M., Berninger, P., Chuma, S., Shah, H., Hosokawa, M., Funaya, C., Antony, C., Sachidanandam, R., and Pillai, R.S. (2011). Miwi catalysis is required for piRNA amplification-independent LINE1 transposon silencing. Nature *480*, 264-267.

Robinson, J.T., Thorvaldsdóttir, H., Winckler, W., Guttman, M., Lander, E.S., Getz, G., and Mesirov, J.P. (2011). Integrative genomics viewer. Nat Biotechnol *29*, 24-26.

Romanenko, S.A., Perelman, P.L., Trifonov, V.A., and Graphodatsky, A.S. (2012). Chromosomal evolution in Rodentia. Heredity (Edinb) *108*, 4-16.

Roovers, E.F., Rosenkranz, D., Mahdipour, M., Han, C.T., He, N., Chuva de Sousa Lopes, S.M., van der Westerlaken, L.A., Zischler, H., Butter, F., Roelen, B.A.*, et al.* (2015). Piwi proteins and piRNAs in mammalian oocytes and early embryos. Cell Rep *10*, 2069-2082.

Rosenkranz, D., and Zischler, H. (2012). proTRAC--a software for probabilistic piRNA cluster detection, visualization and analysis. BMC Bioinformatics *13*, 5.

Saito, K., Inagaki, S., Mituyama, T., Kawamura, Y., Ono, Y., Sakota, E., Kotani, H., Asai, K., Siomi, H., and Siomi, M.C. (2009). A regulatory circuit for piwi by the large Maf gene traffic jam in Drosophila. Nature *461*, 1296-1299.

Saito, K., Sakaguchi, Y., Suzuki, T., Suzuki, T., Siomi, H., and Siomi, M.C. (2007). Pimet, the Drosophila homolog of HEN1, mediates 2'-O-methylation of Piwi- interacting RNAs at their 3' ends. Genes Dev *21*, 1603-1608.

Sasaki, T., Shiohama, A., Minoshima, S., and Shimizu, N. (2003). Identification of eight members of the Argonaute family in the human genome. Genomics *82*, 323-330.

Shen, W., Le, S., Li, Y., and Hu, F. (2016). SeqKit: A Cross-Platform and Ultrafast Toolkit for FASTA/Q File Manipulation. PLoS One *11*, e0163962.

Sheng, G., Zhao, H., Wang, J., Rao, Y., Tian, W., Swarts, D.C., van der Oost, J., Patel, D.J., and Wang, Y. (2014). Structure-based cleavage mechanism of Thermus thermophilus Argonaute DNA guide strand-mediated DNA target cleavage. Proc Natl Acad Sci U S A *111*, 652-657.

Shi, S., Yang, Z.Z., Liu, S., Yang, F., and Lin, H. (2020). PIWIL1 promotes gastric cancer via a piRNA-independent mechanism. Proc Natl Acad Sci U S A *117*, 22390-22401.

Sia, S.F., Yan, L.M., Chin, A.W.H., Fung, K., Choy, K.T., Wong, A.Y.L., Kaewpreedee, P., Perera, R., Poon, L.L.M., Nicholls, J.M.*, et al.* (2020). Pathogenesis and transmission of SARS-CoV-2 in golden hamsters. Nature *583*, 834-838.

Simon, B., Kirkpatrick, J.P., Eckhardt, S., Reuter, M., Rocha, E.A., Andrade-Navarro, M.A., Sehr, P., Pillai, R.S., and Carlomagno, T. (2011). Recognition of 2'-O-methylated 3'-end of piRNA by the PAZ domain of a Piwi protein. Structure *19*, 172-180.

Siomi, M.C., Higashijima, K., Ishizuka, A., and Siomi, H. (2002). Casein kinase II phosphorylates the fragile X mental retardation protein and modulates its biological properties. Mol Cell Biol *22*, 8438-8447.

Smibert, P., Yang, J. S., Azzam, G., Liu, J. L., and Lai, E. C. (2013). Homeostatic control of Argonaute stability by microRNA availability. Nat Struct Mol Biol *20*, 789-795.

Speir, M.L., Zweig, A.S., Rosenbloom, K.R., Raney, B.J., Paten, B., Nejad, P., Lee, B.T., Learned, K., Karolchik, D., Hinrichs, A.S.*, et al.* (2016). The UCSC Genome Browser database: 2016 update. Nucleic Acids Res *44*, D717-725.

Thomson, T., and Lin, H. (2009). The biogenesis and function of PIWI proteins and piRNAs: progress and prospect. Annu Rev Cell Dev Biol *25*, 355-376.

Trapnell, C., Williams, B.A., Pertea, G., Mortazavi, A., Kwan, G., van Baren, M.J., Salzberg, S.L., Wold, B.J., and Pachter, L. (2010). Transcript assembly and quantification by RNA-Seq reveals unannotated transcripts and isoform switching during cell differentiation. Nat Biotechnol *28*, 511-515.

Treiber, T., Treiber, N., and Meister, G. (2019). Regulation of microRNA biogenesis and its crosstalk with other cellular pathways. Nat Rev Mol Cell Biol *20*, 5-20.

Vagin, V.V., Sigova, A., Li, C., Seitz, H., Gvozdev, V., and Zamore, P.D. (2006). A distinct small RNA pathway silences selfish genetic elements in the germline. Science *313*, 320-324.

Vargiu, L., Rodriguez-Tomé, P., Sperber, G.O., Cadeddu, M., Grandi, N., Blikstad, V., Tramontano, E., and Blomberg, J. (2016). Classification and characterization of human endogenous retroviruses; mosaic forms are common. Retrovirology *13*, 7.

Vaser, R., Sović, I., Nagarajan, N., and Šikić, M. (2017). Fast and accurate de novo genome assembly from long uncorrected reads. Genome Res *27*, 737-746.

Vasiliauskaitė L, Berrens RV, Ivanova I, Carrieri C, Reik W, Enright AJ, and O'Carroll D. (2018). Defective germline reprogramming rewires the spermatogonial transcriptome. Nat Struct Mol Biol. *25*, 394-404

Vourekas, A., Zheng, Q., Alexiou, P., Maragkakis, M., Kirino, Y., Gregory, B.D., and Mourelatos, Z. (2012). Mili and Miwi target RNA repertoire reveals piRNA biogenesis and function of Miwi in spermiogenesis. Nat Struct Mol Biol *19*, 773-781.

Wang, Y., Sheng, G., Juranek, S., Tuschl, T., and Patel, D.J. (2008). Structure of the guide-strand-containing argonaute silencing complex. Nature *456*, 209-213.

Waterhouse, R.M., Seppey, M., Simão, F.A., Manni, M., Ioannidis, P., Klioutchnikov, G., Kriventseva, E.V., and Zdobnov, E.M. (2018). BUSCO Applications from Quality Assessments to Gene Prediction and Phylogenomics. Mol Biol Evol *35*, 543-548.

Williams, Z., Morozov, P., Mihailovic, A., Lin, C., Puvvula, P.K., Juranek, S., Rosenwaks, Z., and Tuschl, T. (2015). Discovery and Characterization of piRNAs in the Human Fetal Ovary. Cell Rep *13*, 854-863.

Yamaguchi, S., Oe, A., Nishida, K.M., Yamashita, K., Kajiya, A., Hirano, S., Matsumoto, N., Dohmae, N., Ishitani, R., Saito, K.*, et al.* (2020). Crystal structure of Drosophila Piwi. Nat Commun *11*, 858.

Yang, Q., Li, R., Lyu, Q., Hou, L., Liu, Z., Sun, Q., Liu, M., Shi, H., Xu, B., Yin, M.*, et al.* (2019). Single-cell CAS-seq reveals a class of short PIWI-interacting RNAs in human oocytes. Nat Commun *10*, 3389.

Figure 1

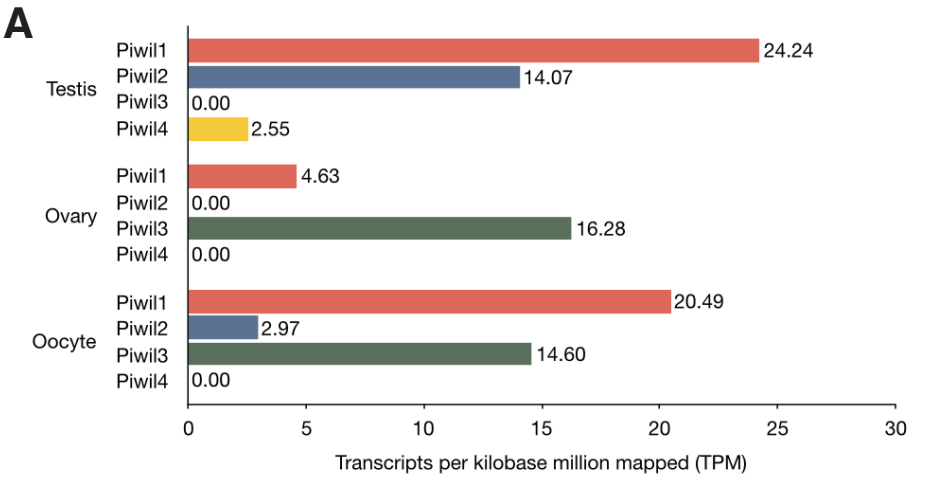

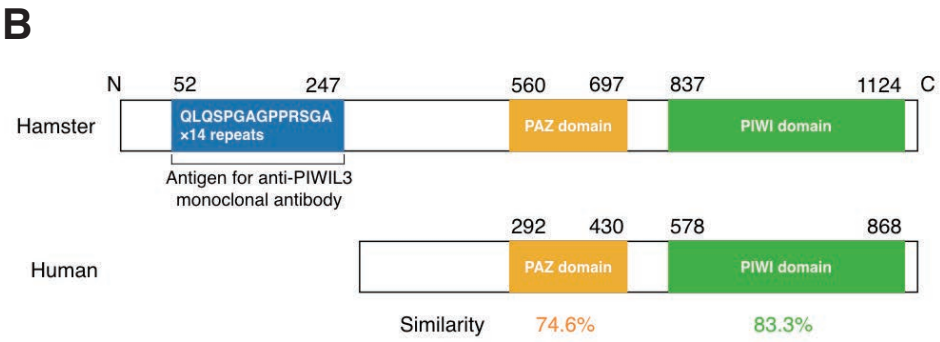

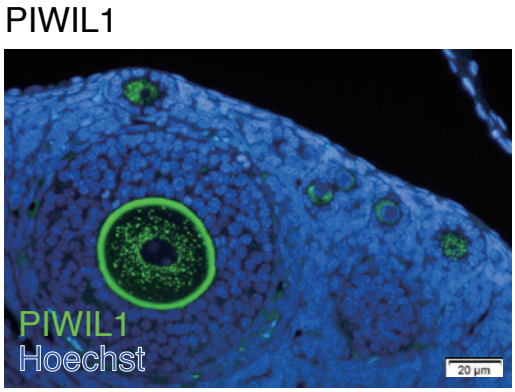

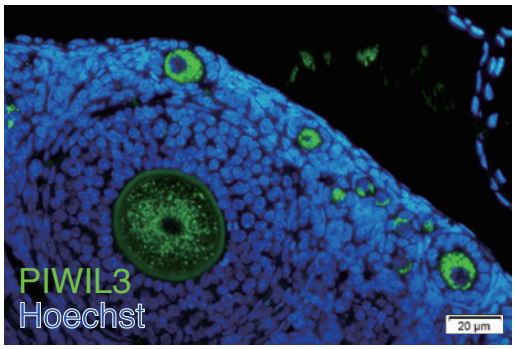

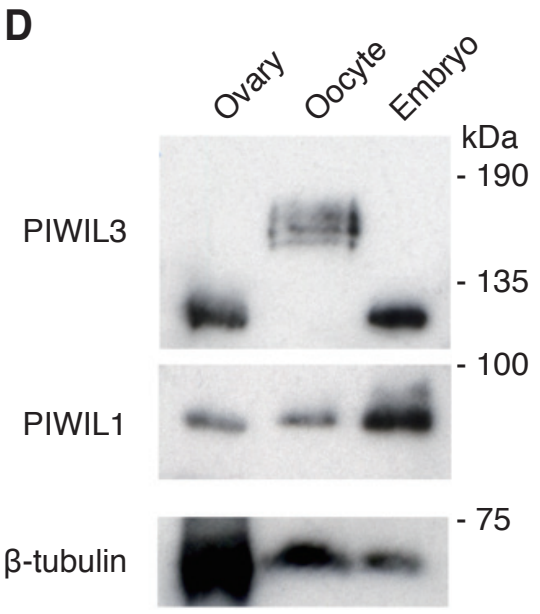

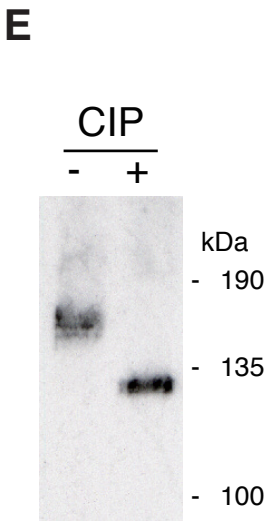

Figure 2

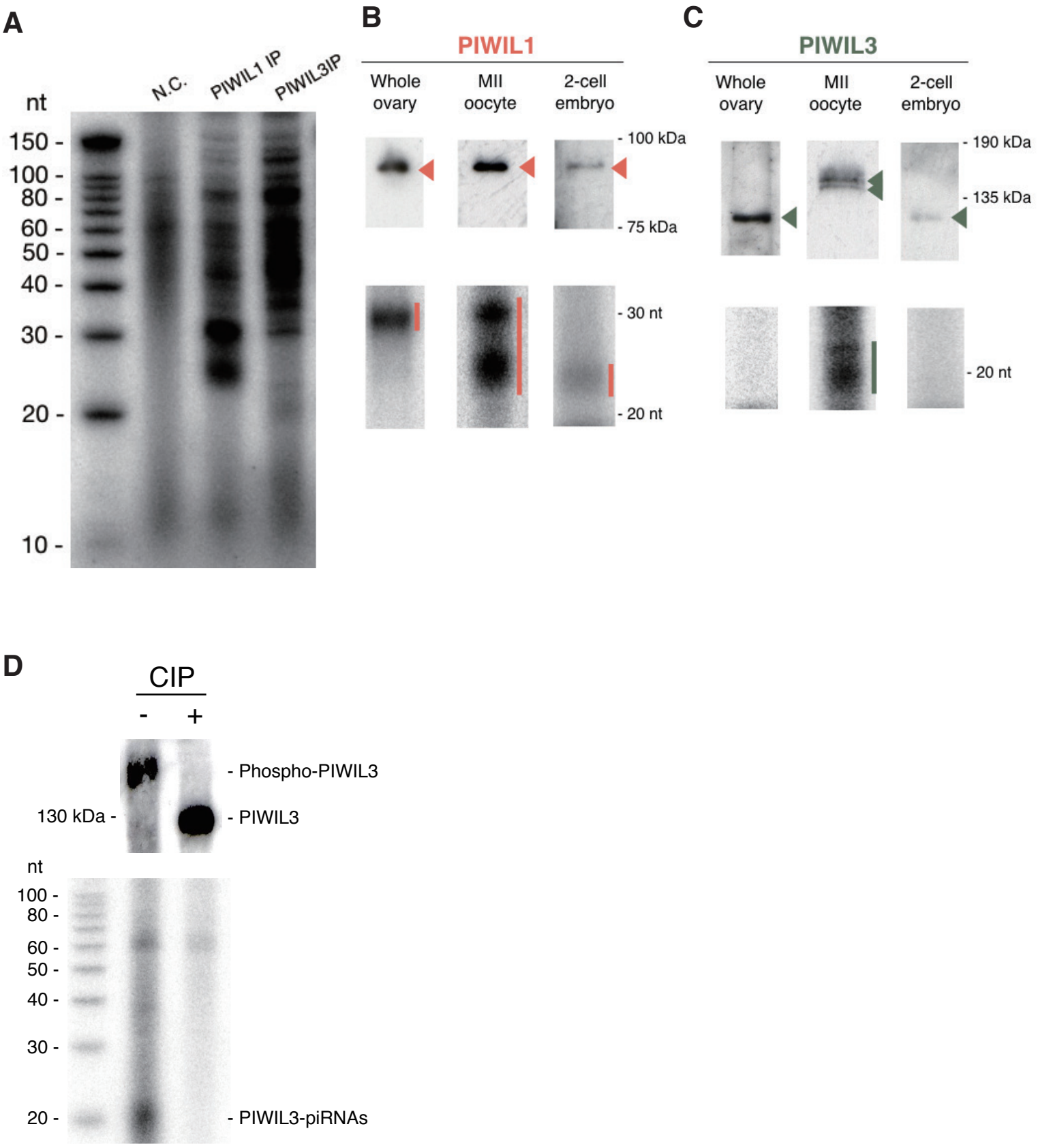

Figure 3

A

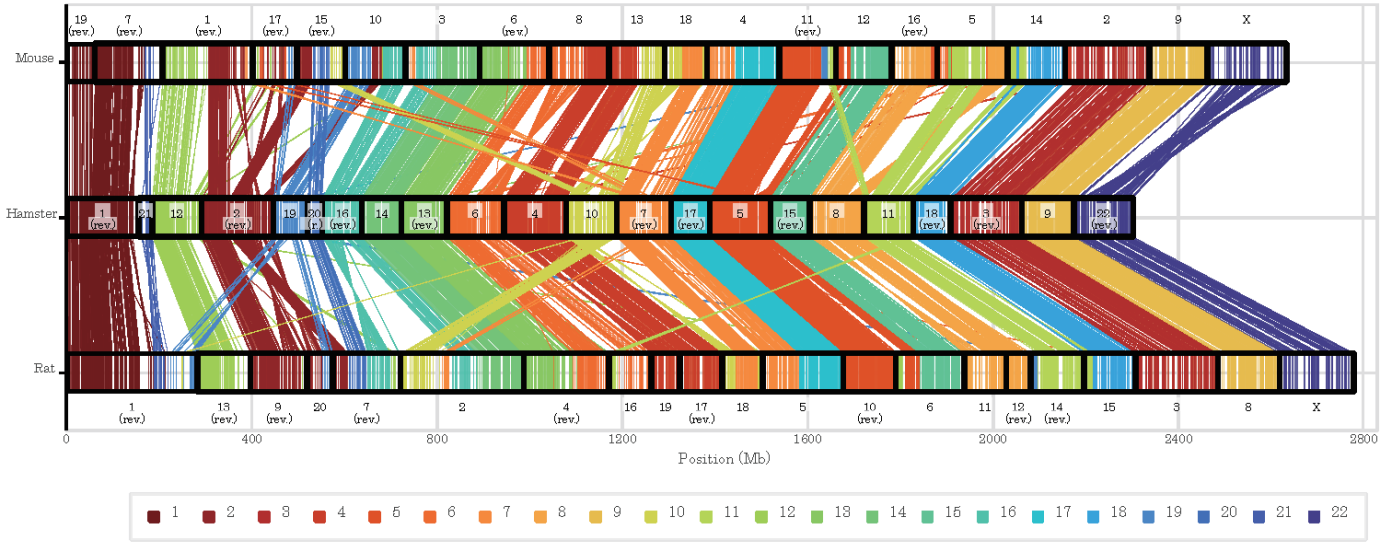

B

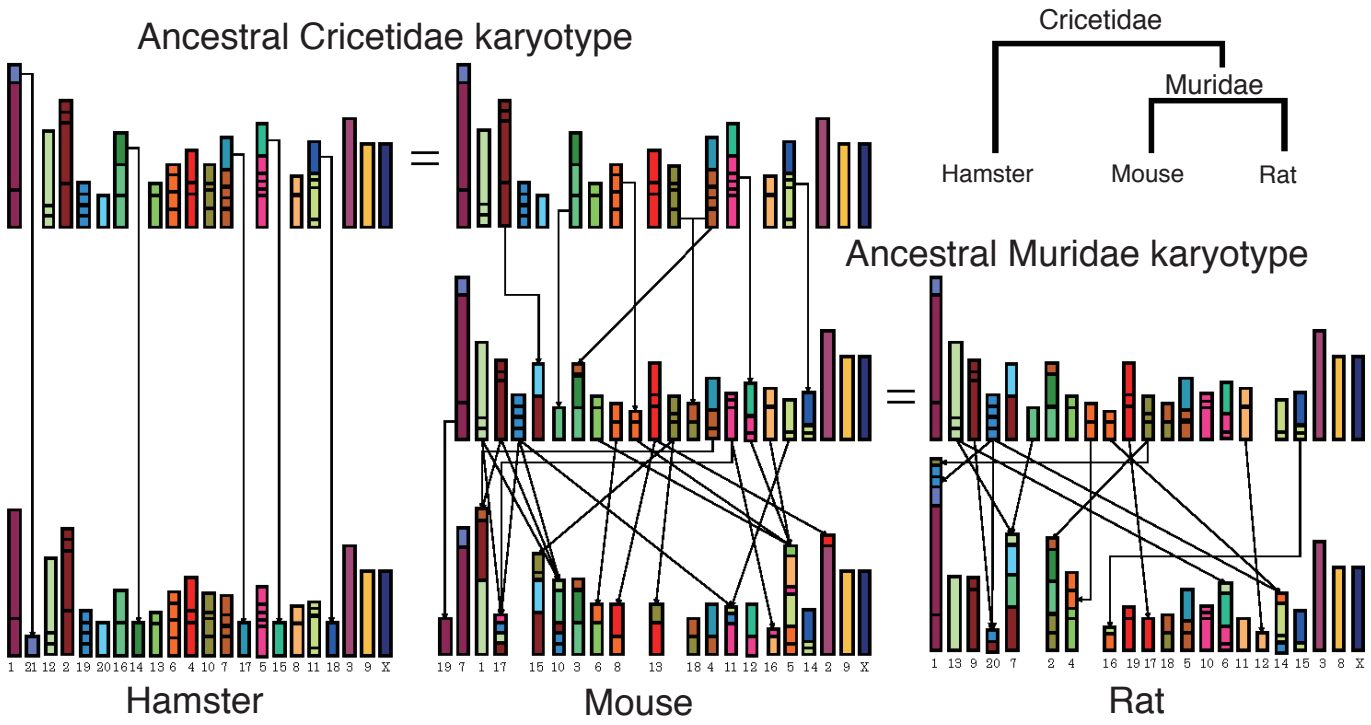

Figure 4

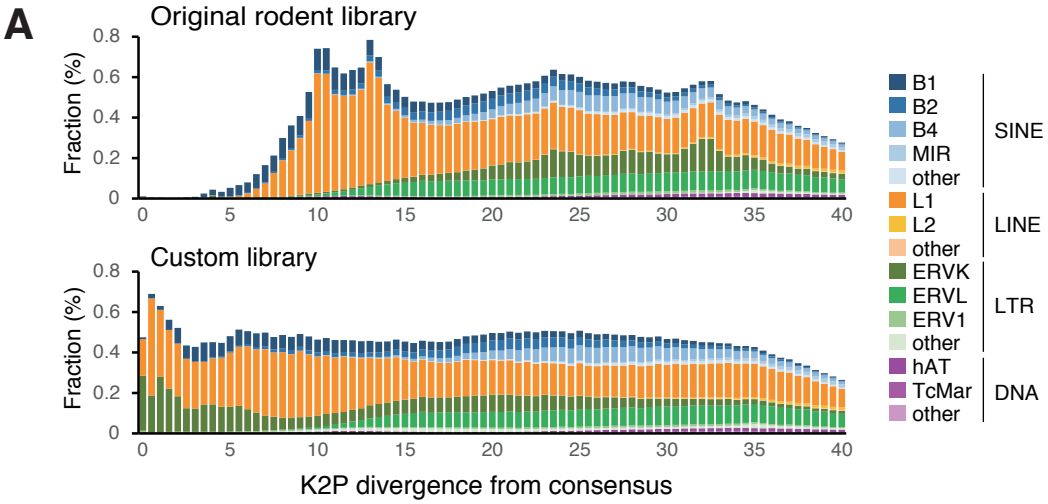

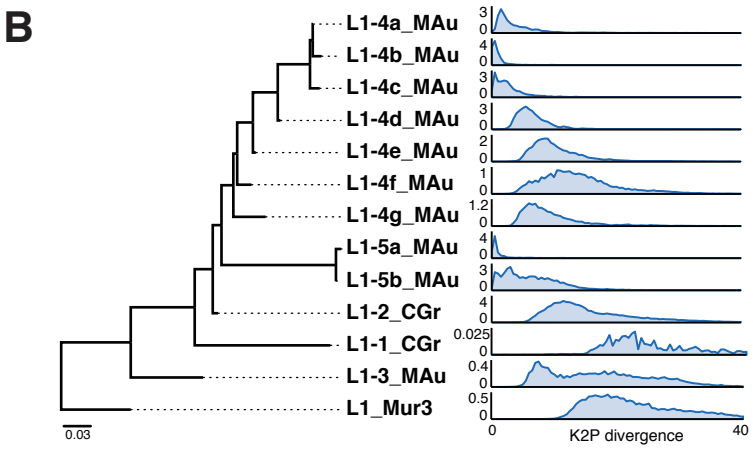

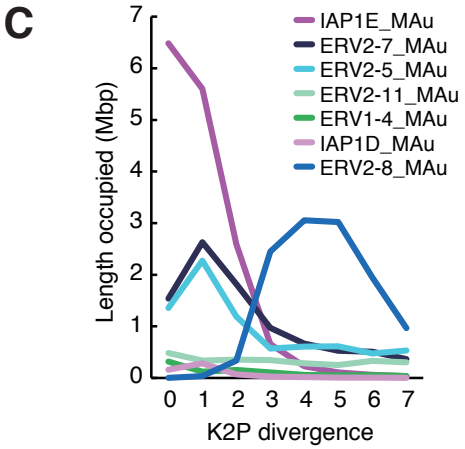

Figure 5

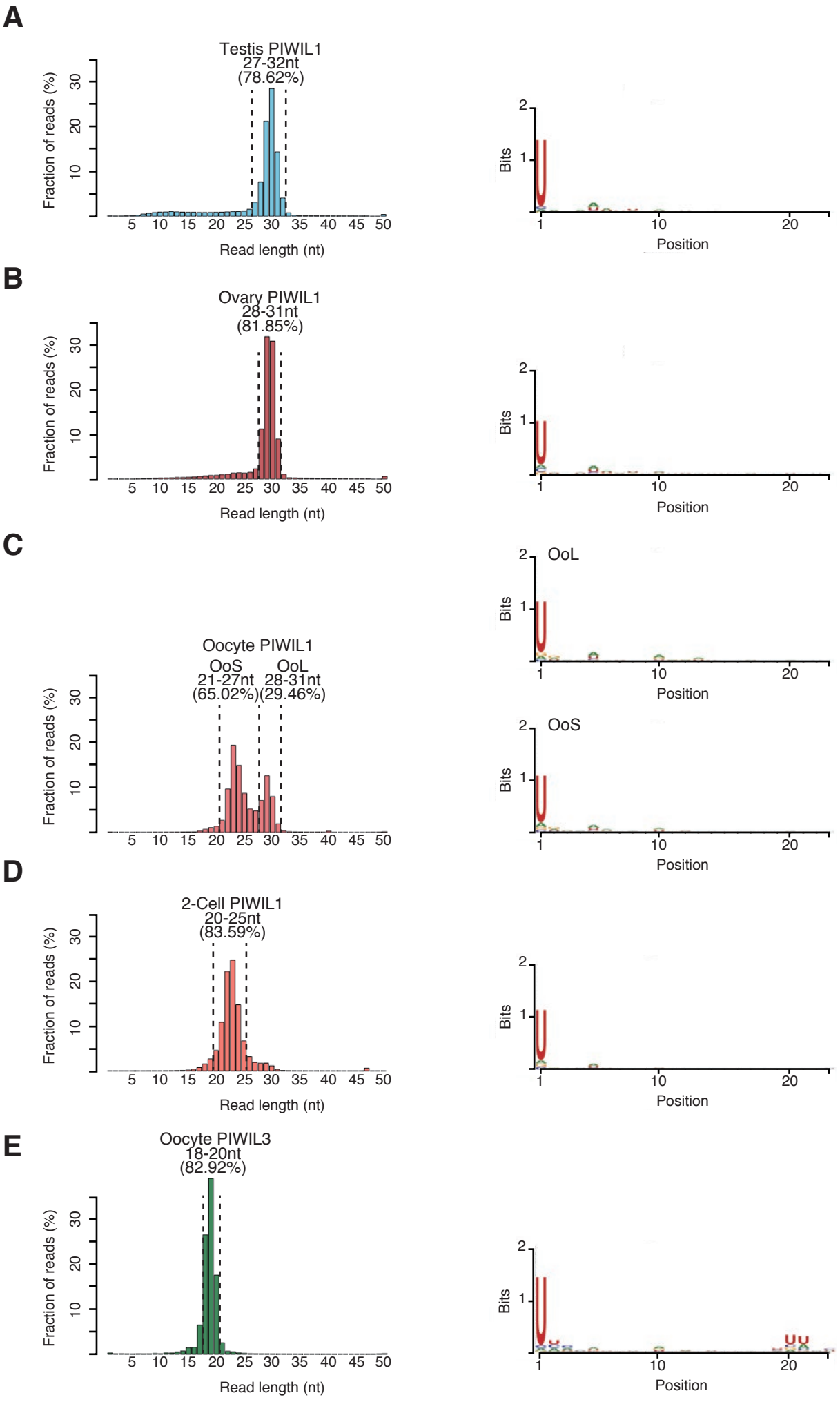

Figure 6

A

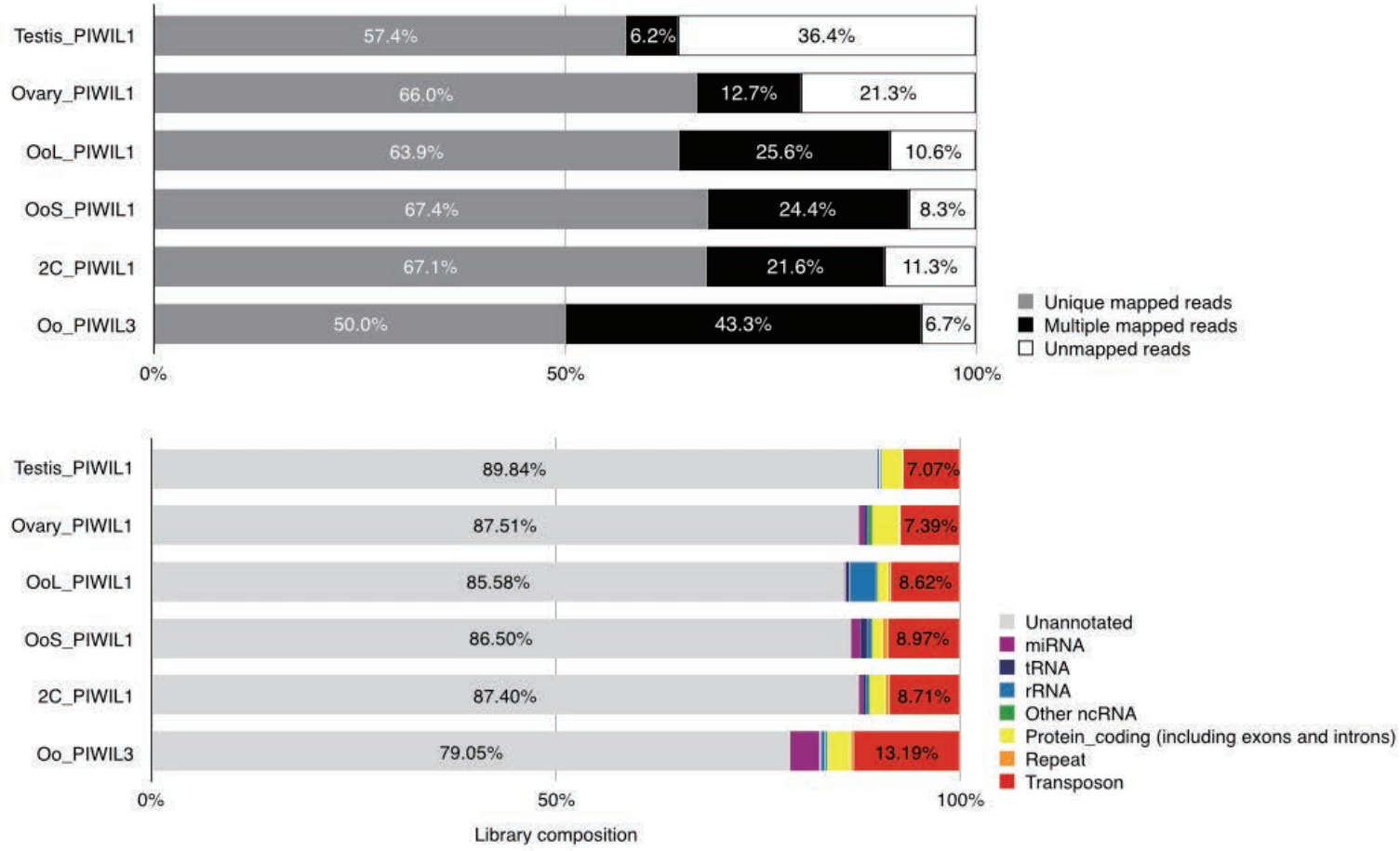

B

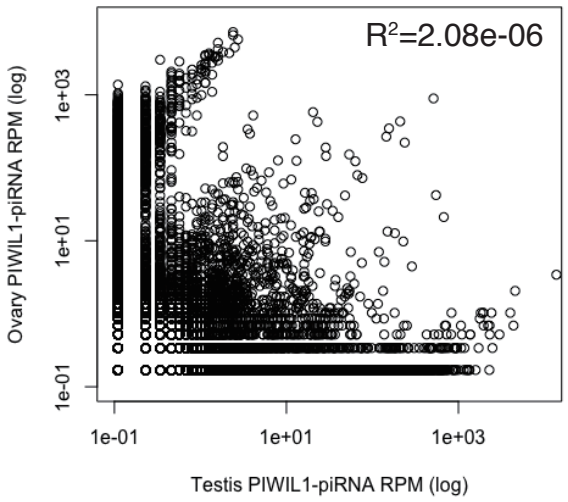

A

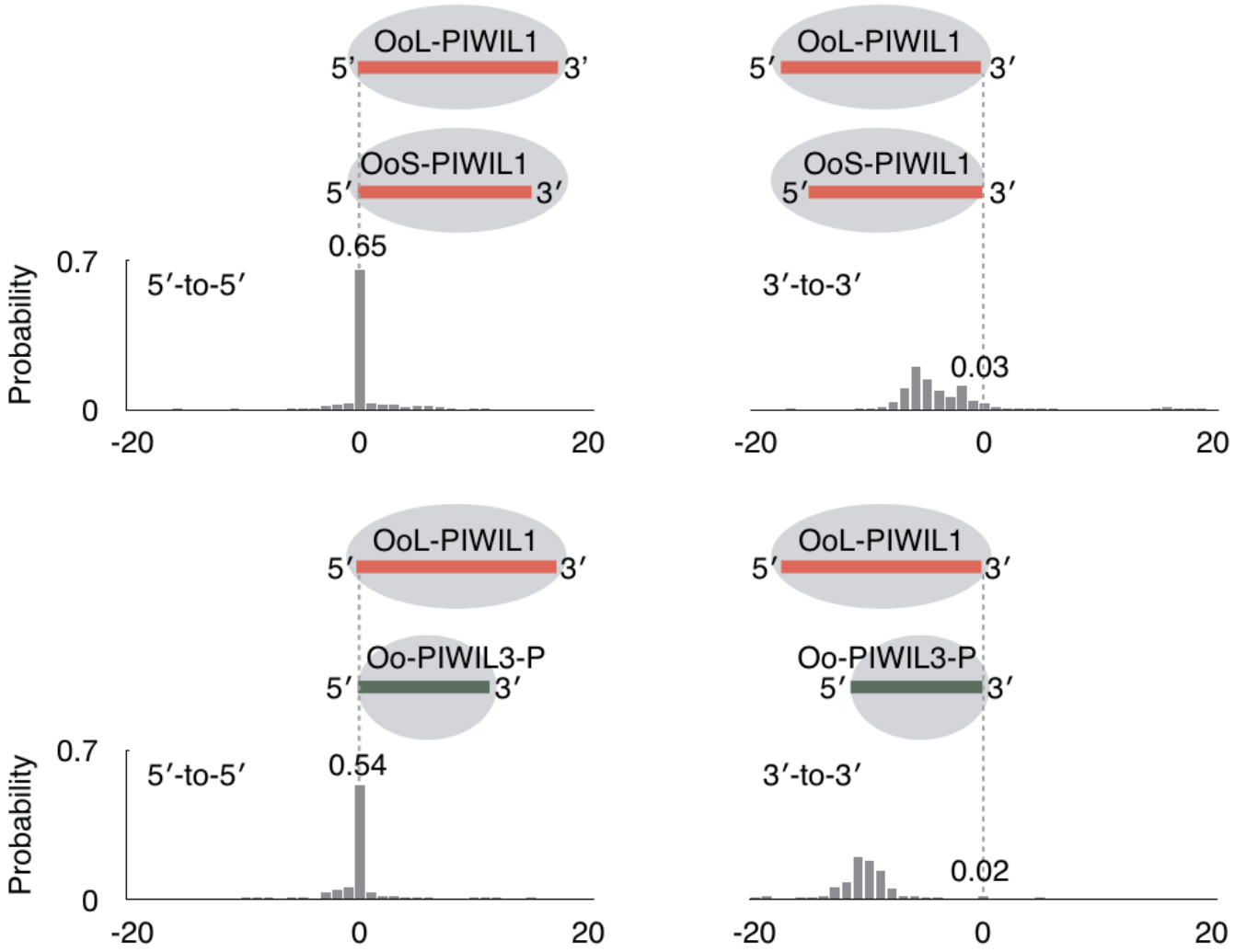

B

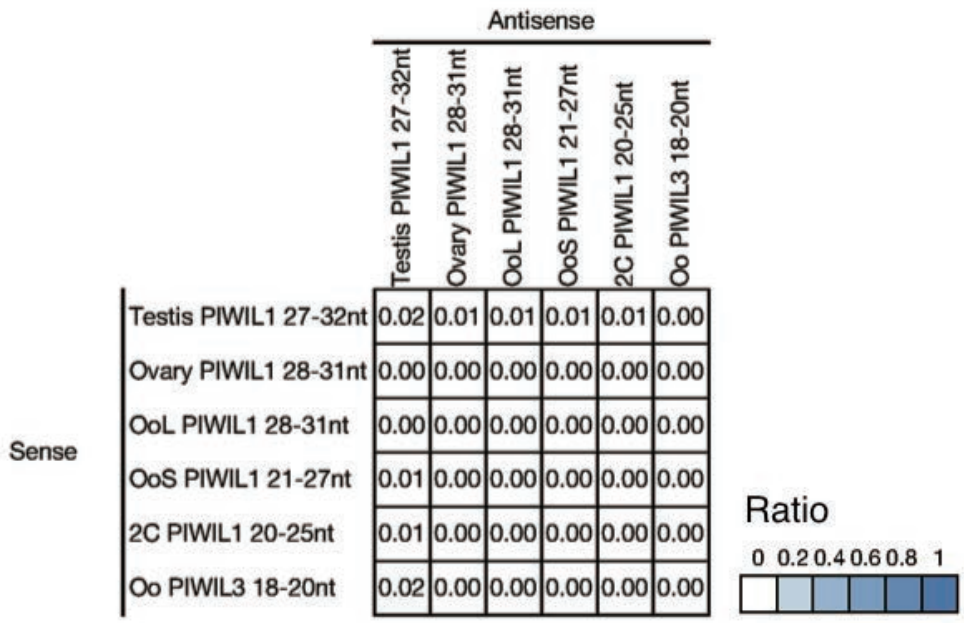

Figure 8

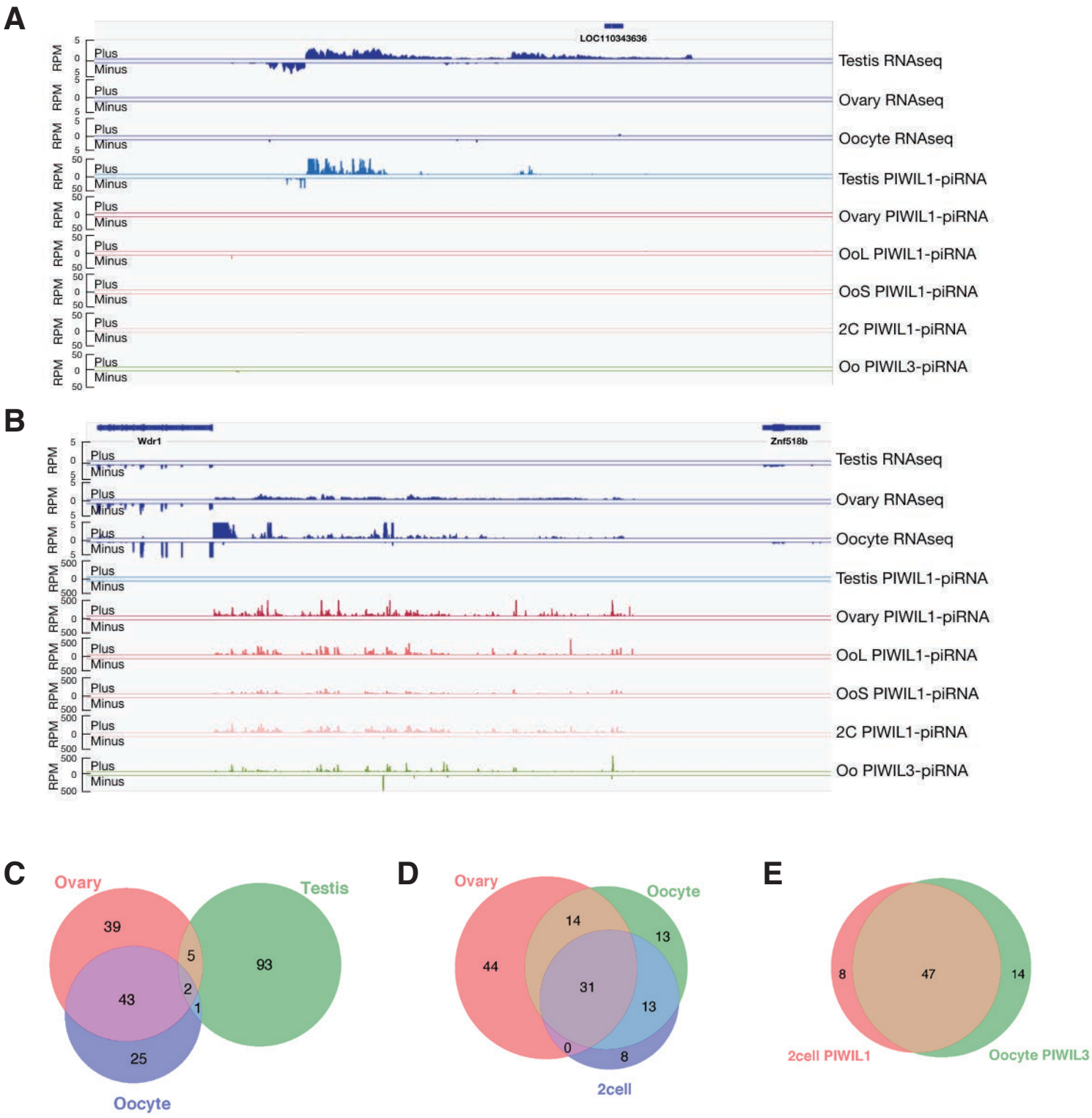

Table 1

	Ensembl Reference (MesAur1.0)		DNA Zoo (Hi-C, MesAur1.0_HiC)		Our Draft Genome	
Number of scaffolds	21,484		22		22	
Total Bases	**2,504,925,039**		**2,351,684,983**		**2,302,785,321**	
Max length	79,790,405		158,839,776		155,812,073	
Min length	1,000		29,446,437		29,820,714	
Average length	116,595		106,894,772		104,672,060	
N10	30,845,043	5	158,364,997	2	155,489,353	2
N20	24,332,566	15	157,194,130	3	153,247,738	3
N30	19,995,379	26	133,100,194	5	130,365,707	5
N40	16,574,428	39	124,260,332	7	122,808,942	7
N50	**12,753,307**	57	**119,733,378**	9	**116,281,491**	9
N60	10,749,540	79	111,148,667	11	108,846,491	11
N70	8,492,120	105	107,481,000	13	105,528,230	13
N80	5,360,393	141	87,854,995	16	85,318,168	16
N90	2,084,661	212	85,557,910	18	83,767,106	18
N99	3,663	9,798	29,446,437	22	29,820,714	22
Number of gaps	216,216		199,141		594	
Total Bases of gaps	**428,748,785**	**17%**	**367,776,424**	**16%**	**5,784,938**	**0.25%**
Max length of gaps	43,810		43,172		48,182	
Average length of gaps	1,983		1,847		9,739	
Number of unanchored contigs			21,762		3,775	
Total bases			141,734,268		234,152,039	
BUSCO complete			3,671 / 4,104	89.4%	3,991 / 4,104	97.2%
BUSCO fragmented			3,722 / 4,104	90.7%	4,028 / 4,104	98.1%
MesAur1.0_HiC identity (%)						99.86%

Class	Clade/Superfamily	Hamster	Mouse	Rat
SINE	B1	3.30	2.32	1.56
	B2	1.96	2.16	2.10
	B4	2.60	2.13	2.12
	ID	0.34	0.17	0.72
	MIR	0.72	0.56	0.53
	other SINE	0.24	0.01	0.01
LINE	L1	16.22	19.75	18.94
	L2	0.57	0.43	0.41
	other LINE	0.13	0.10	0.10
LTR	ERV1	0.64	0.74	0.99
	ERVK	5.02	5.02	3.81
	ERVL	5.55	5.90	5.26
	other LTR	0.87	0.44	0.04
DNA	hAT	0.98	0.82	0.81
	TcMar	0.27	0.22	0.21
	other DNA	0.03	0.03	0.03
Other TE		0.38	0.29	0.27
Unknown TE		0.09	0.12	0.79
Total		**39.90**	**41.22**	**38.70**

Figure S1

Ishino et al.

A

Gene name	Drosophila homolog	Expression level (TPM)		
		Testis	Ovary	Oocyte
Piwil1	Aub	24.24	4.63	20.49
Piwil2	Ago3	14.07	0.00	2.97
Piwil3	-	0.00	16.28	14.60
Piwil4	-	2.55	0.00	0.00
GASZ (Asz1)	GasZ	6.45	2.29	4.20
GTSF1	Asterix/Gtsf1	54.03	2.26	11.10
Henmt1	Hen1	3.25	2.24	18.50
Mael	Mealstrom	389.23	14.05	109.81
MitoPLD (Pld6)	Zucchini	3.83	0.18	12.38
Mov10l1	Armitage	41.34	0.00	12.79
MVH (Ddx4)	Vasa	365.43	27.26	1163.69
Pnldc1	- (Trimmer in silkworm)	12.44	4.94	2.51
SETDB1	Eggless	39.88	26.75	459.95
TDRD1	Vreteno	158.01	19.77	455.42
TDRD2 (Tdrkh)	Papi	12.32	1.42	10.38
TDRD4 (Rnf17)	Qin/Kumo	88.61	5.94	36.19
TDRD5	Tejas	92.64	4.57	3.94
TDRD6	Tudor	15.56	0.00	0.00
TDRD7	Tapas	79.80	10.18	81.32
TDRD9	SpnE	49.70	1.43	0.00
TDRD12	BoYb	0.64	0.54	0.54

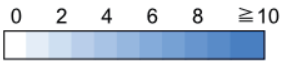

B

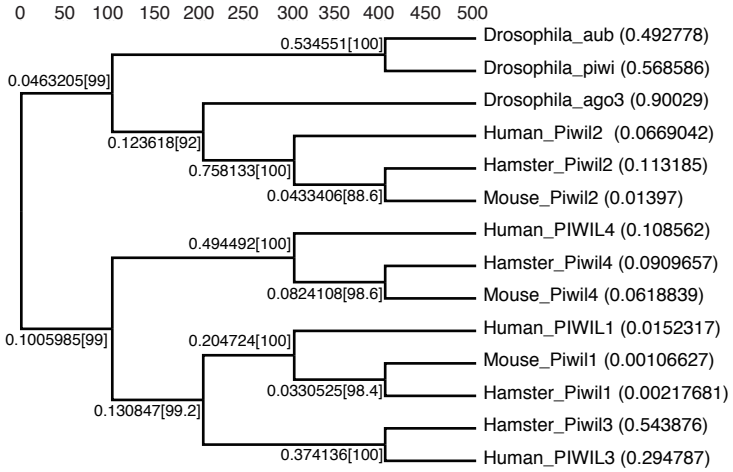

C

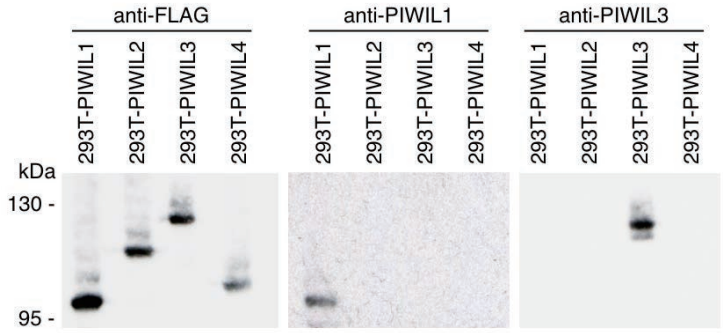

Figure S2

Ishino et al.

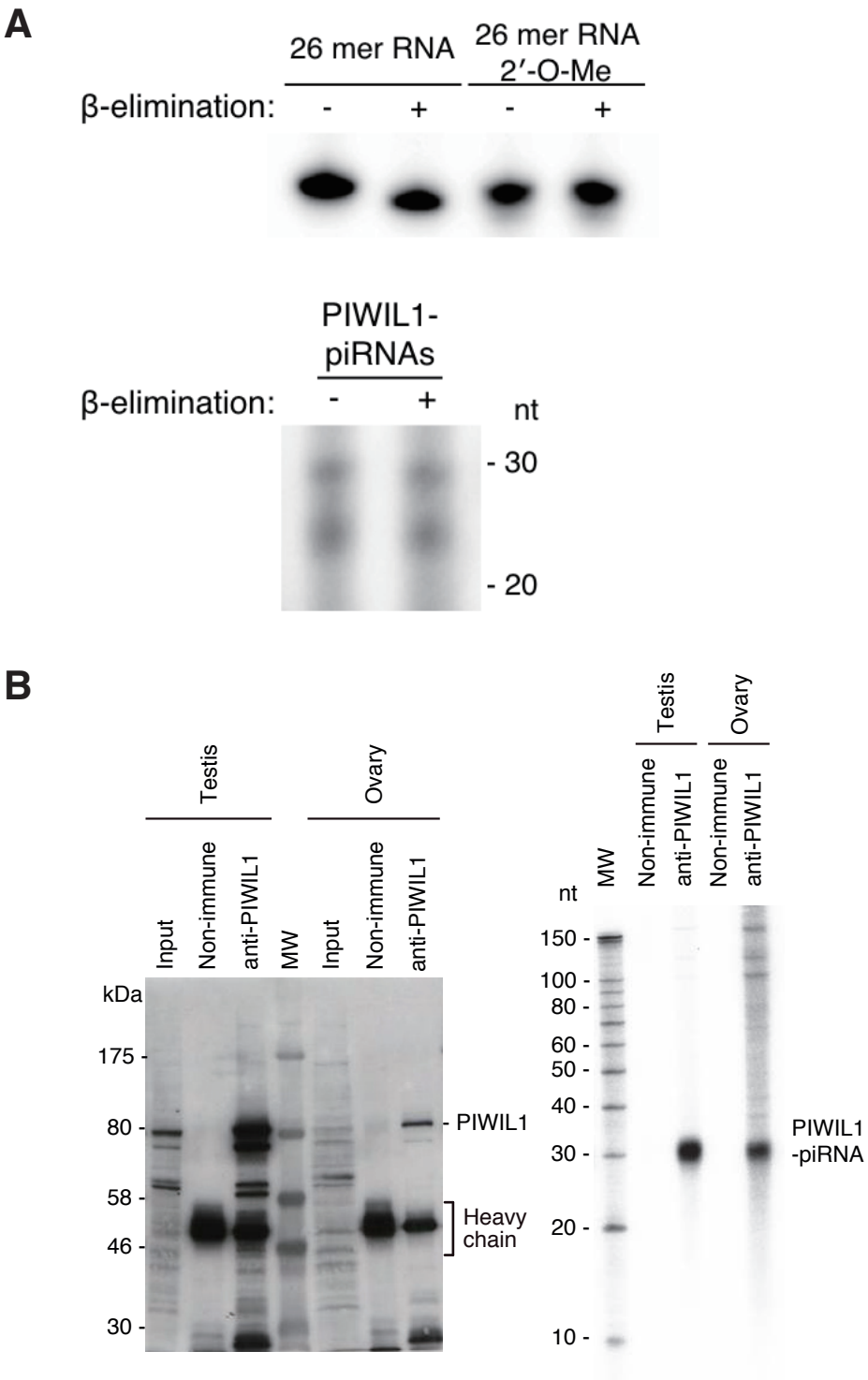

Figure S3

Ishino et al.

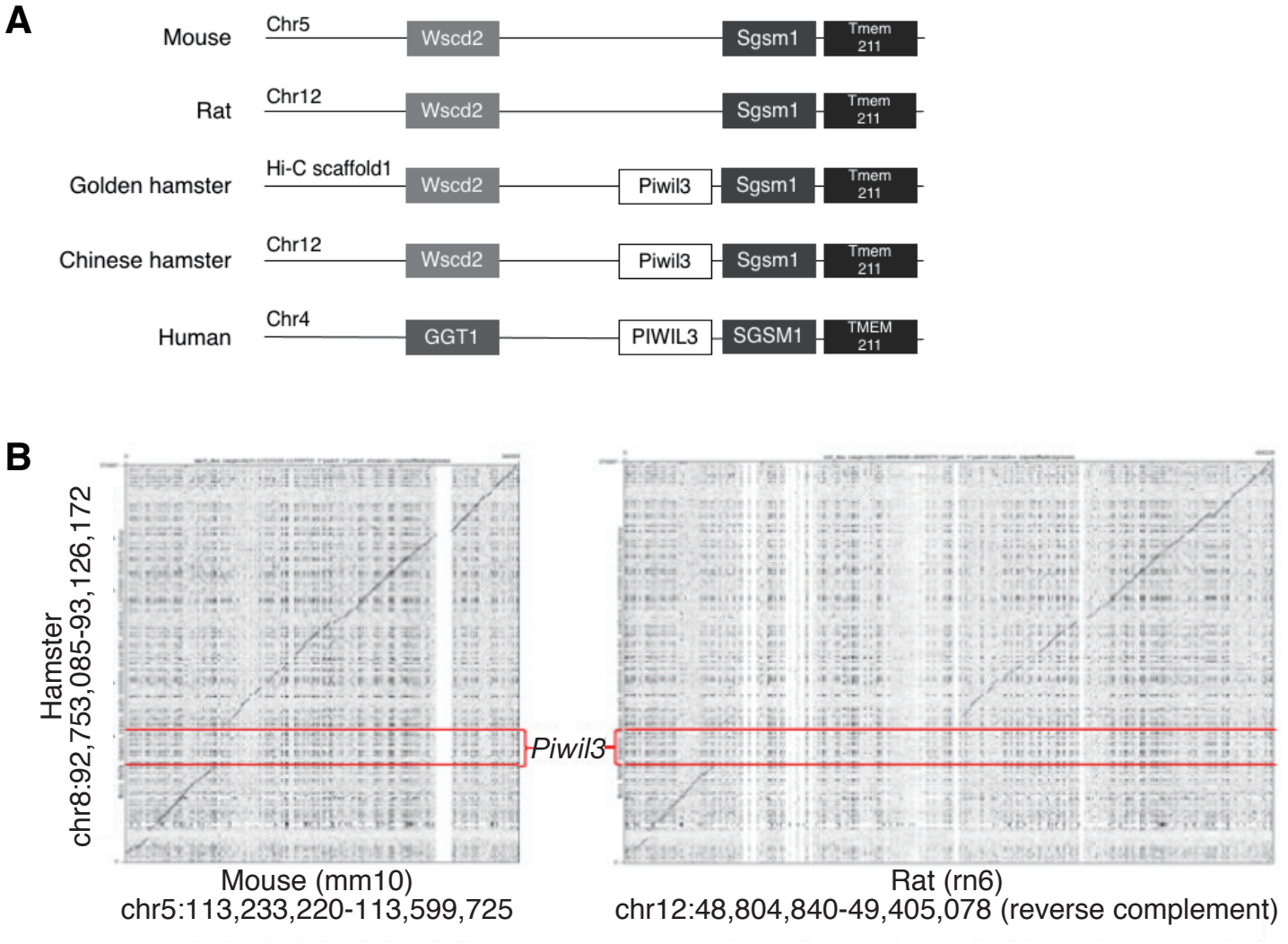

Figure S4

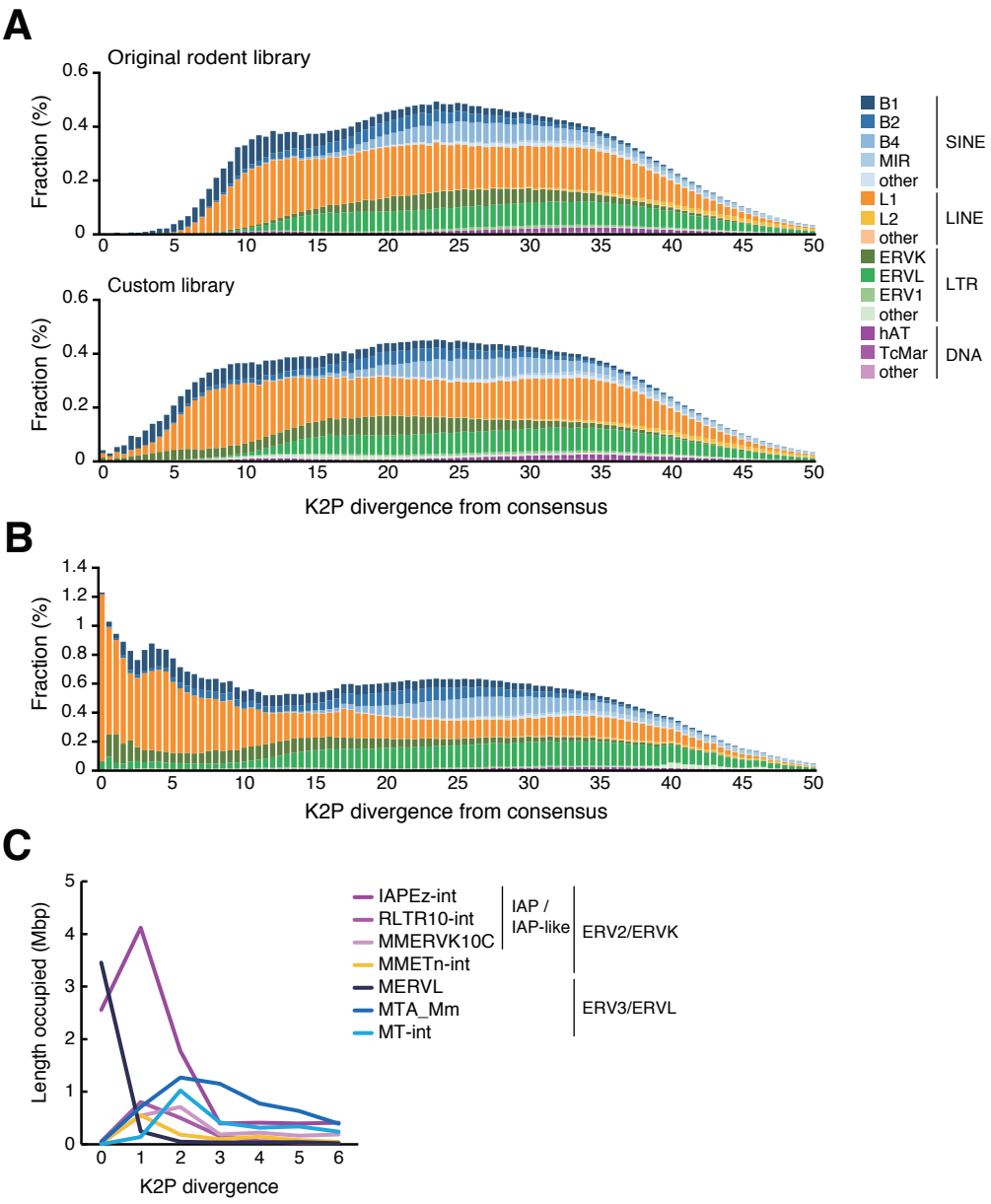

Figure S5

Ishino et al.

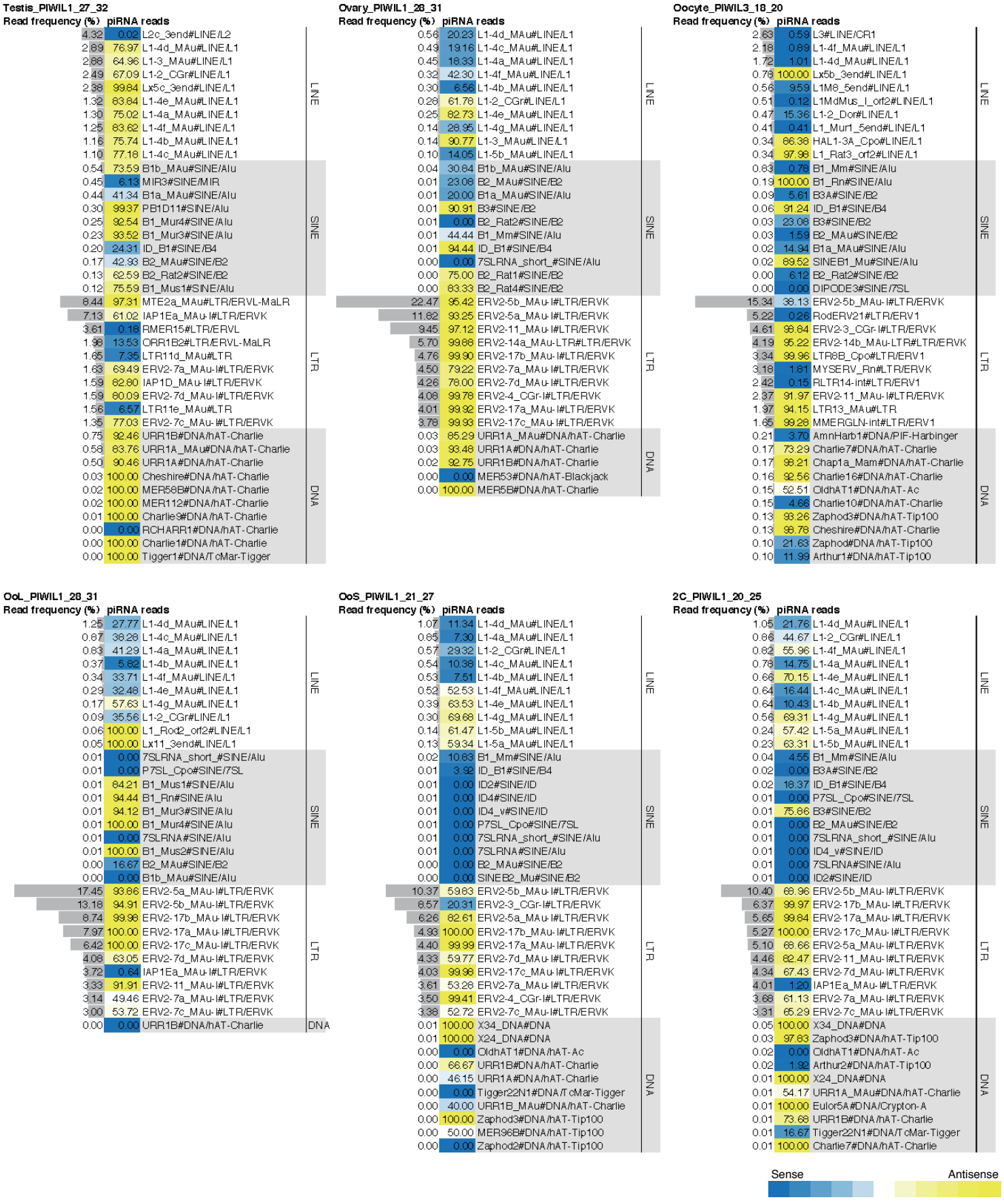

A

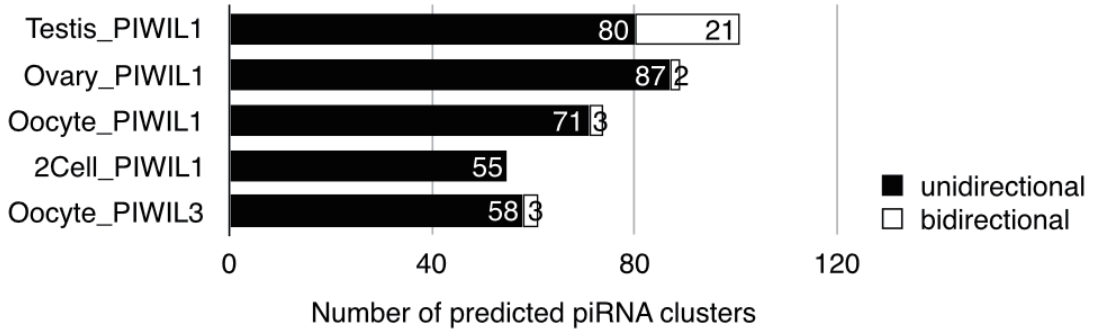

B

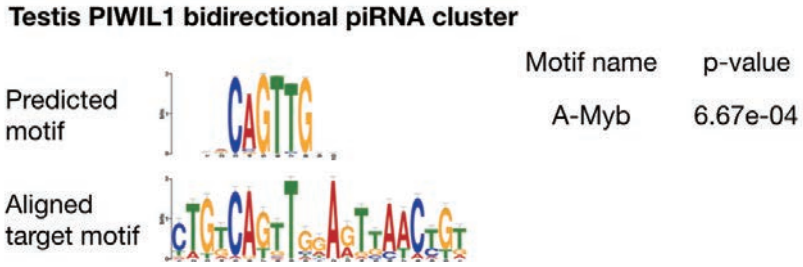

C

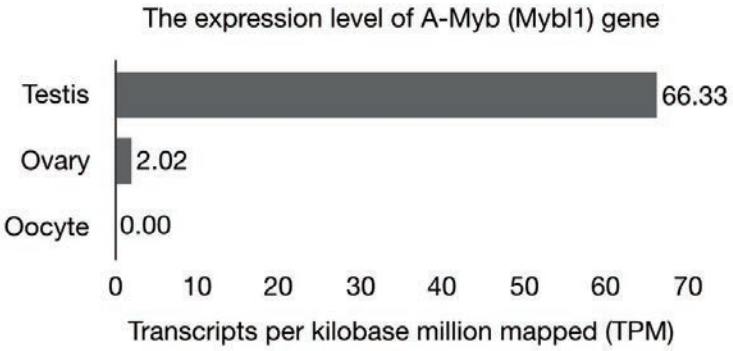

Figure S7

Ishino et al.

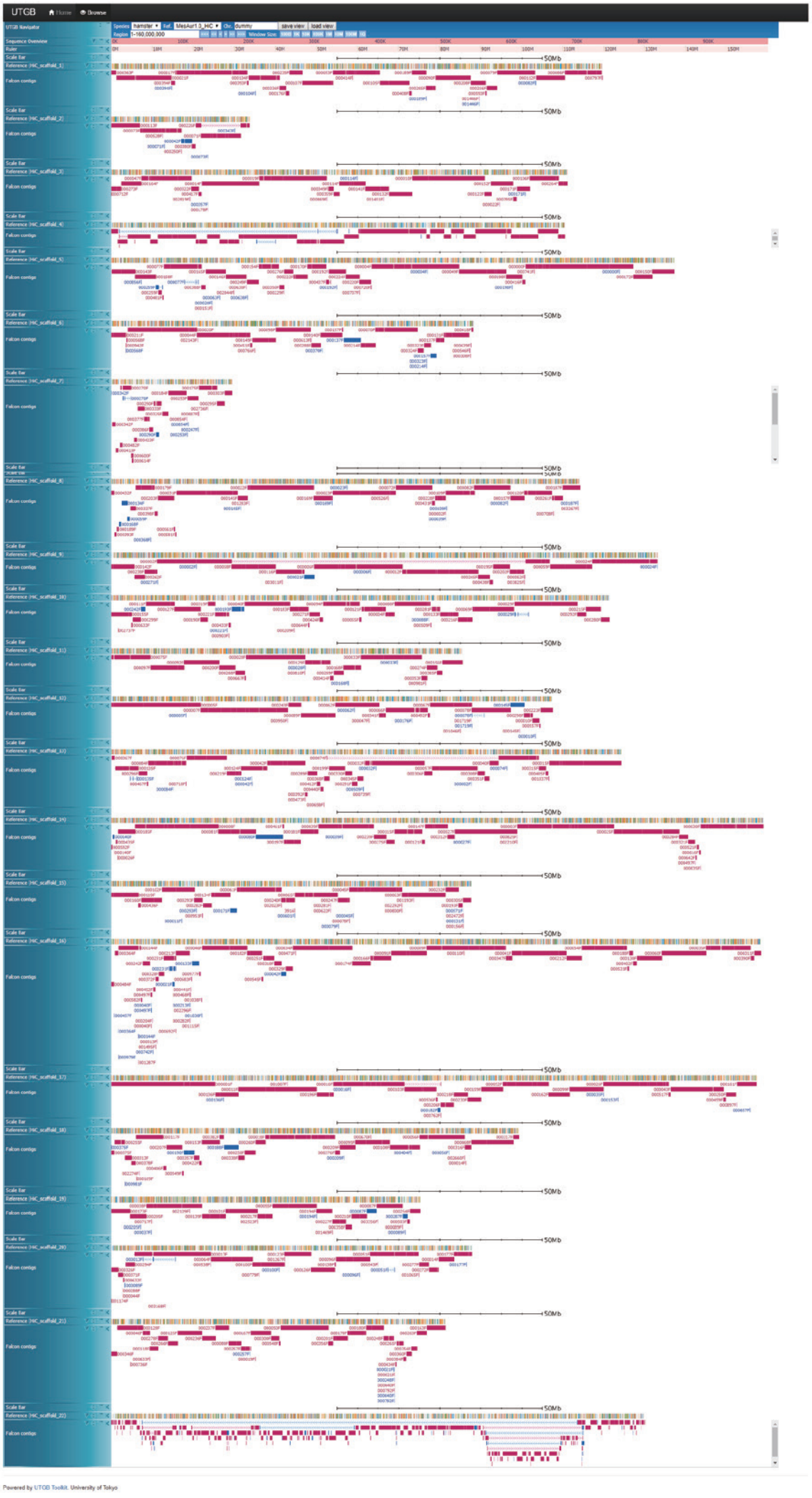

Figure S8

Ishino et al.

A: all chromosomes	
hamster	All
Mus_Musculus	All
Rattus_norvegicus	All

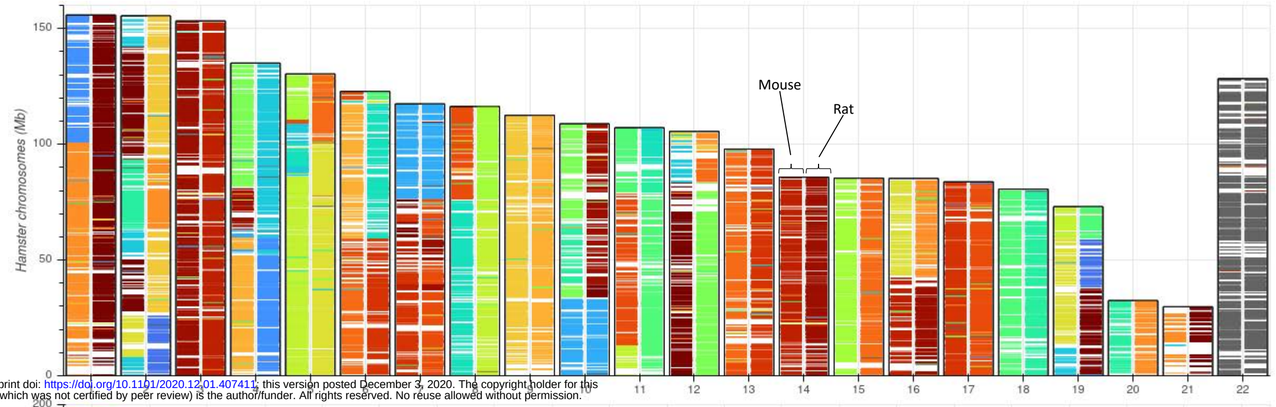

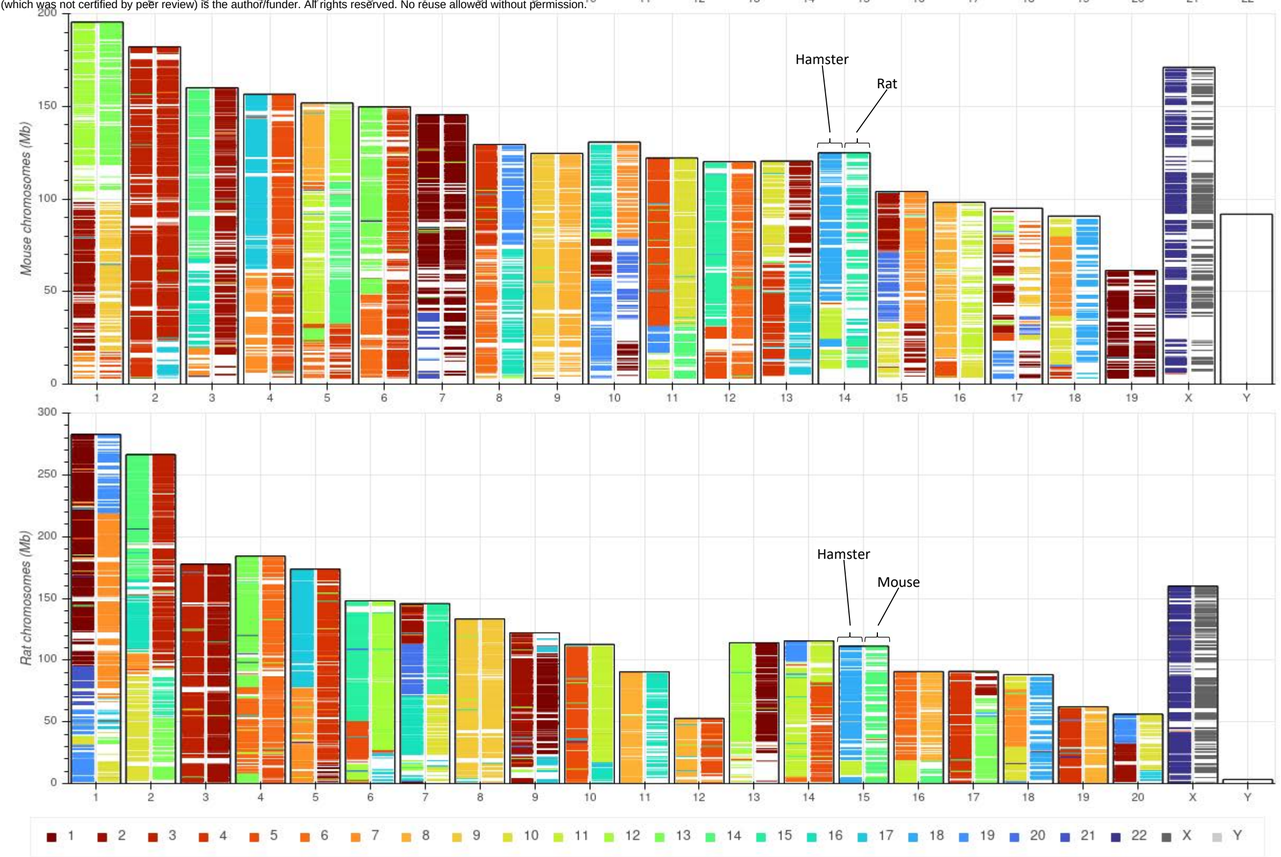

B: all chromosomes

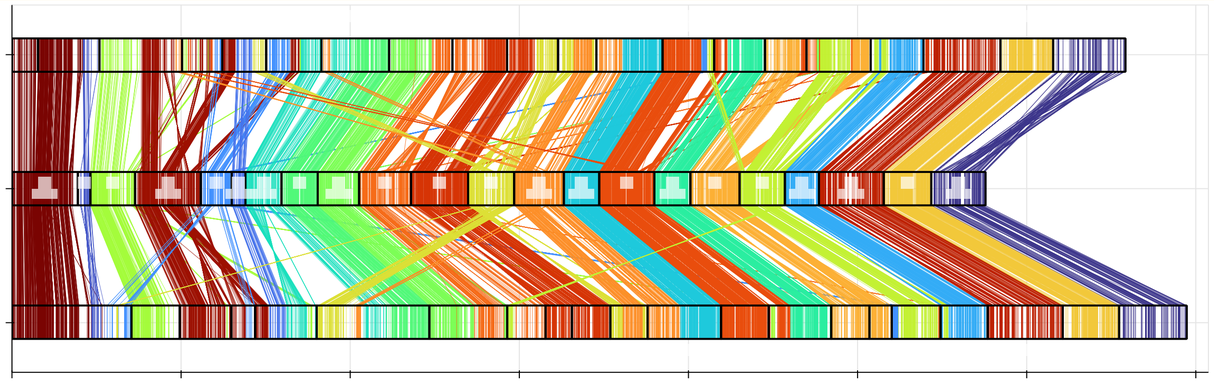

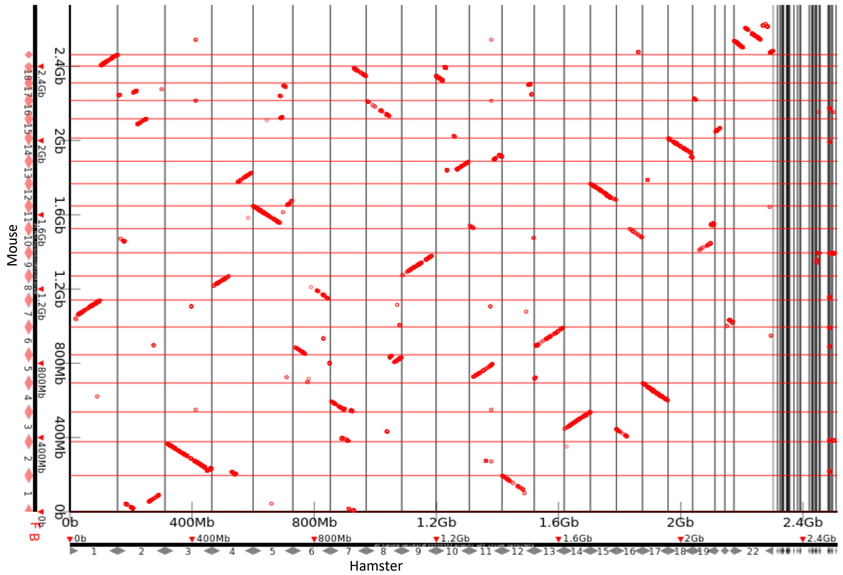

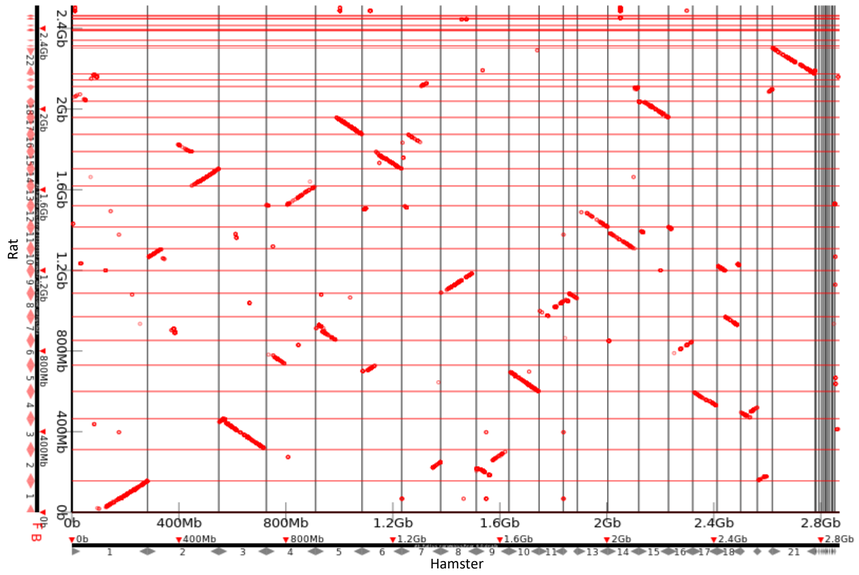

C: each chromosomes

hamster	chr1	HiC_scaffold_16
Mus_Musculus	7 & 19	
Rattus_norvegicus	1	

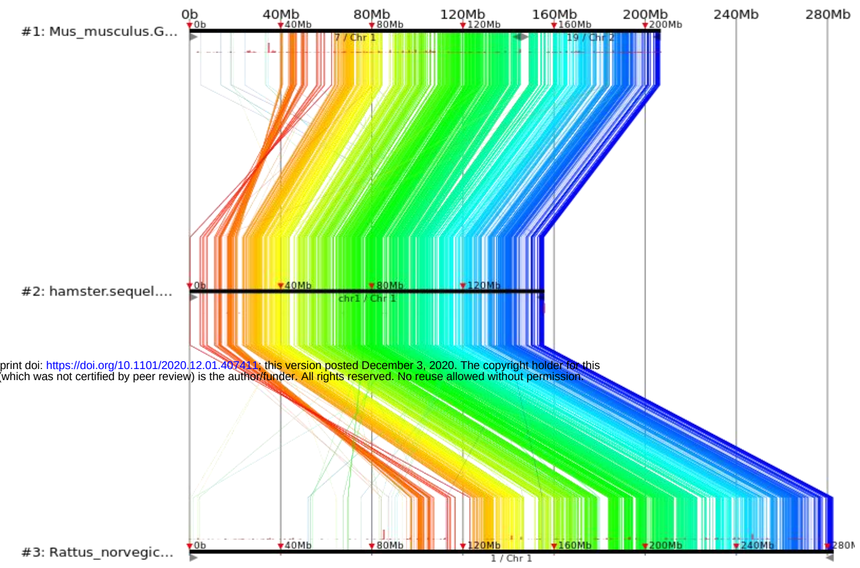

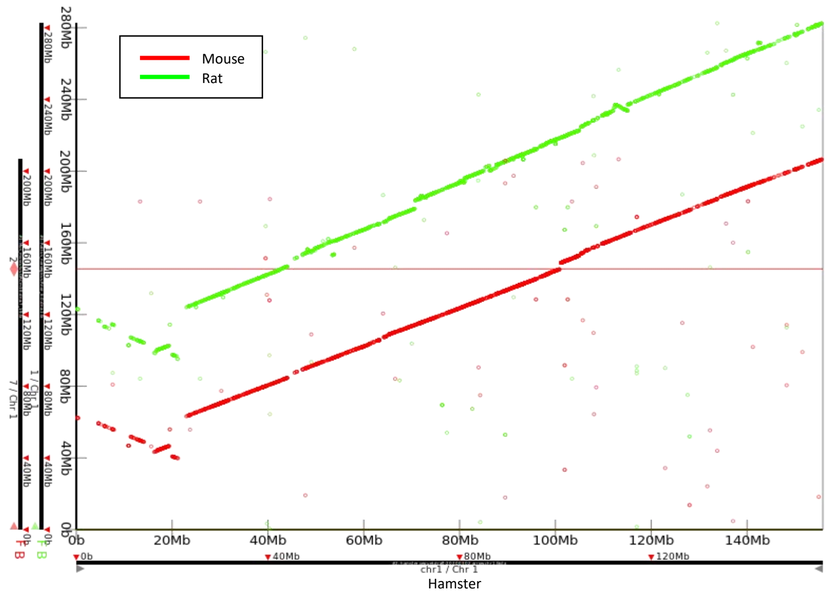

hamster	chr2	HiC_scaffold_14
Mus_Musculus	17 & 10 (rev.) & 15 & 1	
Rattus_norvegicus	20 & 7 & 9	

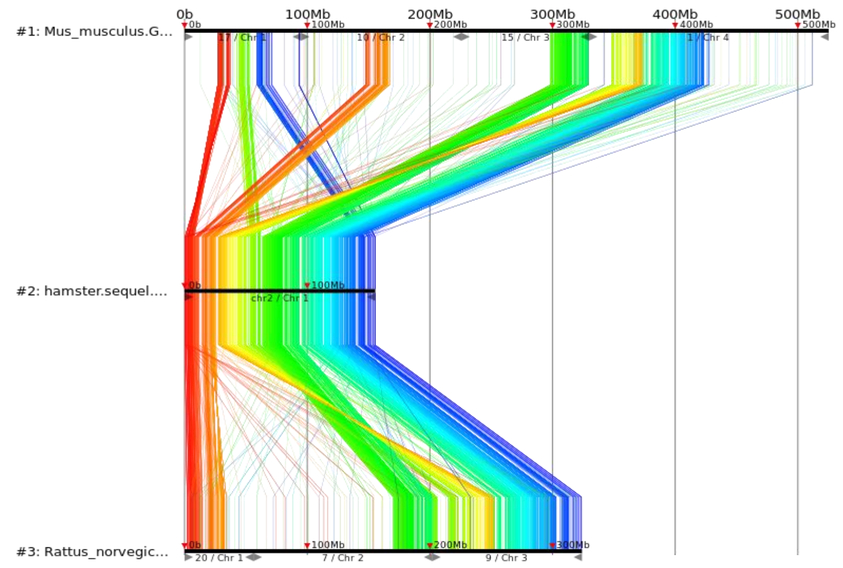

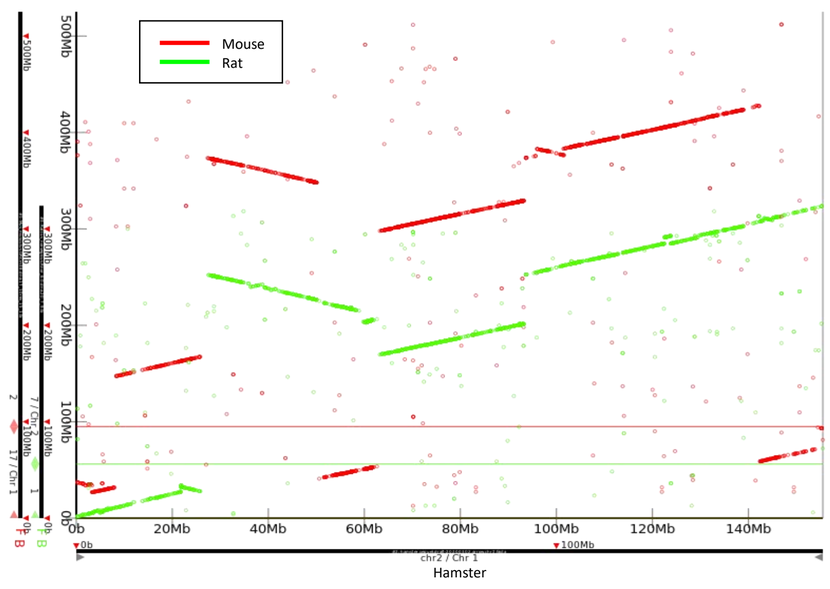

hamster	chr3	HiC_scaffold_17
Mus_Musculus	2 (rev.)	
Rattus_norvegicus	3 (rev.)	

0bp-182,113,224bp of 182,113,224bp (100.00%)

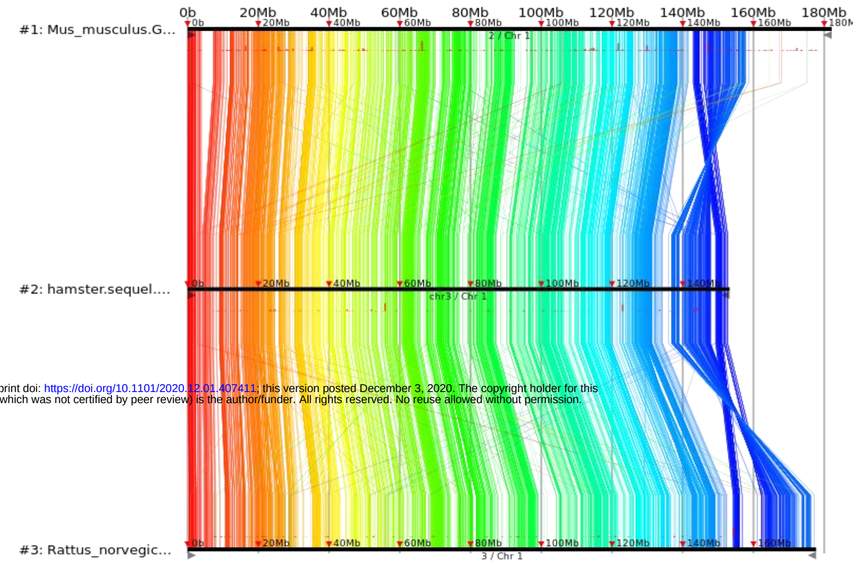

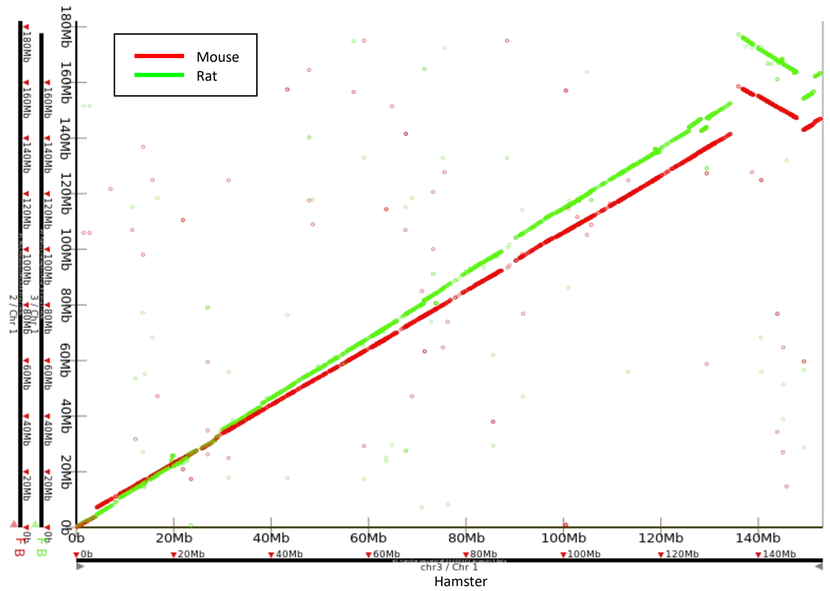

hamster	chr4	HiC_scaffold_5
Mus_Musculus	8 & 2(rev.) & 13	
Rattus_norvegicus	19 & 17 (rev.)	

0bp-431,936,096bp of 431,936,096bp (100.00%)

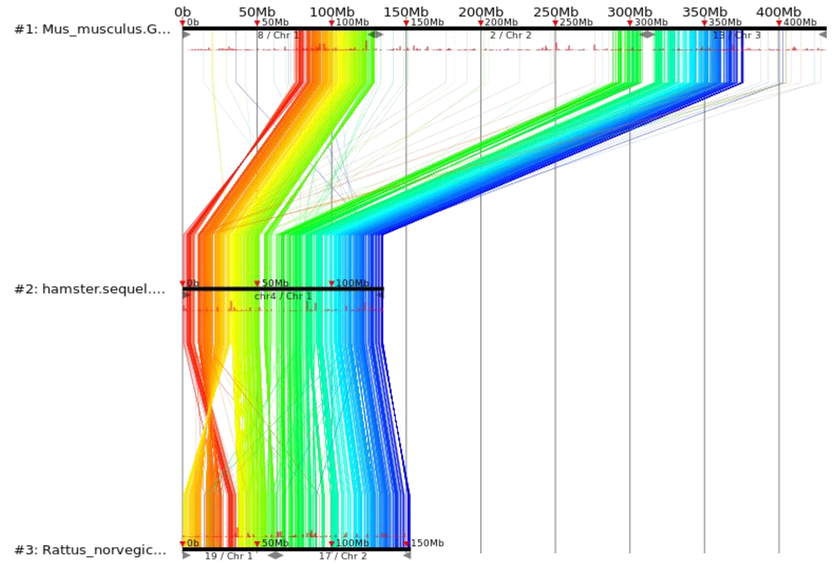

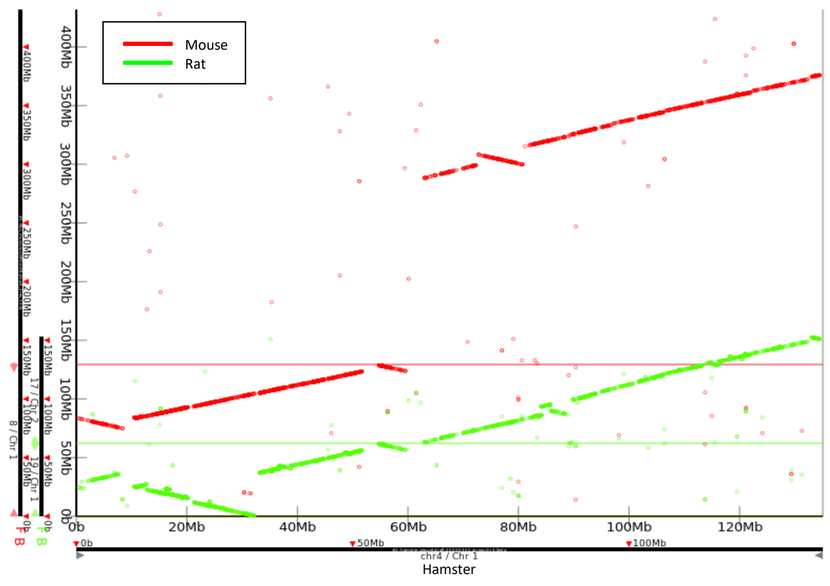

hamster	chr5	HiC_scaffold_9
Mus_Musculus	11 (rev.) & 17 & 16 & 5 (rev.) & 12	
Rattus_norvegicus	10 (rev.) & 6	

0bp-587,241,328bp of 587,241,328bp (100.00%)

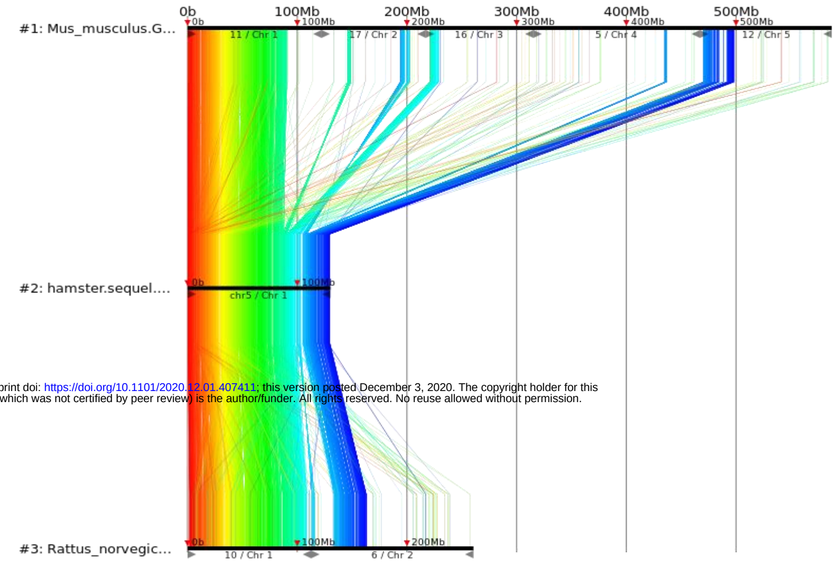

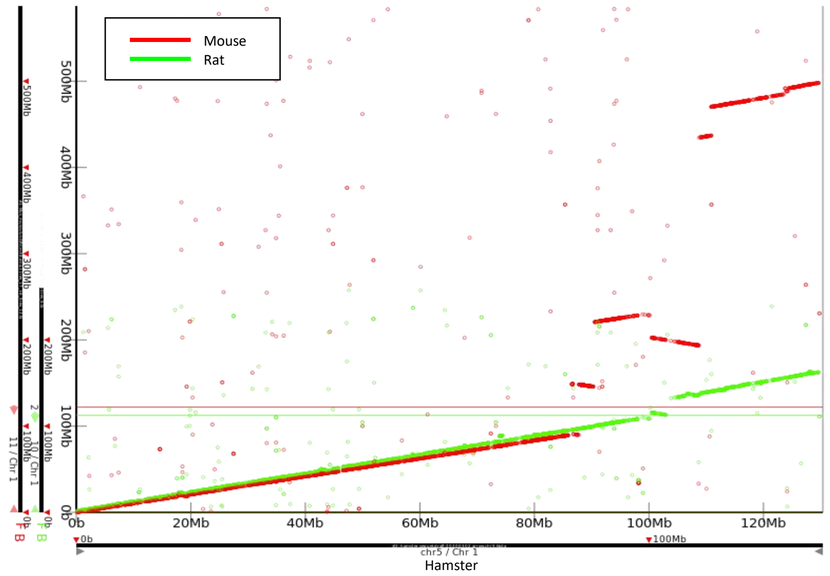

hamster	chr6	HiC_scaffold_13
Mus_Musculus	6(rev.) & 5 & 8(rev.)	
Rattus_norvegicus	4(rev.) & 16 &14(rev.)	

0bp-430,972,463bp of 430,972,463bp (100.00%)

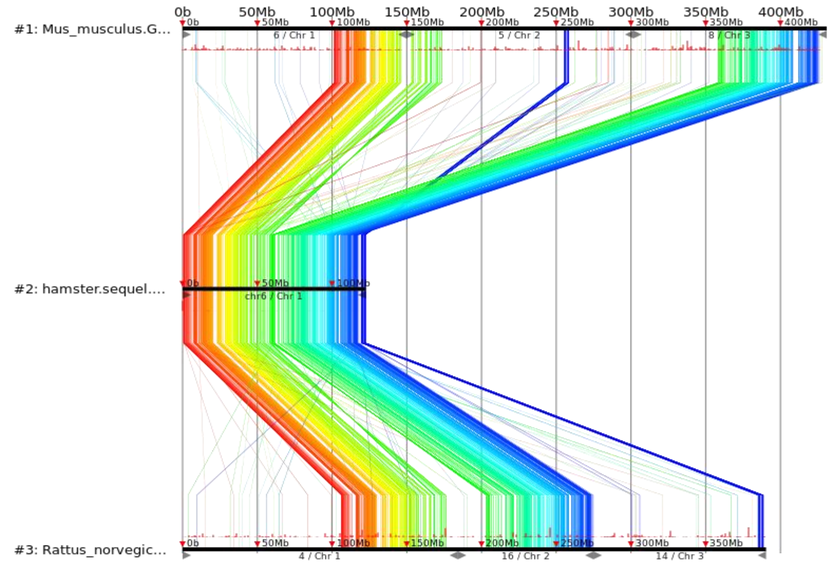

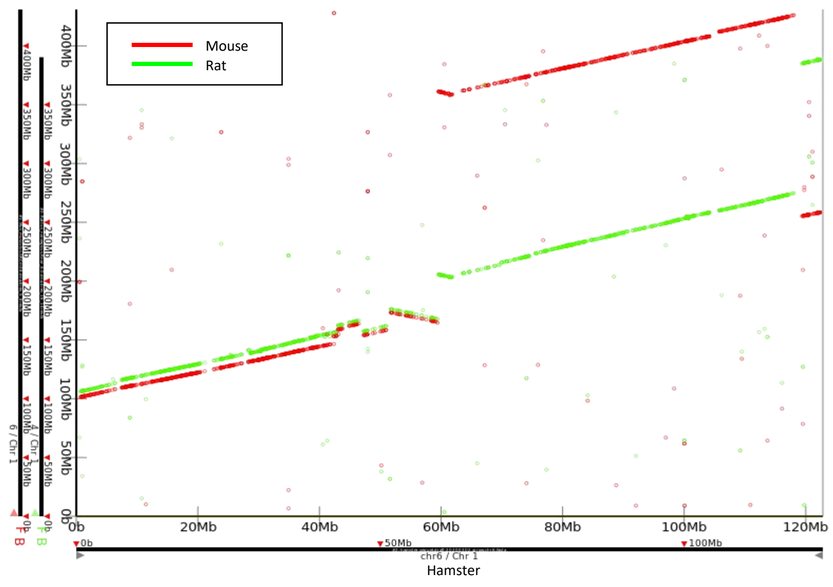

hamster	chr7	HiC_scaffold_10
Mus_Musculus	4(rev.) & 3(rev.) & 1(rev.) & 18(rev.)	
Rattus_norvegicus	5(rev.) & 2 & 18(rev.)	

0bp-602,722,436bp of 602,722,436bp (100.00%)

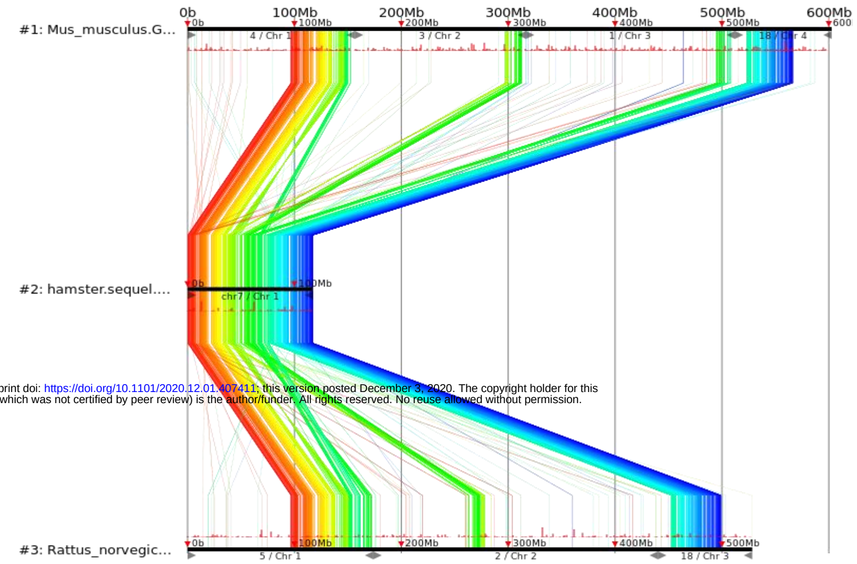

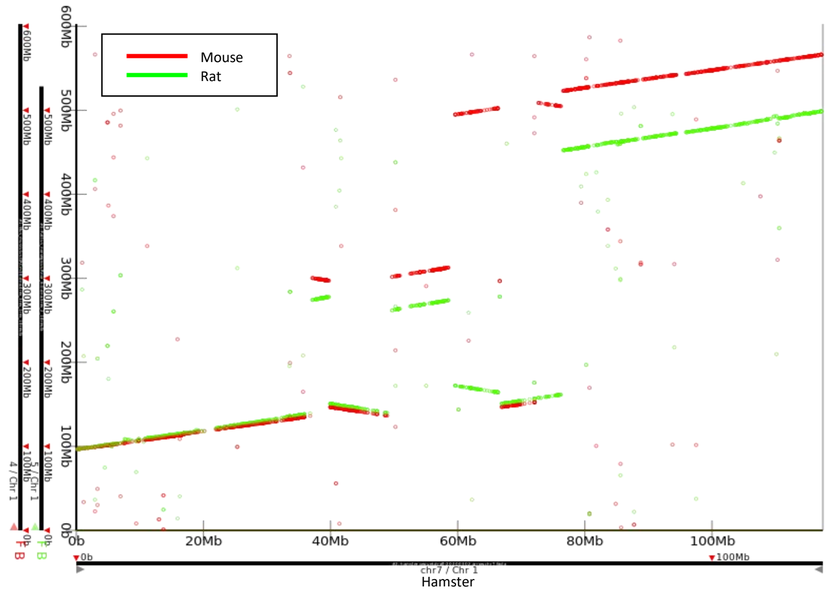

hamster	chr8	HiC_scaffold_1
Mus_Musculus	16(rev.) & 5	
Rattus_norvegicus	11 & 12(rev.)	

0bp-250,042,462bp of 250,042,462bp (100.00%)

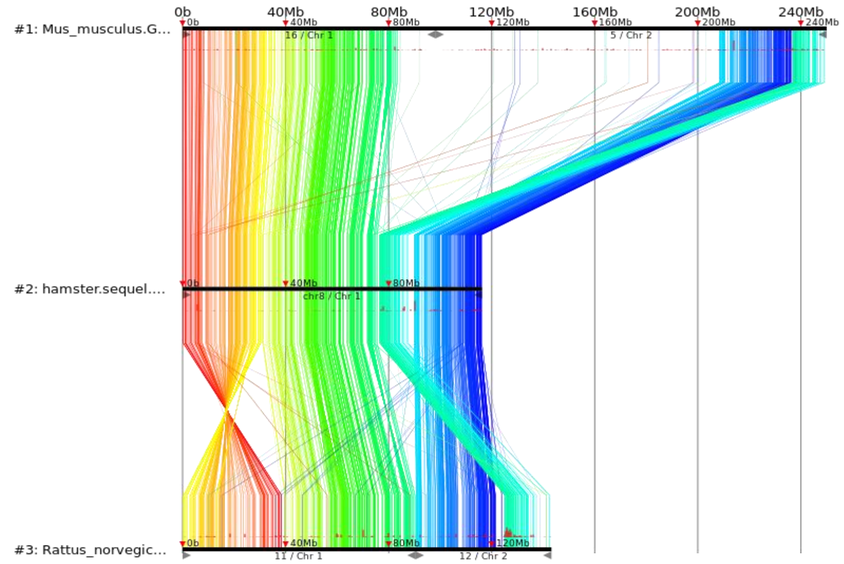

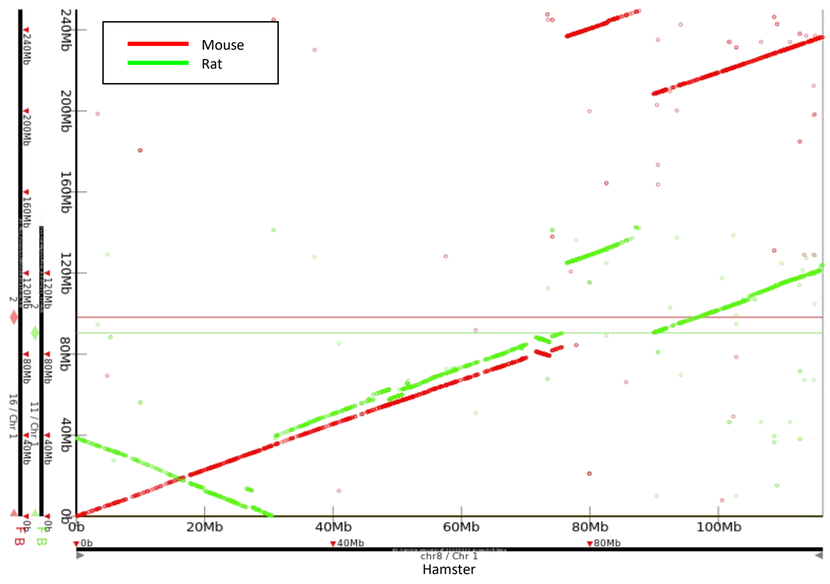

hamster	chr9	HiC_scaffold_8
Mus_Musculus	9	
Rattus_norvegicus	8	

0bp-133,307,652bp of 133,307,652bp (100.00%)

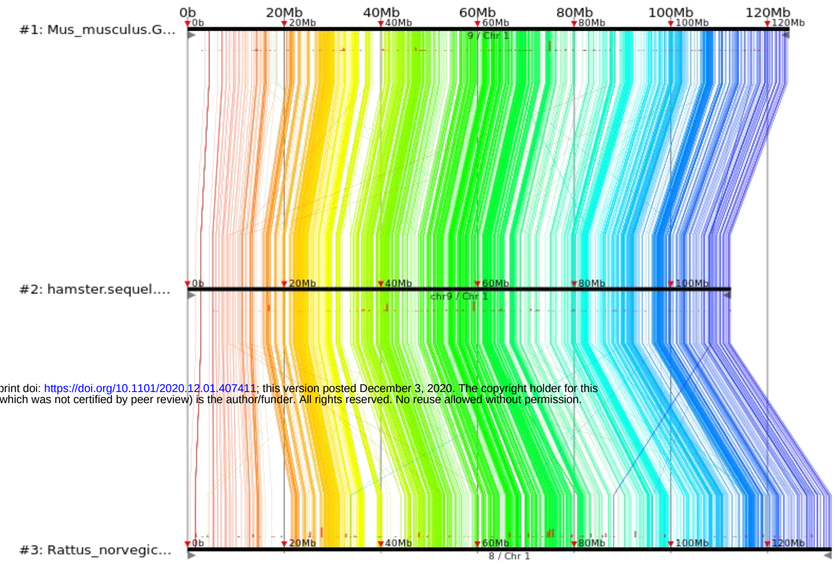

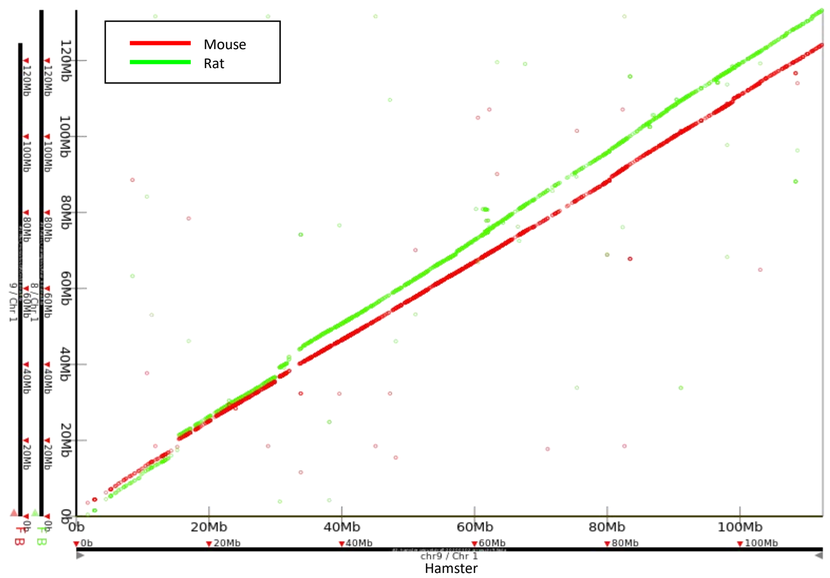

hamster	chr10	HiC_scaffold_3
Mus_Musculus	18(rev.) & 15(rev.) & 13	
Rattus_norvegicus	18(rev.) & 1 & 2(rev.)	

0bp-637,400,148bp of 637,400,148bp (100.00%)

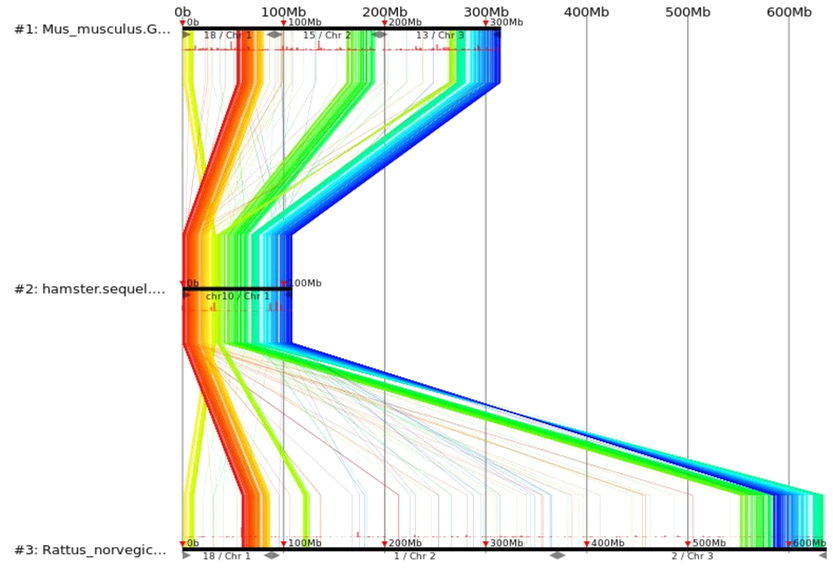

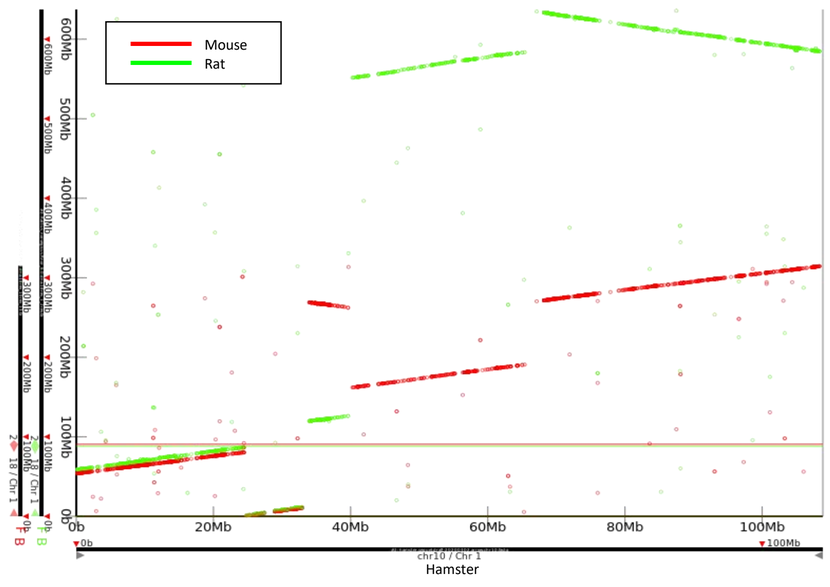

hamster	chr11	HiC_scaffold_4
Mus_Musculus	11(rev.) & 5 & 14(rev.)	
Rattus_norvegicus	14(rev.) & 15(rev.) & 16(rev.)	

0bp-398,819,491bp of 398,819,491bp (100.00%)

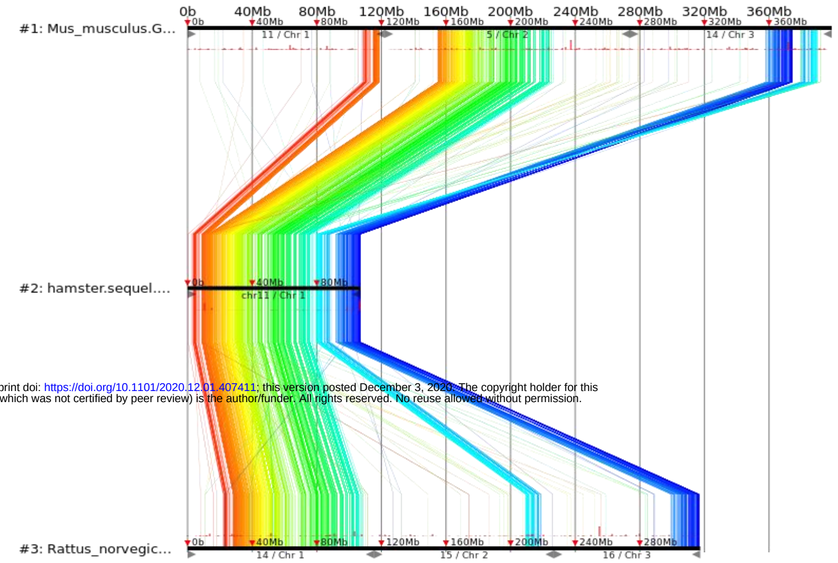

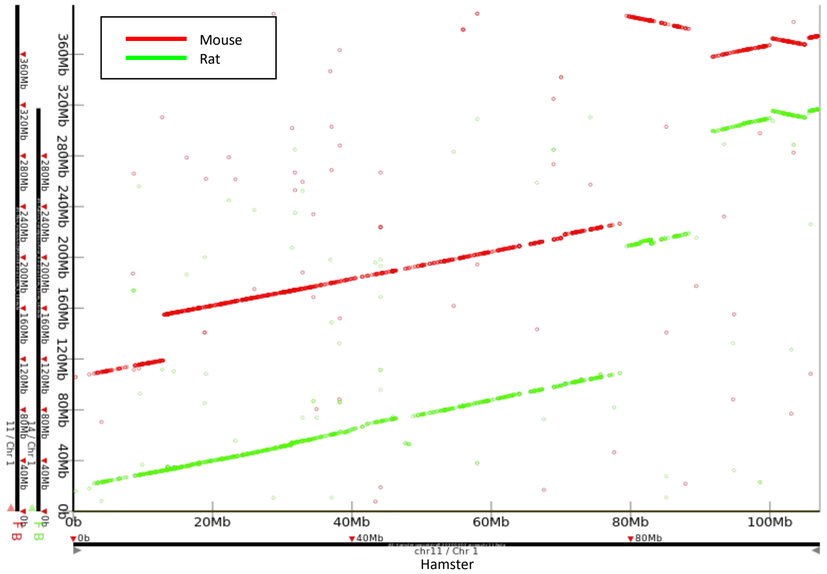

hamster	chr12	HiC_scaffold_12
Mus_Musculus	1(rev.) & 17 & 10	
Rattus_norvegicus	13(rev.) & 6 & 7(rev.)	

0bp-421,154,255bp of 421,154,255bp (100.00%)

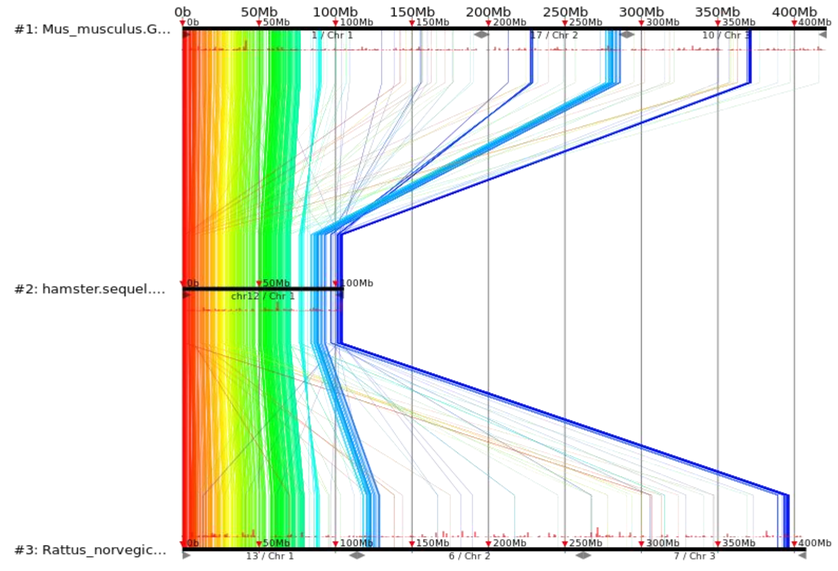

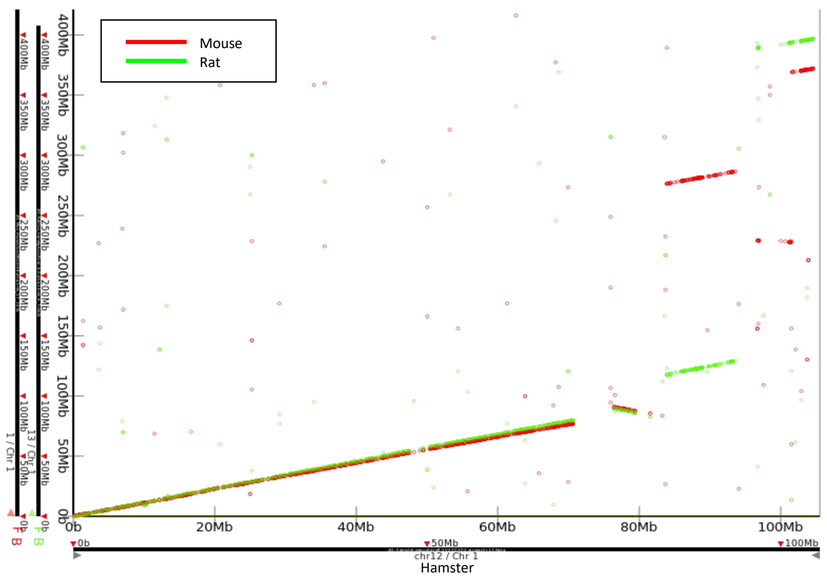

hamster	chr13	HiC_scaffold_18
Mus_Musculus	5 & 6	
Rattus_norvegicus	4	

0bp-301,571,240bp of 301,571,240bp (100.00%)

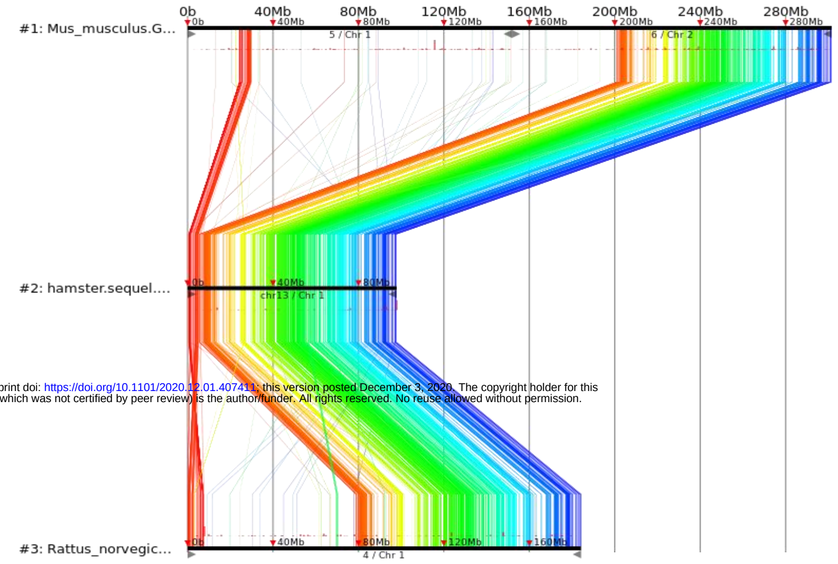

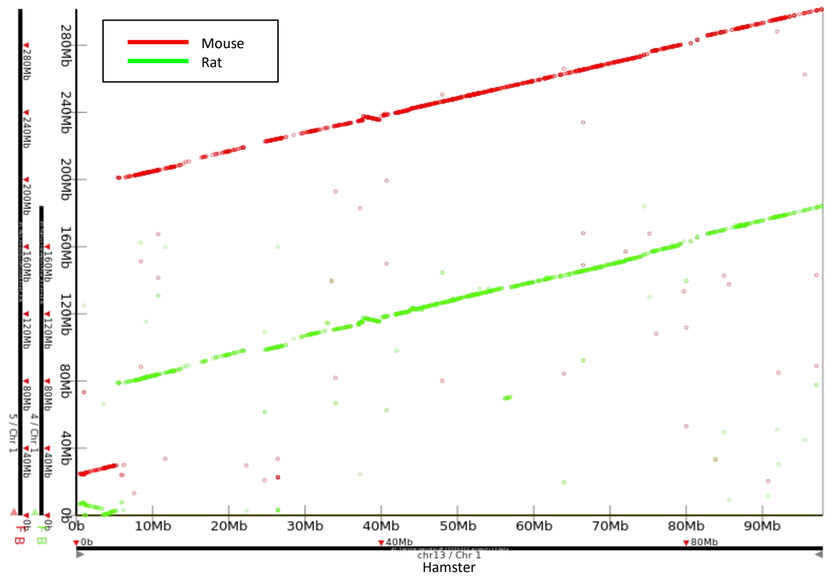

hamster	chr14	HiC_scaffold_20
Mus_Musculus	3	
Rattus_norvegicus	2	

0bp-266,435,125bp of 266,435,125bp (100.00%)

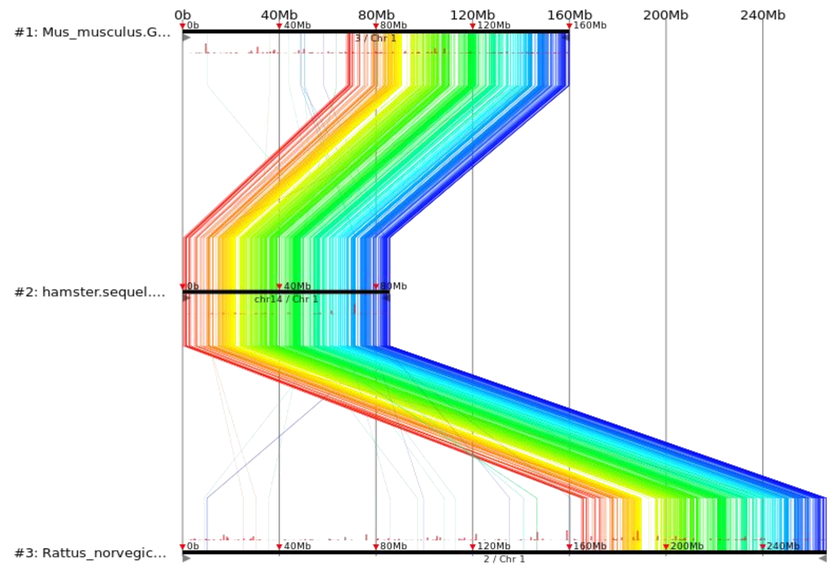

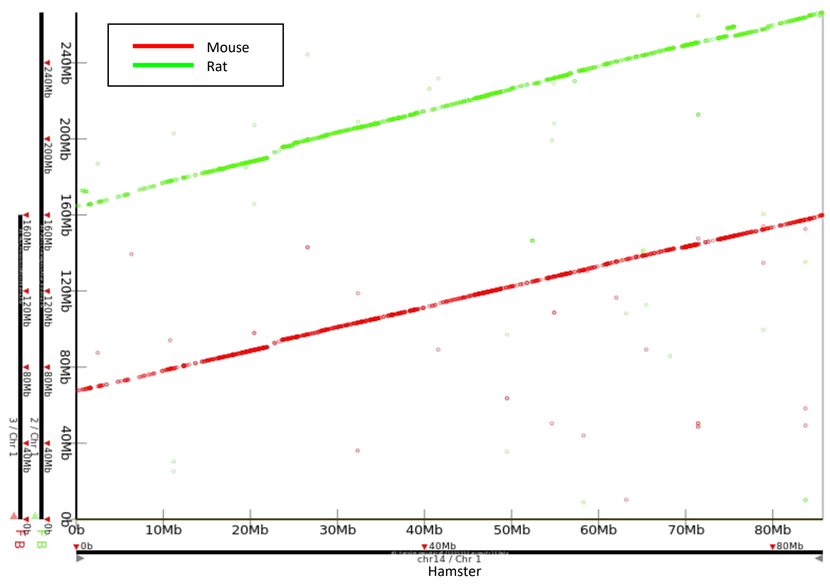

hamster	chr15	HiC_scaffold_6
Mus_Musculus	12(rev.)	
Rattus_norvegicus	6(rev.)	

0bp-147,991,367bp of 147,991,367bp (100.00%)

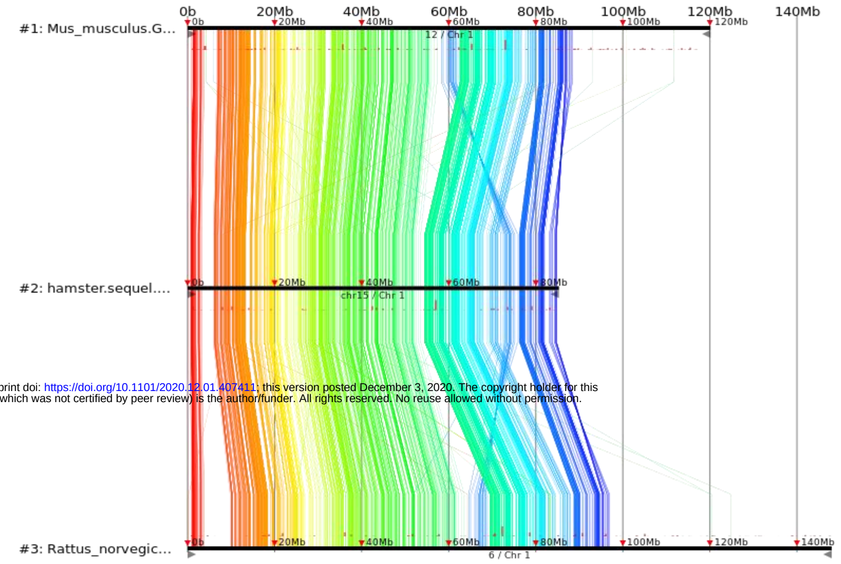

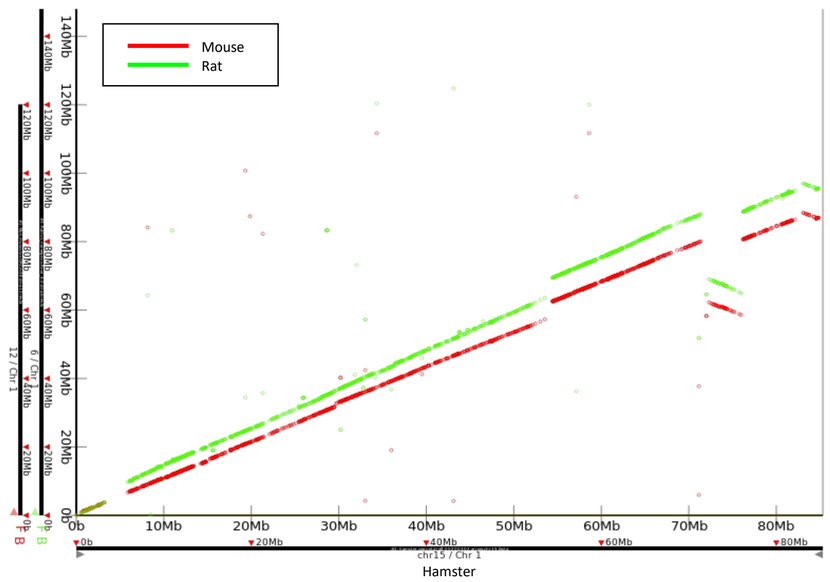

hamster	chr16	HiC_scaffold_15
Mus_Musculus	3(rev.) & 10(rev.)	
Rattus_norvegicus	2(rev.) & 7(rev.)	

0bp-412,164,437bp of 412,164,437bp (100.00%)

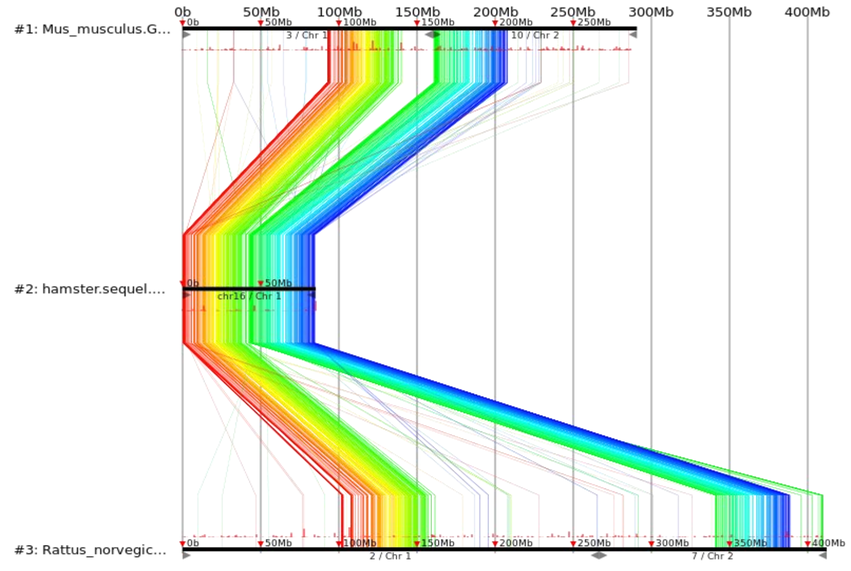

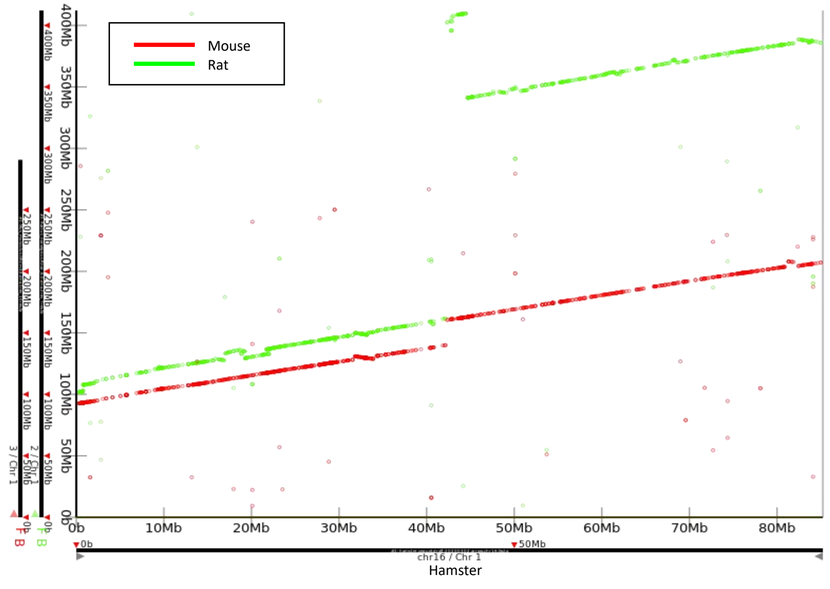

hamster	chr17	HiC_scaffold_11
Mus_Musculus	4(rev.)	
Rattus_norvegicus	5(rev.)	

0bp-173,707,219bp of 173,707,219bp (100.00%)

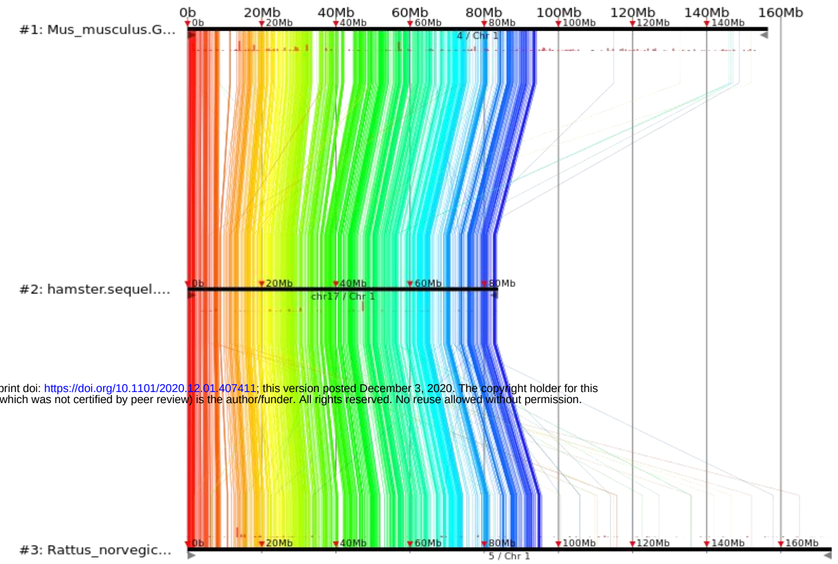

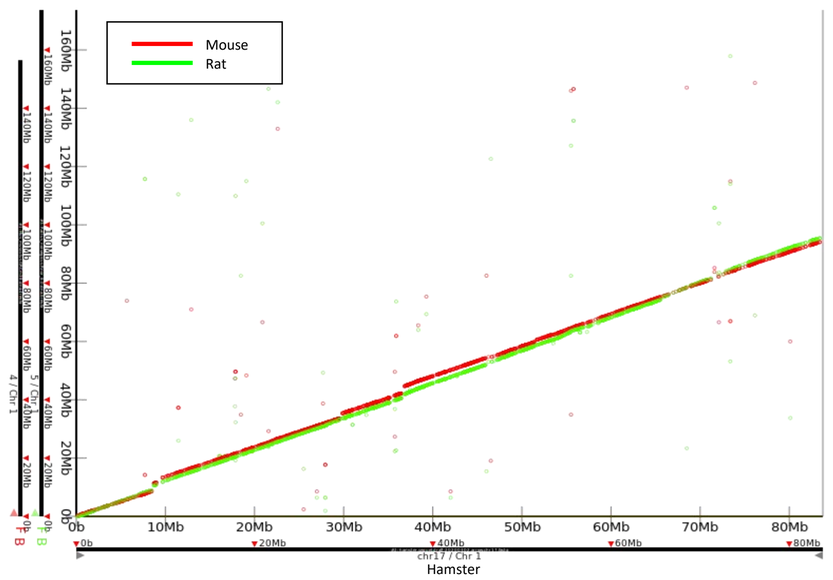

hamster	chr18	HiC_scaffold_21
Mus_Musculus	14(rev.)	
Rattus_norvegicus	15(rev.)	

0bp-124,902,244bp of 124,902,244bp (100.00%)

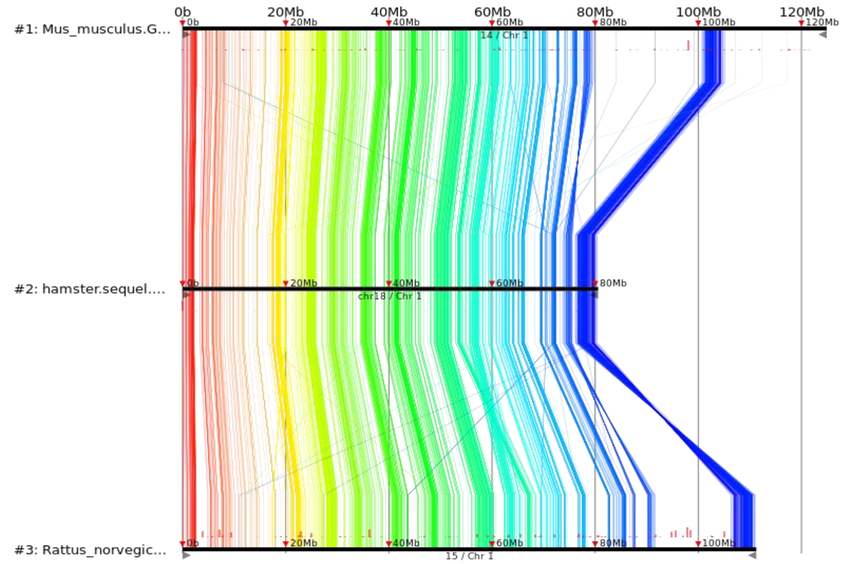

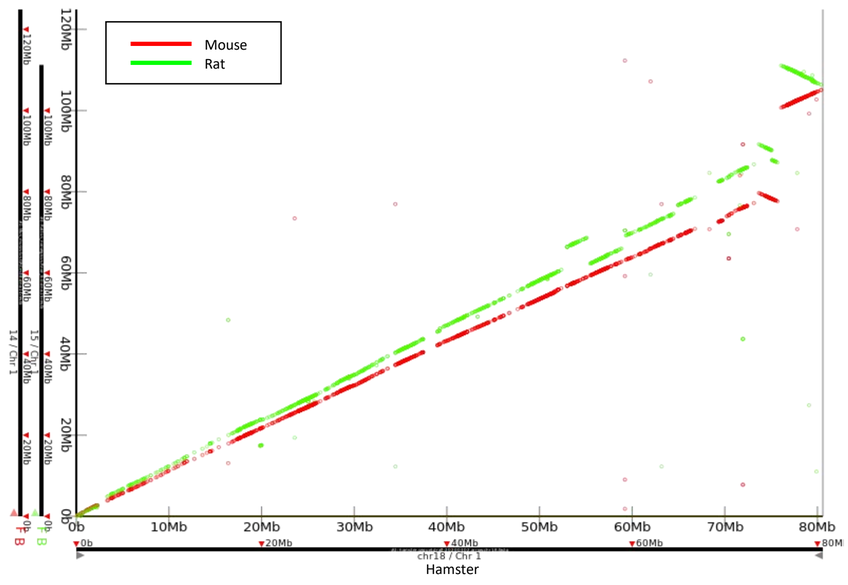

hamster	chr19	HiC_scaffold_19
Mus_Musculus	17(rev.) & 10 & 11	
Rattus_norvegicus	1(rev.) & 20 & 14	

0bp-454,462,496bp of 454,462,496bp (100.00%)

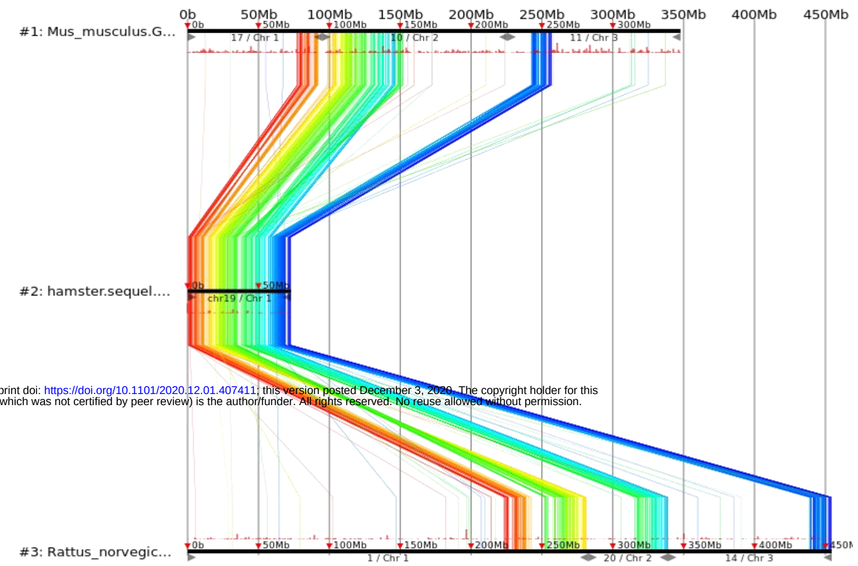

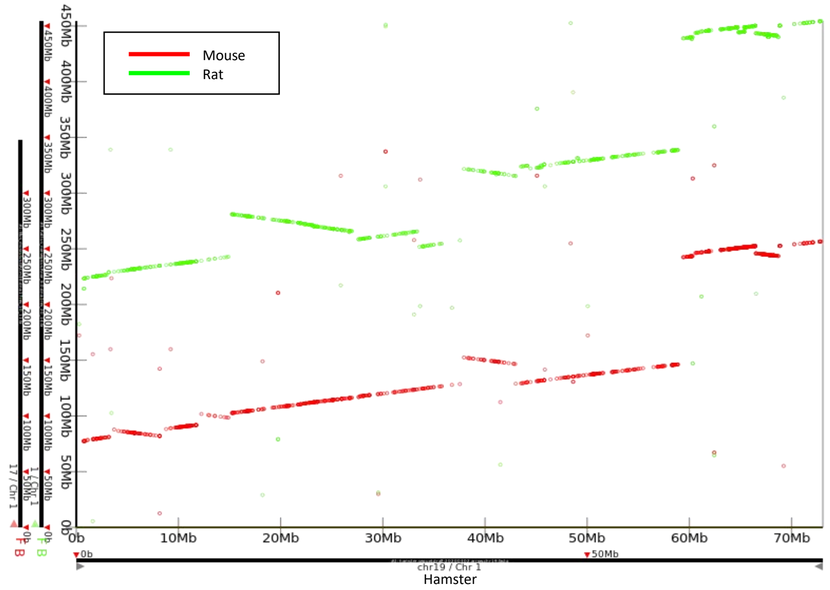

hamster	chr20	HiC_scaffold_2
Mus_Musculus	15	
Rattus_norvegicus	7	

0bp-145,729,302bp of 145,729,302bp (100.00%)

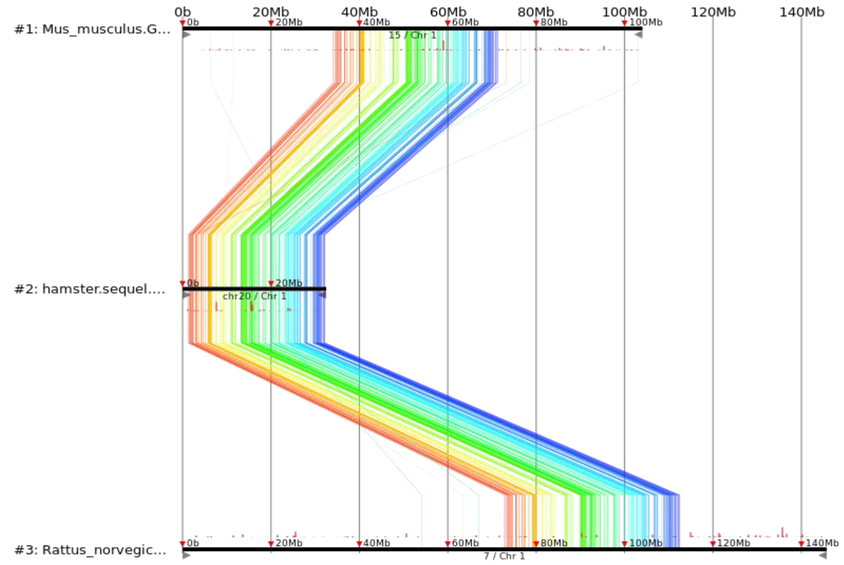

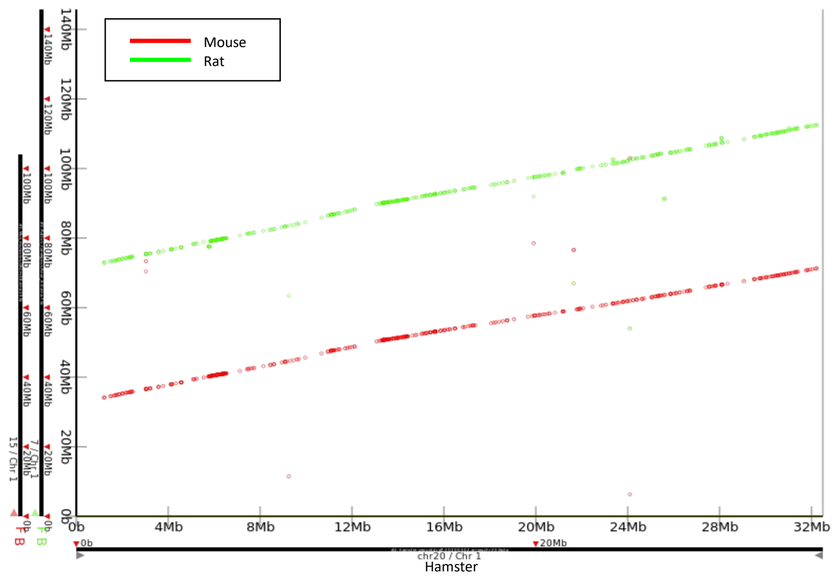

hamster	chr21	HiC_scaffold_7
Mus_Musculus	7	
Rattus_norvegicus	1	

0bp-282,763,074bp of 282,763,074bp (100.00%)

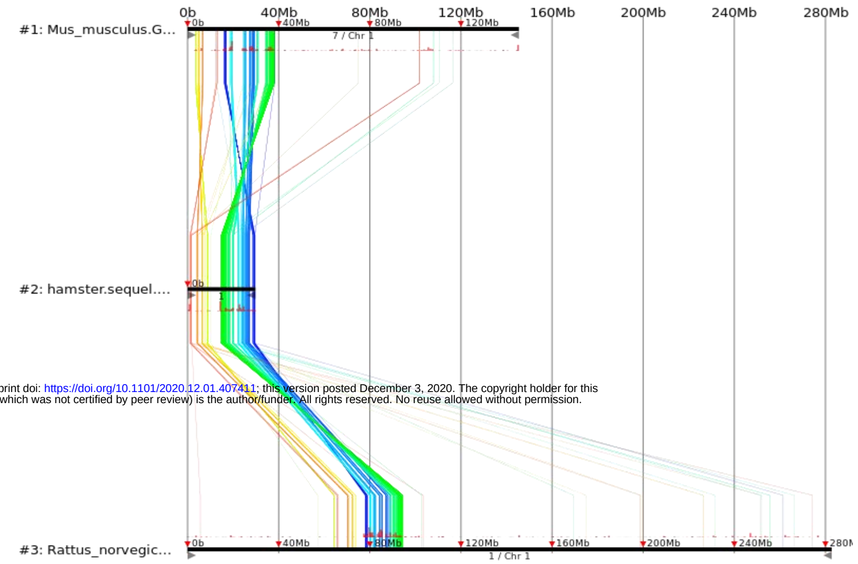

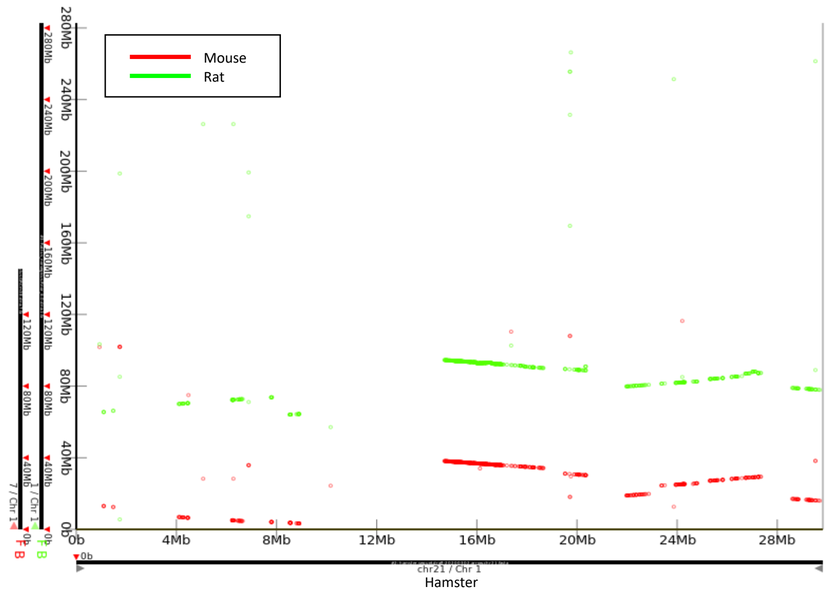

hamster	chr22	HiC_scaffold_22
Mus_Musculus	X (rev.)	
Rattus_norvegicus	X (rev.)	

0bp-171,031,299bp of 171,031,299bp (100.00%)

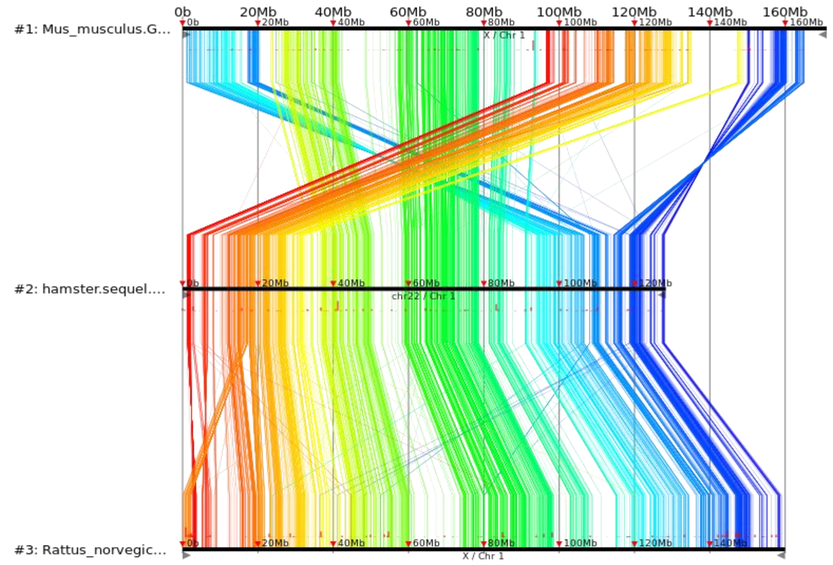

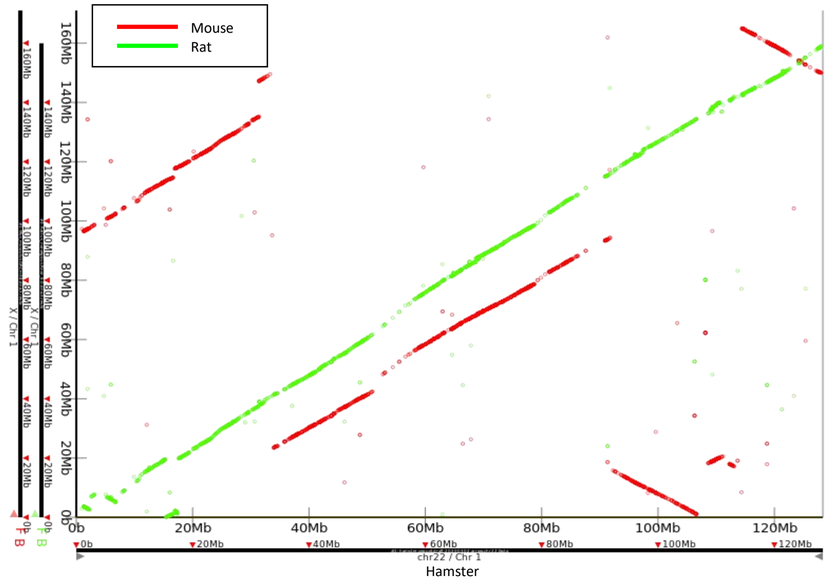

¥

Table S1

	Sequel raw reads		polished Sequel reads	
Number of reads	12,586,368		8,957,271	
Total Bases	234,079,417,624		118,229,107,194	
Coverage (2.5Gb)	**93.6**		**47.3**	
Max length	225,226		65,535	
Min length	50		500	
Average length	18,598		13,199	
N10	46,646	422,154	37,153	269,328
N20	39,659	970,508	31,004	620,374
N30	35,359	1,597,485	26,988	1,029,810
N40	32,142	2,292,726	23,080	1,502,938
N50	**29,513**	3,053,500	**19,413**	2,061,746
N60	26,841	3,883,122	16,115	2,730,037
N70	22,718	4,823,737	12,979	3,546,302
N80	17,327	5,996,473	9,902	4,586,019
N90	11,041	7,662,185	6,659	6,028,787
N99	2,834	10,890,109	2,609	8,339,269

Table S2

chromosome	assembly name	contig name	start position	end position	strand	reference scaffold name	reference start position	reference end position
chr1	falcon	000484F	1	586553	+	HiC_scaffold_16	7681	679067
chr1	falcon	000457F	28651	295533	-	HiC_scaffold_16	679068	883421
chr1	gap		1	500	+	HiC_scaffold_16		
chr1	falcon	000364F	10951	1059725	+	HiC_scaffold_16	883922	1748259
chr1	gap		1	500	+	HiC_scaffold_16		
chr1	falcon	000144F	1	5632105	+	HiC_scaffold_16	1748760	7233876
chr1	gap		1	1817	+	HiC_scaffold_16		
chr1	falcon	000582F	1	391477	+	HiC_scaffold_16	7235694	7644144
chr1	gap		1	17686	+	HiC_scaffold_16		
chr1	falcon	000242F	1	1897450	+	HiC_scaffold_16	7661831	9553494
chr1	subsequence of a corrected read	GGAGAACTGAGGGGGGACAGAAAGCTGAAGTTTATTTTTGTAAGCTTCC				HiC_scaffold_16	9553495	9560590
chr1	falcon	000497F	175955	560430	+	HiC_scaffold_16	9560591	10051720
chr1	falcon	000204F	35336	248737	+	HiC_scaffold_16	10051721	10200984
chr1	gap		1	500	+	HiC_scaffold_16		
chr1	falcon	000452F	1	707132	+	HiC_scaffold_16	10201485	10752916
chr1	gap		1	500	+	HiC_scaffold_16		
chr1	falcon	000372F	316921	1152062	+	HiC_scaffold_16	10753417	11621318
chr1	gap		1	7260	+	HiC_scaffold_16		
chr1	falcon	000328F	1	1077405	+	HiC_scaffold_16	11628579	12739183
chr1	gap		1	7906	+	HiC_scaffold_16		
chr1	falcon	000231F	1	3142160	+	HiC_scaffold_16	12747090	15786090
chr1	gap		1	499	+	HiC_scaffold_16		
chr1	falcon	000213F	254362	3526640	+	HiC_scaffold_16	15786590	19110281
chr1	gap		1	21022	+	HiC_scaffold_16		

chr1	falcon	000468F	1	196482	+	HiC_scaffold_16	19131304	19297433
chr1	gap		1	500	+	HiC_scaffold_16		
chr1	falcon	000441F	1	359997	+	HiC_scaffold_16	19297934	19493278
chr1	gap		1	7085	+	HiC_scaffold_16		
chr1	falcon	000683F	1	256548	+	HiC_scaffold_16	19500364	19753115
chr1	gap		1	9117	+	HiC_scaffold_16		
chr1	falcon	000133F	75691	1599583	-	HiC_scaffold_16	19762233	21382978
chr1	gap		1	27442	+	HiC_scaffold_16		
chr1	falcon	000977F	1	60758	+	HiC_scaffold_16	21410421	
chr1	gap		1	10000	+	HiC_scaffold_16		
chr1	falcon	001115F	1	118050	+	HiC_scaffold_16	21425919	
chr1	gap		1	10000	+	HiC_scaffold_16		
chr1	falcon	000504F	1	486604	+	HiC_scaffold_16	21459729	
chr1	gap		1	10000	+	HiC_scaffold_16		
chr1	falcon	002370F	1	27273	+	HiC_scaffold_16	21959186	21964245
chr1	gap		1	39657	+	HiC_scaffold_16		
chr1	falcon	001038F	1	124245	+	HiC_scaffold_16	22003903	22148781
chr1	gap		1	7708	+	HiC_scaffold_16		
chr1	falcon	000046F	1	10629933	+	HiC_scaffold_16	22156490	33022995
chr1	gap		1	5120	+	HiC_scaffold_16		
chr1	falcon	000182F	736743	4249162	+	HiC_scaffold_16	33028116	36604870
chr1	gap		1	12904	+	HiC_scaffold_16		
chr1	falcon	000545F	1	430094	+	HiC_scaffold_16	36617775	37041999
chr1	gap		1	8109	+	HiC_scaffold_16		
chr1	falcon	000251F	1	2611851	+	HiC_scaffold_16	37050109	39689075
chr1	gap		1	13340	+	HiC_scaffold_16		
chr1	falcon	000318F	1	1644088	+	HiC_scaffold_16	39702416	41392138
chr1	gap		1	8049	+	HiC_scaffold_16		

chr1	falcon	000042F	2478709	3631930	-	HiC_scaffold_16	41400188	42577688
chr1	falcon	000329F	1	1556063	+	HiC_scaffold_16	42577689	44151685
chr1	gap		1	500	+	HiC_scaffold_16		
chr1	falcon	000034F	19791	14104184	+	HiC_scaffold_16	44152186	58706842
chr1	gap		1	7389	+	HiC_scaffold_16		
chr1	falcon	000174F	1	4469547	+	HiC_scaffold_16	58714232	63185131
chr1	gap		1	15855	+	HiC_scaffold_16		
chr1	falcon	000166F	1	4741830	+	HiC_scaffold_16	63200987	68170394
chr1	gap		1	27773	+	HiC_scaffold_16		
chr1	falcon	000091F	1	8426292	+	HiC_scaffold_16	68198168	76787415
chr1	gap		1	24671	+	HiC_scaffold_16		
chr1	falcon	000009F	1	18919549	+	HiC_scaffold_16	76812087	96149439
chr1	gap		1	5707	+	HiC_scaffold_16		
chr1	falcon	000347F	1	1428978	+	HiC_scaffold_16	96155147	97610224
chr1	gap		1	13723	+	HiC_scaffold_16		
chr1	falcon	000041F	1	12991069	+	HiC_scaffold_16	97623948	110946318
chr1	gap		1	8446	+	HiC_scaffold_16		
chr1	falcon	000212F	1	3533511	+	HiC_scaffold_16	110954765	114594271
chr1	gap		1	19368	+	HiC_scaffold_16		
chr1	falcon	000054F	1	10793224	+	HiC_scaffold_16	114613640	125689347
chr1	falcon	000531F	3306	454459	+	HiC_scaffold_16	125689348	126196439
chr1	gap		1	507	+	HiC_scaffold_16		
chr1	falcon	000188F	1	876413	+	HiC_scaffold_16	126196947	127106287
chr1	gap		1	7416	+	HiC_scaffold_16		
chr1	falcon	000402F	1	955378	+	HiC_scaffold_16	127113704	128125539
chr1	falcon	000130F	161327	6042313	+	HiC_scaffold_16	128125540	134150095
chr1	gap		1	8016	+	HiC_scaffold_16		
chr1	falcon	000060F	1	10463776	+	HiC_scaffold_16	134158112	144864221

chr1	gap		1	8025	+	HiC_scaffold_16		
chr1	falcon	000035F	32064	10612044	+	HiC_scaffold_16	144872247	
chr1	gap		1	10000	+	HiC_scaffold_16		
chr1	falcon	000390F	1	1002908	+	HiC_scaffold_16	155745234	156740262
chr1	gap		1	652	+	HiC_scaffold_16		
chr1	falcon	000311F	1	1787224	+	HiC_scaffold_16	156740915	158364997
chr2	falcon	000592F	1	377446	+	HiC_scaffold_14	1	344190
chr2	falcon	000140F	1	689832	-	HiC_scaffold_14	344191	1096645
chr2	falcon	000435F	42362	771658	+	HiC_scaffold_14	1096646	1609021
chr2	falcon	000185F	1	4217309	+	HiC_scaffold_14	1609022	5784168
chr2	gap		1	4546	+	HiC_scaffold_14		
chr2	falcon	000008F	1	19884822	+	HiC_scaffold_14	5788715	26054938
chr2	gap		1	501	+	HiC_scaffold_14		
chr2	falcon	000081F	1	9049130	+	HiC_scaffold_14	26055440	35216794
chr2	gap		1	1765	+	HiC_scaffold_14		
chr2	falcon	000080F	1	6289368	-	HiC_scaffold_14	35218560	41721953
chr2	gap		1	9904	+	HiC_scaffold_14		
chr2	falcon	000461F	309938	630770	+	HiC_scaffold_14	41731858	42083134
chr2	falcon	000197F	77361	3909103	+	HiC_scaffold_14	42083135	46068987
chr2	falcon	000181F	21	4263883	+	HiC_scaffold_14	46068988	50456908
chr2	gap		1	30101	+	HiC_scaffold_14		
chr2	falcon	000039F	1	13235795	+	HiC_scaffold_14	50487010	63965772
chr2	gap		1	499	+	HiC_scaffold_14		
chr2	falcon	000239F	1	3052675	+	HiC_scaffold_14	63966272	66960159
chr2	gap		1	500	+	HiC_scaffold_14		
chr2	falcon	000275F	12988	2290566	+	HiC_scaffold_14	66960660	68990046
chr2	gap		1	500	+	HiC_scaffold_14		
chr2	falcon	000115F	814	6715047	+	HiC_scaffold_14	68990547	75751552

chr2	gap		1	374	+	HiC_scaffold_14		
chr2	falcon	000121F	1	641413	+	HiC_scaffold_14	75751927	76432954
chr2	gap		1	685	+	HiC_scaffold_14		
chr2	falcon	000147F	1	5447046	+	HiC_scaffold_14	76433640	
chr2	gap		1	10000	+	HiC_scaffold_14		
chr2	falcon	000312F	1	1751465	+	HiC_scaffold_14	81942147	83703190
chr2	gap		1	2278	+	HiC_scaffold_14		
chr2	falcon	000027F	208	14726910	+	HiC_scaffold_14	83705469	98830411
chr2	gap		1	8128	+	HiC_scaffold_14		
chr2	falcon	000825F	1	197098	+	HiC_scaffold_14	98838540	98950389
chr2	gap		1	500	+	HiC_scaffold_14		
chr2	falcon	000003F	88578	22775273	+	HiC_scaffold_14	98950890	122442117
chr2	falcon	000025F	1323	15378484	+	HiC_scaffold_14	122442118	138353912

chr2	subsequence of a corrected read	GGAAACAAAATCAGGGCATCCAT TCTGCGGATATCTCCTATAGAGA GTAAACTGAGGCATGAGAAAGTT TTTTTTTATTTTCCATTTTAAATT TAGATAAGAAACAAGGTTGCTTC ACAAGTCAGTACGAGGTCCCTCT CCCTTTCCCTCCCCTCCTCCCGTG CCCTCCCCCCATCCCCCCCCCGTT ATCCCCTCATTCCCCCAGGGAGG GTGAGGCCCTCCATGGGGGTGTC CATAGTCTGTCATTTCATATAGG GCAGGGCCTAGACCCTTCCCCAA GAGTTCAGGGTGAGAGTGCACCT CACATTGTTCTATGGGAGTCCAG AGACCGTGTGTATACTTGGGATG GGTACTGATCTGCT			HiC_scaffold_14	138353913	138353912
chr2	falcon	000284F	300	2159844 +	HiC_scaffold_14	138353913	140526097
chr2	falcon	000321F	78	1626835 +	HiC_scaffold_14	140526098	142220266
chr2	falcon	000497F	7005	168210 +	HiC_scaffold_14	142220267	142374643
chr2	gap		1	7439 +	HiC_scaffold_14		
chr2	falcon	000642F	1	298487 +	HiC_scaffold_14	142382083	142691467
chr2	gap		1	19799 +	HiC_scaffold_14		
chr2	falcon	000521F	18	463328 +	HiC_scaffold_14	142711267	143205951
chr2	falcon	000616F	1	305886 +	HiC_scaffold_14	143205952	143540314
chr2	falcon	000030F	1	14734960 +	HiC_scaffold_14	143540315	158839776
chr3	falcon	000001F	1	25233264 +	HiC_scaffold_17	1	
chr3	gap		1	10000 +	HiC_scaffold_17		
chr3	falcon	000136F	1	5542034 +	HiC_scaffold_17	25319561	30908838

chr3	falcon	000011F	1	18310114	+	HiC_scaffold_17	30908839	50012861
chr3	gap		1	7834	+	HiC_scaffold_17		
chr3	falcon	000196F	107	3924259	+	HiC_scaffold_17	50020696	54060255
chr3	gap		1	9299	+	HiC_scaffold_17		
chr3	falcon	000016F	34761	16913623	+	HiC_scaffold_17	54069555	71440982
chr3	gap		1	8555	+	HiC_scaffold_17		
chr3	falcon	000103F	1	7416981	+	HiC_scaffold_17	71449538	79122605
chr3	gap		1	7702	+	HiC_scaffold_17		
chr3	falcon	000536F	1	468325	+	HiC_scaffold_17	79130308	79506171
chr3	falcon	000182F	1	699703	-	HiC_scaffold_17	79506172	80257242
chr3	falcon	000206F	38681	3060765	+	HiC_scaffold_17	80257243	83405230
chr3	gap		1	7251	+	HiC_scaffold_17		
chr3	falcon	000218F	58229	3381417	+	HiC_scaffold_17	83412482	86818498
chr3	gap		1	8037	+	HiC_scaffold_17		
chr3	falcon	000230F	501	3192630	+	HiC_scaffold_17	86826536	90145664
chr3	gap		1	977	+	HiC_scaffold_17		
chr3	falcon	000159F	6791	4866412	+	HiC_scaffold_17	90146642	95404240
chr3	falcon	000052F	244997	11059275	+	HiC_scaffold_17	95404241	106579280
chr3	subsequence of a corrected read	CTGGAATAAAGGAACCTCAGCTT AAAAATGCTTCCTTCAGATTGGCC CGTAGGTGTGAGGAGC				HiC_scaffold_17	106579281	106579327
chr3	falcon	000162F	1	4815025	+	HiC_scaffold_17	106579328	
chr3	gap		1	10000	+	HiC_scaffold_17		
chr3	falcon	000099F	1	7928744	+	HiC_scaffold_17	111629131	119889055
chr3	falcon	000026F	419	15388079	+	HiC_scaffold_17	119889056	135842976
chr3	falcon	000517F	3005	453739	+	HiC_scaffold_17	135842977	136327675
chr3	gap		1	7611	+	HiC_scaffold_17		
chr3	falcon	000043F	1	12671037	+	HiC_scaffold_17	136335287	149146624

chr3	gap		1	500	+	HiC_scaffold_17		
chr3	falcon	000459F	1	673966	+	HiC_scaffold_17	149147125	149737909
chr3	gap		1	500	+	HiC_scaffold_17		
chr3	falcon	000250F	1	2668574	+	HiC_scaffold_17	149738410	152313533
chr3	gap		1	26078	+	HiC_scaffold_17		
chr3	falcon	000897F	1	170284	+	HiC_scaffold_17	152339612	152483542
chr3	gap		1	77	+	HiC_scaffold_17		
chr3	falcon	000161F	1	4801766	+	HiC_scaffold_17	152483620	157194130
chr4	falcon	000143F	1	5648125	+	HiC_scaffold_5	1	5771123
chr4	gap		1	14195	+	HiC_scaffold_5		
chr4	falcon	000158F	1	4763458	+	HiC_scaffold_5	5785319	10823291
chr4	gap		1	499	+	HiC_scaffold_5		
chr4	falcon	000259F	1	1982545	-	HiC_scaffold_5	10823791	12459654
chr4	gap		1	11405	+	HiC_scaffold_5		
chr4	falcon	000481F	160371	456313	+	HiC_scaffold_5	12471060	12770296
chr4	gap		1	500	+	HiC_scaffold_5		
chr4	falcon	000077F	1	9138869	+	HiC_scaffold_5	12770797	21993692
chr4	gap		1	500	+	HiC_scaffold_5		
chr4	falcon	000388F	46058	1055302	+	HiC_scaffold_5	21994193	23026364
chr4	gap		1	3119	+	HiC_scaffold_5		
chr4	falcon	000165F	1	4758682	+	HiC_scaffold_5	23029484	27969559
chr4	falcon	000146F	667362	5477212	+	HiC_scaffold_5	27969560	32819206
chr4	gap		1	500	+	HiC_scaffold_5		
chr4	falcon	000638F	1	241703	+	HiC_scaffold_5	32819707	32995989
chr4	gap		1	22424	+	HiC_scaffold_5		
chr4	falcon	000703F	38361	91929	+	HiC_scaffold_5	33018414	33076542
chr4	gap		1	6176	+	HiC_scaffold_5		
chr4	falcon	000249F	1	2677104	+	HiC_scaffold_5	33082719	35852030

chr4	gap		1	500	+	HiC_scaffold_5		
chr4	falcon	000154F	155979	5046034	+	HiC_scaffold_5	35852531	40876705
chr4	gap		1	3805	+	HiC_scaffold_5		
chr4	falcon	000350F	1	1390809	+	HiC_scaffold_5	40880511	42127407
chr4	falcon	000276F	6577	2265482	+	HiC_scaffold_5	42127408	44435343
chr4	gap		1	9865	+	HiC_scaffold_5		
chr4	falcon	000222F	1	3301786	+	HiC_scaffold_5	44445209	47770109
chr4	gap		1	175	+	HiC_scaffold_5		
chr4	falcon	000170F	1	4568271	+	HiC_scaffold_5	47770285	52320051
chr4	gap		1	3578	+	HiC_scaffold_5		
chr4	falcon	000437F	1	797937	+	HiC_scaffold_5	52323630	53062332
chr4	falcon	000192F	80402	4081166	+	HiC_scaffold_5	53062333	57142699
chr4	gap		1	8478	+	HiC_scaffold_5		
chr4	falcon	000224F	1	3242736	+	HiC_scaffold_5	57151178	60401810
chr4	gap		1	501	+	HiC_scaffold_5		
chr4	falcon	000220F	352139	3350498	+	HiC_scaffold_5	60402312	63293802
chr4	gap		1	500	+	HiC_scaffold_5		
chr4	falcon	000720F	1	226677	+	HiC_scaffold_5	63294303	63469730
chr4	gap		1	8044	+	HiC_scaffold_5		
chr4	falcon	000004F	7	20646533	+	HiC_scaffold_5	63477775	84732822
chr4	gap		1	7820	+	HiC_scaffold_5		
chr4	falcon	000049F	145	11089655	+	HiC_scaffold_5	84740643	96258777
chr4	falcon	000198F	1	3945754	+	HiC_scaffold_5	96258778	100079090
chr4	gap		1	8639	+	HiC_scaffold_5		
chr4	falcon	000416F	1	813508	+	HiC_scaffold_5	100087730	100937278
chr4	gap		1	8014	+	HiC_scaffold_5		
chr4	falcon	000000F	1	25639206	+	HiC_scaffold_5	100945293	127220383
chr4	gap		1	2092	+	HiC_scaffold_5		

chr4	falcon	000172F	1	4552453	+	HiC_scaffold_5	127222476	131814787
chr4	gap		1	689	+	HiC_scaffold_5		
chr4	falcon	000150F	1	5291852	+	HiC_scaffold_5	131815477	137107746
chr5	falcon	000142F	1	5624441	+	HiC_scaffold_9	1	5657204
chr5	gap		1	6481	+	HiC_scaffold_9		
chr5	falcon	000262F	3816	2461928	+	HiC_scaffold_9	5663686	8139108
chr5	gap		1	10620	+	HiC_scaffold_9		
chr5	falcon	000238F	1	3039661	+	HiC_scaffold_9	8149729	11217876
chr5	falcon	000002F	15477	17633046	+	HiC_scaffold_9	11217877	29272759
chr5	falcon	000058F	1	10597359	+	HiC_scaffold_9	29272760	40096321
chr5	gap		1	7270	+	HiC_scaffold_9		
chr5	falcon	000116F	7	6721333	+	HiC_scaffold_9	40103592	47026006
chr5	gap		1	14685	+	HiC_scaffold_9		
chr5	falcon	000021F	13522125	15778618	-	HiC_scaffold_9	47040692	49417578
chr5	gap		1	7578	+	HiC_scaffold_9		
chr5	falcon	000006F	1	20996585	+	HiC_scaffold_9	49425157	70864013
chr5	falcon	000012F	1	17788885	+	HiC_scaffold_9	70864014	89342344
chr5	gap		1	8021	+	HiC_scaffold_9		
chr5	falcon	000245F	1	2755889	+	HiC_scaffold_9	89350366	92220311
chr5	gap		1	50	+	HiC_scaffold_9		
chr5	falcon	000438F	1	775273	+	HiC_scaffold_9	92220362	93002419
chr5	gap		1	5419	+	HiC_scaffold_9		
chr5	falcon	000195F	1	3976367	+	HiC_scaffold_9	93007839	97096912
chr5	subsequence of a corrected read	CTGTCAGGATAGACTGCAGACAGTGAGTGTTTAACACTGTGGAGGATGT				HiC_scaffold_9	97096913	97097412
chr5	falcon	000202F	1	3822540	+	HiC_scaffold_9	97097413	100616944
chr5	gap		1	26521	+	HiC_scaffold_9		

chr5	falcon	000052F	1	239039	+	HiC_scaffold_9	100643466	100878276
chr5	gap		1	5381	+	HiC_scaffold_9		
chr5	falcon	000002F	17657928	23750703	+	HiC_scaffold_9	100883658	106921021
chr5	gap		1	14604	+	HiC_scaffold_9		
chr5	falcon	000059F	630661	10653164	+	HiC_scaffold_9	106935626	117176881
chr5	gap		1	8739	+	HiC_scaffold_9		
chr5	falcon	000024F	1	15584437	+	HiC_scaffold_9	117185621	133094598
chr6	falcon	000367F	1	1177383	+	HiC_scaffold_13	1	996671
chr6	gap		1	2262	+	HiC_scaffold_13		
chr6	falcon	000135F	1	5777853	+	HiC_scaffold_13	998934	6628207
chr6	gap		1	499	+	HiC_scaffold_13		
chr6	falcon	000296F	1	1983052	+	HiC_scaffold_13	6628707	8633383
chr6	gap		1	2450	+	HiC_scaffold_13		
chr6	falcon	000467F	1	483065	+	HiC_scaffold_13	8635834	9097365
chr6	gap		1	2325	+	HiC_scaffold_13		
chr6	falcon	000084F	444	8913275	+	HiC_scaffold_13	9099691	18143777
chr6	gap		1	68	+	HiC_scaffold_13		
chr6	falcon	000718F	1	217904	+	HiC_scaffold_13	18143846	18393793
chr6	falcon	000076F	1	9360244	+	HiC_scaffold_13	18393794	28161989
chr6	falcon	000219F	12267	3341668	+	HiC_scaffold_13	28161990	31569461
chr6	falcon	000124F	2	6218713	+	HiC_scaffold_13	31569462	37925145
chr6	gap		1	1232	+	HiC_scaffold_13		
chr6	falcon	000042F	3639637	12779646	+	HiC_scaffold_13	37926378	47198059
chr6	gap		1	530	+	HiC_scaffold_13		
chr6	falcon	000392F	1	1019505	+	HiC_scaffold_13	47198590	47817710
chr6	gap		1	7054	+	HiC_scaffold_13		
chr6	falcon	000289F	3348	2120244	+	HiC_scaffold_13	47824765	50041772
chr6	gap		1	7947	+	HiC_scaffold_13		

chr6	falcon	000412F	1	884705	+	HiC_scaffold_13	50049720	50984316
chr6	gap		1	7891	+	HiC_scaffold_13		
chr6	falcon	000440F	1	717877	+	HiC_scaffold_13	50992208	51723050
chr6	gap		1	3501	+	HiC_scaffold_13		
chr6	falcon	000658F	2804	114142	+	HiC_scaffold_13	51726552	51829780
chr6	gap		1	27774	+	HiC_scaffold_13		
chr6	falcon	000368F	46812	1216279	+	HiC_scaffold_13	51857555	53052863
chr6	falcon	000199F	1	3924852	+	HiC_scaffold_13	53052864	56986021
chr6	gap		1	1949	+	HiC_scaffold_13		
chr6	falcon	000330F	1	1603475	+	HiC_scaffold_13	56987971	58638788
chr6	gap		1	7835	+	HiC_scaffold_13		
chr6	falcon	000291F	1	1266415	+	HiC_scaffold_13	58646624	59931950
chr6	gap		1	500	+	HiC_scaffold_13		
chr6	falcon	000345F	1	1426943	+	HiC_scaffold_13	59932451	61339396
chr6	falcon	000509F	315291	515610	-	HiC_scaffold_13	61339397	61562063
chr6	gap		1	36380	+	HiC_scaffold_13		
chr6	falcon	000032F	248	14394033	+	HiC_scaffold_13	61598444	76290617
chr6	gap		1	500	+	HiC_scaffold_13		
chr6	falcon	000306F	1	1853291	+	HiC_scaffold_13	76291118	78174694
chr6	gap		1	2845	+	HiC_scaffold_13		
chr6	falcon	000057F	1	10719182	+	HiC_scaffold_13	78177540	89178752
chr6	gap		1	8336	+	HiC_scaffold_13		
chr6	falcon	000308F	81461	1771215	+	HiC_scaffold_13	89187089	90945027
chr6	gap		1	7397	+	HiC_scaffold_13		
chr6	falcon	000351F	1	1360575	+	HiC_scaffold_13	90952425	92163022
chr6	gap		1	8219	+	HiC_scaffold_13		
chr6	falcon	000040F	269333	2385656	+	HiC_scaffold_13	92171242	94376685
chr6	gap		1	7940	+	HiC_scaffold_13		

chr6	falcon	000074F	1	9605744	+	HiC_scaffold_13	94384626	104132502
chr6	gap		1	623	+	HiC_scaffold_13		
chr6	falcon	000315F	6986	1704419	+	HiC_scaffold_13	104133126	105811307
chr6	gap		1	499	+	HiC_scaffold_13		
chr6	falcon	000405F	1	953706	+	HiC_scaffold_13	105811807	106581122
chr6	gap		1	23102	+	HiC_scaffold_13		
chr6	falcon	001037F	1	140114	+	HiC_scaffold_13	106604225	106720252
chr6	subsequence of a corrected read	ATGAGAGCATCATTGTCCCGCGC TACCGTCTCGCCAGCAAGAACGA CGCAGAACACTCGGATCCTTCTG CAGTAAAGCTTTAATGCATCTTGA GAGATAGATGATCAGCTTCTTAG AGGGAGACCCCAAGCTAAGAAAC CCAGCCCCTTATATAAGCCTAGGA GCTCCGAGTGAGACGTGTAGAGC CGGGATTGGTGGTTTGCACATCA CCCCAGATGACGCCACGGGAGAG GCACAGCTTAAACGGTTAACTCCA ACTGACAGCAGATGTCAGCGCCA TCTTCTAACGGTTAACTCCAACTG ACAGCAGATGTCAGCGCCATCTT CTAACGGCAATAGCGATAGCGAG GGCGGCTCCTCACATCTCCCCCTA TTCATTTATTTTTGAAGCAATAGG ACACCCACAACTTTGGAGTGGAG ATAGAGGTCAAATCCCCATGTGC AAATTCGGAACATGTACAAAGCTC CTCTCCAGGGTCTTATCCCCA			HiC_scaffold_13	106720253	106720259

chr6	falcon	000015F	1	17145014	+	HiC_scaffold_13	106720260	124260332
chr7	falcon	000155F	1	4937991	+	HiC_scaffold_10	1	4979563
chr7	gap		1	7639	+	HiC_scaffold_10		
chr7	falcon	000633F	1	270444	+	HiC_scaffold_10	4987203	5256653
chr7	gap		1	20241	+	HiC_scaffold_10		
chr7	falcon	000299F	1	1925818	+	HiC_scaffold_10	5276895	7239838
chr7	gap		1	8080	+	HiC_scaffold_10		
chr7	falcon	000242F	1905537	2963291	-	HiC_scaffold_10	7247919	8382054
chr7	gap		1	17735	+	HiC_scaffold_10		
chr7	falcon	000111F	1	6790279	+	HiC_scaffold_10	8399790	15384328
chr7	gap		1	6497	+	HiC_scaffold_10		
chr7	falcon	000127F	1	6136878	+	HiC_scaffold_10	15390826	21757733
chr7	gap		1	16350	+	HiC_scaffold_10		
chr7	falcon	000190F	2410829	4090200	+	HiC_scaffold_10	21774084	23504430
chr7	gap		1	13793	+	HiC_scaffold_10		
chr7	falcon	000319F	1	1671412	+	HiC_scaffold_10	23518224	25274419
chr7	gap		1	8004	+	HiC_scaffold_10		
chr7	falcon	000221F	1	3293608	+	HiC_scaffold_10	25282424	28648513
chr7	falcon	000433F	1	724288	+	HiC_scaffold_10	28648514	29283193
chr7	gap		1	9222	+	HiC_scaffold_10		
chr7	falcon	000193F	1137186	4043622	-	HiC_scaffold_10	29292416	32331050
chr7	gap		1	24983	+	HiC_scaffold_10		
chr7	falcon	000040F	2408438	13085936	+	HiC_scaffold_10	32356034	43515517
chr7	gap		1	14541	+	HiC_scaffold_10		
chr7	falcon	000183F	1	4239627	+	HiC_scaffold_10	43530059	47951396
chr7	gap		1	8040	+	HiC_scaffold_10		
chr7	falcon	000644F	1	297225	+	HiC_scaffold_10	47959437	48281735
chr7	gap		1	23264	+	HiC_scaffold_10		

chr7	falcon	000271F	1	2313109	+	HiC_scaffold_10	48305000	50806981
chr7	gap		1	23656	+	HiC_scaffold_10		
chr7	falcon	000424F	1	833713	+	HiC_scaffold_10	50830638	51645569
chr7	gap		1	7799	+	HiC_scaffold_10		
chr7	falcon	000094F	25151	8236271	+	HiC_scaffold_10	51653369	60370013
chr7	falcon	000055F	10259036	10917344	+	HiC_scaffold_10	60370014	61065304
chr7	gap		1	18556	+	HiC_scaffold_10		
chr7	falcon	000121F	659315	6246238	+	HiC_scaffold_10	61083861	66808980
chr7	falcon	000004F	20664692	22774601	+	HiC_scaffold_10	66808981	69005532
chr7	gap		1	11871	+	HiC_scaffold_10		
chr7	falcon	000088F	1	8501069	+	HiC_scaffold_10	69017404	77785222
chr7	falcon	000509F	1	309856	+	HiC_scaffold_10	77785223	78098499
chr7	gap		1	6493	+	HiC_scaffold_10		
chr7	falcon	000281F	1	2097896	+	HiC_scaffold_10	78104993	80092158
chr7	falcon	000133F	1606603	5883547	+	HiC_scaffold_10	80092159	84505300
chr7	gap		1	500	+	HiC_scaffold_10		
chr7	falcon	000216F	1	3366572	+	HiC_scaffold_10	84505801	88027514
chr7	falcon	000069F	722	9859064	+	HiC_scaffold_10	88027515	98229270
chr7	gap		1	2197	+	HiC_scaffold_10		
chr7	falcon	000029F	1	14673280	+	HiC_scaffold_10	98231468	113507716
chr7	gap		1	9249	+	HiC_scaffold_10		
chr7	falcon	000292F	1	2098899	+	HiC_scaffold_10	113516966	115682563
chr7	gap		1	8456	+	HiC_scaffold_10		
chr7	falcon	000215F	1	3498475	+	HiC_scaffold_10	115691020	119247784
chr7	gap		1	31178	+	HiC_scaffold_10		
chr7	falcon	000280F	1	2206830	+	HiC_scaffold_10	119278963	121354536
chr8	falcon	000363F	1	1264047	+	HiC_scaffold_1	1	1304646
chr8	gap		1	6487	+	HiC_scaffold_1		

chr8	falcon	000021F	661193	13503735	+	HiC_scaffold_1	1311134	14625668
chr8	falcon	000394F	1	1001448	+	HiC_scaffold_1	14625669	15665393
chr8	gap		1	7528	+	HiC_scaffold_1		
chr8	falcon	000017F	1	16724009	+	HiC_scaffold_1	15672922	33095499
chr8	gap		1	6727	+	HiC_scaffold_1		
chr8	falcon	000393F	617658	998836	+	HiC_scaffold_1	33102227	33501938
chr8	falcon	000104F	5108	7028777	+	HiC_scaffold_1	33501939	41007642
chr8	falcon	000336F	1	1481302	+	HiC_scaffold_1	41007643	42537471
chr8	gap		1	7090	+	HiC_scaffold_1		
chr8	falcon	000176F	24309	830690	+	HiC_scaffold_1	42544562	43414696
chr8	gap		1	2449	+	HiC_scaffold_1		
chr8	falcon	000235F	1	3097516	+	HiC_scaffold_1	43417146	46620504
chr8	gap		1	5995	+	HiC_scaffold_1		
chr8	falcon	000107F	1	7128496	+	HiC_scaffold_1	46626500	53990565
chr8	gap		1	19058	+	HiC_scaffold_1		
chr8	falcon	000053F	1	11027616	+	HiC_scaffold_1	54009624	65422312
chr8	gap		1	7467	+	HiC_scaffold_1		
chr8	falcon	000105F	1	7000714	+	HiC_scaffold_1	65429780	72583789
chr8	gap		1	499	+	HiC_scaffold_1		
chr8	falcon	000408F	400347	955985	+	HiC_scaffold_1	72584289	73153860
chr8	falcon	000189F	569291	4054011	+	HiC_scaffold_1	73153861	76683604
chr8	falcon	000285F	1	2202827	+	HiC_scaffold_1	76683605	78970875
chr8	gap		1	13333	+	HiC_scaffold_1		
chr8	falcon	000090F	1	8392793	+	HiC_scaffold_1	78984209	87494751
chr8	gap		1	7635	+	HiC_scaffold_1		
chr8	falcon	000208F	1	3600336	+	HiC_scaffold_1	87502387	
chr8	gap		1	10000	+	HiC_scaffold_1		
chr8	falcon	000593F	109	370706	+	HiC_scaffold_1	91144971	91429975

chr8	gap		1	7133	+	HiC_scaffold_1		
chr8	falcon	000256F	1	2554935	+	HiC_scaffold_1	91437109	94054521
chr8	subsequence of a corrected read	CCACAGAAGAACACAGGTCTACAC CACAGT				HiC_scaffold_1	94054522	94055021
chr8	falcon	000079F	1	9126671	+	HiC_scaffold_1	94055022	103253269
chr8	gap		1	20136	+	HiC_scaffold_1		
chr8	falcon	000082F	8751874	9047432	-	HiC_scaffold_1	103273406	103530212
chr8	gap		1	8201	+	HiC_scaffold_1		
chr8	falcon	000112F	1	6732382	+	HiC_scaffold_1	103538414	110430532
chr8	falcon	000086F	1	8915674	+	HiC_scaffold_1	110430533	119542279
chr8	gap		1	21495	+	HiC_scaffold_1		
chr8	falcon	000797F	731	205127	+	HiC_scaffold_1	119563775	119733378
chr9	falcon	000063F	1	191159	+	HiC_scaffold_8	1	4614
chr9	gap		1	5528	+	HiC_scaffold_8		
chr9	falcon	000432F	1	773251	+	HiC_scaffold_8	10143	866263
chr9	gap		1	12058	+	HiC_scaffold_8		
chr9	falcon	000393F	1	608899	+	HiC_scaffold_8	878322	1338979
chr9	gap		1	34944	+	HiC_scaffold_8		
chr9	falcon	000189F	1	550593	+	HiC_scaffold_8	1373924	1917106
chr9	gap		1	13192	+	HiC_scaffold_8		
chr9	falcon	000168F	4076244	4571413	-	HiC_scaffold_8	1930299	2479669
chr9	gap		1	405	+	HiC_scaffold_8		
chr9	falcon	000134F	2	1385646	-	HiC_scaffold_8	2480075	3948899
chr9	falcon	000059F	9809	602506	-	HiC_scaffold_8	3948900	4543364
chr9	gap		1	4051	+	HiC_scaffold_8		
chr9	falcon	000337F	179104	1497952	+	HiC_scaffold_8	4547416	5966040
chr9	subsequence of a corrected read	AGTCTCTT				HiC_scaffold_8	5966041	5966044

chr9	gap		1	1000	+	HiC_scaffold_8		
chr9	falcon	000179F	1	4372643	+	HiC_scaffold_8	5967045	10522360
chr9	gap		1	7675	+	HiC_scaffold_8		
chr9	falcon	000398F	1	835974	+	HiC_scaffold_8	10530036	
chr9	gap		1	10000	+	HiC_scaffold_8		
chr9	falcon	000203F	2152	3780957	+	HiC_scaffold_8	11408385	15337952
chr9	gap		1	9485	+	HiC_scaffold_8		
chr9	falcon	000561F	1	283981	+	HiC_scaffold_8	15347438	15652861
chr9	gap		1	501	+	HiC_scaffold_8		
chr9	falcon	000581F	1	380782	+	HiC_scaffold_8	15653363	15910436
chr9	gap		1	11398	+	HiC_scaffold_8		
chr9	falcon	000031F	1	14618795	+	HiC_scaffold_8	15921835	30791394
chr9	falcon	000145F	1	2354867	+	HiC_scaffold_8	30791395	33199167
chr9	gap		1	7716	+	HiC_scaffold_8		
chr9	falcon	000022F	1	15829378	+	HiC_scaffold_8	33206884	49318198
chr9	gap		1	4456	+	HiC_scaffold_8		
chr9	falcon	000169F	24360	4616618	+	HiC_scaffold_8	49322655	53930072
chr9	gap		1	500	+	HiC_scaffold_8		
chr9	falcon	000023F	117685	15730818	+	HiC_scaffold_8	53930573	69328562
chr9	gap		1	6738	+	HiC_scaffold_8		
chr9	falcon	000072F	1188953	9614333	+	HiC_scaffold_8	69335301	78193883
chr9	gap		1	7561	+	HiC_scaffold_8		
chr9	falcon	000431F	1	827570	+	HiC_scaffold_8	78201445	78950606
chr9	falcon	000228F	666615	3238262	+	HiC_scaffold_8	78950607	81437308
chr9	gap		1	500	+	HiC_scaffold_8		
chr9	falcon	000109F	194846	6920192	+	HiC_scaffold_8	81437809	88433549
chr9	falcon	000082F	1	8732100	+	HiC_scaffold_8	88433550	97224215
chr9	falcon	000157F	1	3391009	+	HiC_scaffold_8	97224216	100673658

chr9	falcon	000120F	1	6480300	+	HiC_scaffold_8	100673659	107390249
chr9	gap		1	399	+	HiC_scaffold_8		
chr9	falcon	000261F	1	2472361	+	HiC_scaffold_8	107390649	109984972
chr9	gap		1	8080	+	HiC_scaffold_8		
chr9	falcon	000187F	1	4208207	+	HiC_scaffold_8	109993053	114151860
chr10	falcon	000273F	1	2355442	+	HiC_scaffold_3	1	2342321
chr10	gap		1	37251	+	HiC_scaffold_3		
chr10	falcon	000164F	1	4814620	+	HiC_scaffold_3	2379573	7342457
chr10	gap		1	100	+	HiC_scaffold_3		
chr10	falcon	000047F	4	11784337	+	HiC_scaffold_3	7342558	19546332
chr10	falcon	000322F	4	1634951	+	HiC_scaffold_3	19546333	21201442
chr10	gap		1	4847	+	HiC_scaffold_3		
chr10	falcon	000417F	1	861512	+	HiC_scaffold_3	21206290	22077260
chr10	gap		1	7980	+	HiC_scaffold_3		
chr10	falcon	000014F	3696189	17218038	+	HiC_scaffold_3	22085241	36079653
chr10	gap		1	15829	+	HiC_scaffold_3		
chr10	falcon	000019F	1	16411431	+	HiC_scaffold_3	36095483	52539995
chr10	gap		1	100	+	HiC_scaffold_3		
chr10	falcon	000869F	1	180761	+	HiC_scaffold_3	52540096	52755085
chr10	falcon	000349F	81919	1403413	+	HiC_scaffold_3	52755086	54118553
chr10	gap		1	29822	+	HiC_scaffold_3		
chr10	falcon	000359F	1	1277269	+	HiC_scaffold_3	54148376	55522668
chr10	falcon	000114F	1	6351188	+	HiC_scaffold_3	55522669	61820196
chr10	falcon	000141F	1	5602472	+	HiC_scaffold_3	61820197	67603610
chr10	gap		1	19003	+	HiC_scaffold_3		
chr10	falcon	000132F	368258	5847321	+	HiC_scaffold_3	67622614	73352396
chr10	gap		1	7434	+	HiC_scaffold_3		
chr10	falcon	000010F	1	17113741	+	HiC_scaffold_3	73359831	90964248

chr10	falcon	000122F	6624	1552800	+	HiC_scaffold_3	90964249	92579253
chr10	falcon	000152F	24861	5189078	+	HiC_scaffold_3	92579254	97875460
chr10	falcon	000395F	10565	962246	+	HiC_scaffold_3	97875461	98877417
chr10	gap		1	8063	+	HiC_scaffold_3		
chr10	falcon	000171F	1572750	4538192	+	HiC_scaffold_3	98885481	101935968
chr10	gap		1	8931	+	HiC_scaffold_3		
chr10	falcon	000106F	1	7028230	+	HiC_scaffold_3	101944900	108997527
chr10	falcon	000264F	1	2410051	+	HiC_scaffold_3	108997528	111148667
chr11	falcon	000331F	1	1526096	+	HiC_scaffold_4	1	1615069
chr11	gap		1	100	+	HiC_scaffold_4		
chr11	falcon	000309F	1	1770555	+	HiC_scaffold_4	1615170	3539083
chr11	subsequence of a corrected read	AACCGTTTAAGCTGTGCCTCTCCC GTGGCGTCATCTGGGGTGATGT GCAAACCACCAATCCCGGCTCTAC ACGTCTCACTCGGAGCTCCTAGG CTTATATAAGGGGCTGGGTTTCT TAGCTTGGGGTCTCCCTCTAAGA AGCTGATCATCTATCTCTCAAGAT GCATTAAAGCTTTACTGCAGAAG GATCCGAGTGTTCTGCGTCGTTC TTGCTGGCGAGACGGTAGCGCG GGACATCTGGTGCCGAAACCCGG GAACTCTTCAACATCGCCGGCGC CGCGGGAGACCCCTCGGAAGACG GGGCGGATTCAGAACTGCAGGGA CGTAAGTTCAGAGAGGTATG				HiC_scaffold_4	3539084	3539246
chr11	falcon	000514F	1	502849	+	HiC_scaffold_4	3539247	4034127

chr11	subsequence of a corrected read	TGCTT				HiC_scaffold_4	4034128	4034627
chr11	falcon	000151F	1	5300539	+	HiC_scaffold_4	4034628	9537515
chr11	gap		1	8480	+	HiC_scaffold_4		
chr11	falcon	000343F	33568	1413053	+	HiC_scaffold_4	9545996	10990388
chr11	gap		1	5058	+	HiC_scaffold_4		
chr11	falcon	000591F	1	389161	+	HiC_scaffold_4	10995447	11362218
chr11	gap		1	9347	+	HiC_scaffold_4		
chr11	falcon	000085F	1	8908242	+	HiC_scaffold_4	11371566	20586570
chr11	gap		1	7907	+	HiC_scaffold_4		
chr11	falcon	000252F	1	2590268	+	HiC_scaffold_4	20594478	23270745
chr11	gap		1	24892	+	HiC_scaffold_4		
chr11	falcon	000233F	2	3109685	+	HiC_scaffold_4	23295638	26403395
chr11	falcon	000118F	1959936	6503124	+	HiC_scaffold_4	26403396	31088959
chr11	falcon	000037F	23310	13477457	+	HiC_scaffold_4	31088960	45240034
chr11	falcon	000048F	1	11893145	+	HiC_scaffold_4	45240035	56760310
chr11	gap		1	5096	+	HiC_scaffold_4		
chr11	falcon	000225F	1	3256611	+	HiC_scaffold_4	56765407	60160323
chr11	gap		1	22127	+	HiC_scaffold_4		
chr11	falcon	000110F	1	6831635	+	HiC_scaffold_4	60182451	67418300
chr11	gap		1	23067	+	HiC_scaffold_4		
chr11	falcon	000083F	1	8965241	+	HiC_scaffold_4	67441368	76701122
chr11	subsequence of a corrected read	ATACCAGGTTTTTGAATGTTCAG TGCCCAGACCCTGGACTGGCACA GTCAGGTCCACAACTCCAACCTGA GAGGCGGGGCCTGCTGCTTCGG GTTTTAAAAGCTGTTGTTGTAGA TCCTGAAGACAGAAGT				HiC_scaffold_4	76701123	76701623

chr11	falcon	000404F	1	972073	+	HiC_scaffold_4	76701624	77733875
chr11	falcon	000234F	4831	3067087	+	HiC_scaffold_4	77733876	80977548
chr11	gap		1	15747	+	HiC_scaffold_4		
chr11	falcon	000307F	1	1752265	+	HiC_scaffold_4	80993296	82772628
chr11	gap		1	5795	+	HiC_scaffold_4		
chr11	falcon	000241F	1	3043299	+	HiC_scaffold_4	82778424	85869977
chr11	gap		1	8637	+	HiC_scaffold_4		
chr11	falcon	000244F	1	2772660	+	HiC_scaffold_4	85878615	88751673
chr11	falcon	000093F	37	8299621	+	HiC_scaffold_4	88751674	97356670
chr11	gap		1	8030	+	HiC_scaffold_4		
chr11	falcon	000176F	838303	4434410	+	HiC_scaffold_4	97364701	101009716
chr11	gap		1	7938	+	HiC_scaffold_4		
chr11	falcon	000246F	1	2775603	+	HiC_scaffold_4	101017655	103907462
chr11	gap		1	144	+	HiC_scaffold_4		
chr11	falcon	000122F	1560248	6341392	+	HiC_scaffold_4	103907607	108848677
chr11	gap		1	1449	+	HiC_scaffold_4		
chr11	falcon	000332F	1	1585396	+	HiC_scaffold_4	108850127	110478139
chr12	falcon	000005F	1	21436847	+	HiC_scaffold_12	1	21770601
chr12	gap		1	8233	+	HiC_scaffold_12		
chr12	falcon	000007F	1	20659751	+	HiC_scaffold_12	21778835	42990748
chr12	gap		1	7897	+	HiC_scaffold_12		
chr12	falcon	000950F	1	153474	+	HiC_scaffold_12	42998646	43134813
chr12	gap		1	9526	+	HiC_scaffold_12		
chr12	falcon	000243F	1	2831724	+	HiC_scaffold_12	43144340	46193033
chr12	gap		1	7083	+	HiC_scaffold_12		
chr12	falcon	000089F	1	8103676	+	HiC_scaffold_12	46200117	54615548
chr12	gap		1	7017	+	HiC_scaffold_12		
chr12	falcon	000062F	1	10480951	+	HiC_scaffold_12	54622566	65296450

chr12	gap		1	7699	+	HiC_scaffold_12		
chr12	falcon	000341F	1	1431822	+	HiC_scaffold_12	65304150	66811699
chr12	gap		1	6262	+	HiC_scaffold_12		
chr12	falcon	000066F	1	9988464	+	HiC_scaffold_12	66817962	77070996
chr12	gap		1	7254	+	HiC_scaffold_12		
chr12	falcon	000492F	1	569419	+	HiC_scaffold_12	77078251	77689911
chr12	gap		1	1525	+	HiC_scaffold_12		
chr12	falcon	000067F	1	9946877	+	HiC_scaffold_12	77691437	
chr12	gap		1	10000	+	HiC_scaffold_12		
chr12	falcon	000078F	1	9339808	+	HiC_scaffold_12	87822026	97256908
chr12	gap		1	9300	+	HiC_scaffold_12		
chr12	falcon	000145F	2377373	5553824	-	HiC_scaffold_12	97266209	100591552
chr12	falcon	000298F	1	1963902	+	HiC_scaffold_12	100591553	102641841
chr12	gap		1	8991	+	HiC_scaffold_12		
chr12	falcon	000010F	17126285	18847059	+	HiC_scaffold_12	102650833	104198721
chr12	gap		1	18601	+	HiC_scaffold_12		
chr12	falcon	000557F	1	407526	+	HiC_scaffold_12	104217323	104698548
chr12	gap		1	500	+	HiC_scaffold_12		
chr12	falcon	000223F	1	3274275	+	HiC_scaffold_12	104699049	107481000
chr13	falcon	000375F	1	1043559	+	HiC_scaffold_18	1	895204
chr13	gap		1	500	+	HiC_scaffold_18		
chr13	falcon	000255F	1	2535068	+	HiC_scaffold_18	895705	3337830
chr13	gap		1	8557	+	HiC_scaffold_18		
chr13	falcon	000313F	3605	1712917	+	HiC_scaffold_18	3346388	4978743
chr13	gap		1	500	+	HiC_scaffold_18		
chr13	falcon	000378F	1	1080740	+	HiC_scaffold_18	4979244	6032945
chr13	gap		1	501	+	HiC_scaffold_18		
chr13	falcon	000117F	1	6596176	+	HiC_scaffold_18	6033447	12614650

chr13	gap		1	501	+	HiC_scaffold_18		
chr13	falcon	000406F	16	957828	+	HiC_scaffold_18	12615152	13508833
chr13	gap		1	501	+	HiC_scaffold_18		
chr13	falcon	000207F	1	3701161	+	HiC_scaffold_18	13509335	17237989
chr13	gap		1	19222	+	HiC_scaffold_18		
chr13	falcon	000549F	1	420031	+	HiC_scaffold_18	17257212	17715216
chr13	falcon	000190F	1	2380667	-	HiC_scaffold_18	17715217	20194881
chr13	gap		1	13300	+	HiC_scaffold_18		
chr13	falcon	000357F	25368	1289203	+	HiC_scaffold_18	20208182	21478736
chr13	gap		1	8035	+	HiC_scaffold_18		
chr13	falcon	000422F	1	672996	+	HiC_scaffold_18	21486772	22109874
chr13	gap		1	4576	+	HiC_scaffold_18		
chr13	falcon	000153F	958153	5103142	+	HiC_scaffold_18	22114451	26388264
chr13	gap		1	500	+	HiC_scaffold_18		
chr13	falcon	000382F	1	1083696	+	HiC_scaffold_18	26388765	27463140
chr13	gap		1	8424	+	HiC_scaffold_18		
chr13	falcon	000188F	877645	4096537	-	HiC_scaffold_18	27471565	
chr13	gap		1	10000	+	HiC_scaffold_18		
chr13	falcon	000338F	1	1476153	+	HiC_scaffold_18	30953737	32477133
chr13	gap		1	6775	+	HiC_scaffold_18		
chr13	falcon	000258F	1	2498857	+	HiC_scaffold_18	32483909	35118175
chr13	gap		1	6385	+	HiC_scaffold_18		
chr13	falcon	000260F	1	2497321	+	HiC_scaffold_18	35124561	37538764
chr13	gap		1	500	+	HiC_scaffold_18		
chr13	falcon	000018F	1	16695792	+	HiC_scaffold_18	37539265	54438994
chr13	gap		1	24372	+	HiC_scaffold_18		
chr13	falcon	000376F	1	1148400	+	HiC_scaffold_18	54463367	55656593
chr13	gap		1	8128	+	HiC_scaffold_18		

chr13	falcon	000209F	1	3625592	+	HiC_scaffold_18	55664722	59438017
chr13	gap		1	27042	+	HiC_scaffold_18		
chr13	falcon	000095F	1	8175151	+	HiC_scaffold_18	59465060	67868441
chr13	gap		1	25100	+	HiC_scaffold_18		
chr13	falcon	000108F	1	7027136	+	HiC_scaffold_18	67893542	75056232
chr13	falcon	000056F	2171	10897349	+	HiC_scaffold_18	75056233	86101360
chr13	gap		1	9165	+	HiC_scaffold_18		
chr13	falcon	002660F	1	12753	+	HiC_scaffold_18	86110526	86120977
chr13	gap		1	6858	+	HiC_scaffold_18		
chr13	falcon	000316F	4694	1606408	+	HiC_scaffold_18	86127836	87744835
chr13	gap		1	8144	+	HiC_scaffold_18		
chr13	falcon	000068F	1	9861613	+	HiC_scaffold_18	87752980	97874415
chr13	gap		1	6601	+	HiC_scaffold_18		
chr13	falcon	000317F	235714	1689273	+	HiC_scaffold_18	97881017	99274718
chr14	falcon	001174F	1	108251	+	HiC_scaffold_20	1	33705
chr14	gap		1	14836	+	HiC_scaffold_20		
chr14	falcon	000326F	1	1598495	+	HiC_scaffold_20	48542	1683371
chr14	gap		1	38180	+	HiC_scaffold_20		
chr14	falcon	000371F	1	1185269	+	HiC_scaffold_20	1721552	2888267
chr14	gap		1	33615	+	HiC_scaffold_20		
chr14	falcon	000632F	1	304280	+	HiC_scaffold_20	2921883	3239500
chr14	gap		1	8749	+	HiC_scaffold_20		
chr14	falcon	000089F	8109037	8345697	-	HiC_scaffold_20	3248250	3496717
chr14	gap		1	19391	+	HiC_scaffold_20		
chr14	falcon	000294F	1	2038727	+	HiC_scaffold_20	3516109	5668021
chr14	gap		1	21562	+	HiC_scaffold_20		
chr14	falcon	000013F	40731	17767327	+	HiC_scaffold_20	5689584	24194809
chr14	falcon	000538F	1	119085	+	HiC_scaffold_20	24194810	24306489

chr14	gap		1	500	+	HiC_scaffold_20		
chr14	falcon	000064F	1	10389687	+	HiC_scaffold_20	24306990	34395673
chr14	gap		1	7737	+	HiC_scaffold_20		
chr14	falcon	000100F	1	7804135	+	HiC_scaffold_20	34403411	42203822
chr14	falcon	000123F	1	6196873	+	HiC_scaffold_20	42203823	48677488
chr14	falcon	000126F	608545	6074579	+	HiC_scaffold_20	48677489	54381478
chr14	falcon	000138F	1	357586	+	HiC_scaffold_20	54381479	54759222
chr14	gap		1	18861	+	HiC_scaffold_20		
chr14	falcon	000096F	1	8068893	+	HiC_scaffold_20	54778084	63086613
chr14	gap		1	8610	+	HiC_scaffold_20		
chr14	falcon	000051F	5713	11156214	+	HiC_scaffold_20	63095224	74793652
chr14	gap		1	7821	+	HiC_scaffold_20		
chr14	falcon	001065F	2307	130518	+	HiC_scaffold_20	74801474	74928479
chr14	gap		1	4955	+	HiC_scaffold_20		
chr14	falcon	000277F	1	2264601	+	HiC_scaffold_20	74933435	77350862
chr14	gap		1	14295	+	HiC_scaffold_20		
chr14	falcon	000272F	1	2350555	+	HiC_scaffold_20	77365158	79823138
chr14	gap		1	7952	+	HiC_scaffold_20		
chr14	falcon	000014F	1	3689669	+	HiC_scaffold_20	79831091	83396219
chr14	gap		1	17898	+	HiC_scaffold_20		
chr14	falcon	000177F	1161	4412533	+	HiC_scaffold_20	83414118	87854995
chr15	falcon	000211F	1	3547655	+	HiC_scaffold_6	1	3694810
chr15	falcon	000568F	88194	416154	+	HiC_scaffold_6	3694811	4034462
chr15	gap		1	30677	+	HiC_scaffold_6		
chr15	falcon	000020F	1	16351333	+	HiC_scaffold_6	4065140	20826100
chr15	gap		1	9298	+	HiC_scaffold_6		
chr15	falcon	000044F	1	12558169	+	HiC_scaffold_6	20835399	33819596
chr15	gap		1	8739	+	HiC_scaffold_6		

chr15	falcon	000451F	3151	679200	+	HiC_scaffold_6	33828336	34421486
chr15	gap		1	8164	+	HiC_scaffold_6		
chr15	falcon	000149F	1	5420795	+	HiC_scaffold_6	34429651	40003888
chr15	gap		1	7998	+	HiC_scaffold_6		
chr15	falcon	000098F	1562	8025863	+	HiC_scaffold_6	40011887	48586673
chr15	gap		1	7805	+	HiC_scaffold_6		
chr15	falcon	000613F	1	336811	+	HiC_scaffold_6	48594479	48807977
chr15	falcon	000288F	35602	2108753	+	HiC_scaffold_6	48807978	50996287
chr15	gap		1	88	+	HiC_scaffold_6		
chr15	falcon	000140F	699833	5612819	+	HiC_scaffold_6	50996376	
chr15	gap		1	10000	+	HiC_scaffold_6		
chr15	falcon	000214F	72772	3469584	+	HiC_scaffold_6	60737207	64317922
chr15	gap		1	19769	+	HiC_scaffold_6		
chr15	falcon	000070F	4933	9646566	+	HiC_scaffold_6	64337692	74611065
chr15	gap		1	8072	+	HiC_scaffold_6		
chr15	falcon	000324F	1	1611222	+	HiC_scaffold_6	74619138	76087288
chr15	gap		1	15502	+	HiC_scaffold_6		
chr15	falcon	000323F	1	1625411	+	HiC_scaffold_6	76102791	77799882
chr15	gap		1	6980	+	HiC_scaffold_6		
chr15	falcon	000157F	3411291	4985286	-	HiC_scaffold_6	77806863	
chr15	gap		1	10000	+	HiC_scaffold_6		
chr15	falcon	000137F	1	5721134	+	HiC_scaffold_6	79066330	80979120
chr15	gap		1	13910	+	HiC_scaffold_6		
chr15	falcon	000131F	1	5943813	+	HiC_scaffold_6	80993031	87169159
chr15	gap		1	13377	+	HiC_scaffold_6		
chr15	falcon	000546F	196008	428375	+	HiC_scaffold_6	87182537	87415047
chr15	gap		1	14863	+	HiC_scaffold_6		
chr15	falcon	000308F	1	74956	+	HiC_scaffold_6	87429911	87493036

chr15	gap		1	3404	+	HiC_scaffold_6		
chr15	falcon	000639F	1	293031	+	HiC_scaffold_6	87496441	87748692
chr15	gap		1	22743	+	HiC_scaffold_6		
chr15	falcon	000418F	1	824327	+	HiC_scaffold_6	87771436	88323766
chr16	falcon	000119F	1	6507223	+	HiC_scaffold_15	1	6525550
chr16	gap		1	99	+	HiC_scaffold_15		
chr16	falcon	000436F	1	799067	+	HiC_scaffold_15	6525650	7332422
chr16	gap		1	9899	+	HiC_scaffold_15		
chr16	falcon	000160F	1	4837371	+	HiC_scaffold_15	7342322	12241594
chr16	gap		1	24933	+	HiC_scaffold_15		
chr16	falcon	000102F	1	7627344	+	HiC_scaffold_15	12266528	20218070
chr16	falcon	000293F	1	1923010	+	HiC_scaffold_15	20218071	22204893
chr16	falcon	000951F	1	163518	+	HiC_scaffold_15	22204894	22359387
chr16	gap		1	6794	+	HiC_scaffold_15		
chr16	falcon	000282F	244424	2229215	+	HiC_scaffold_15	22366182	24372216
chr16	falcon	000134F	1407949	5855931	+	HiC_scaffold_15	24372217	28970298
chr16	falcon	000171F	4756	1556766	-	HiC_scaffold_15	28970299	30581465
chr16	gap		1	27135	+	HiC_scaffold_15		
chr16	falcon	000061F	1	10463620	+	HiC_scaffold_15	30608601	41369718
chr16	gap		1	16973	+	HiC_scaffold_15		
chr16	falcon	002023F	1	38543	+	HiC_scaffold_15	41386692	41411854
chr16	gap		1	5826	+	HiC_scaffold_15		
chr16	falcon	000240F	1	3044126	+	HiC_scaffold_15	41417681	44679120
chr16	gap		1	26000	+	HiC_scaffold_15		
chr16	falcon	000065F	60	10121793	+	HiC_scaffold_15	44705121	55187790
chr16	gap		1	10370	+	HiC_scaffold_15		
chr16	falcon	000247F	1	2702874	+	HiC_scaffold_15	55198161	57977170
chr16	gap		1	7716	+	HiC_scaffold_15		

chr16	falcon	000045F	1	12397204	+	HiC_scaffold_15	57984887	70753153
chr16	falcon	000063F	198198	10482355	+	HiC_scaffold_15	70753154	81432301
chr16	gap		1	6820	+	HiC_scaffold_15		
chr16	falcon	000232F	1	3081013	+	HiC_scaffold_15	81439122	84571688
chr16	gap		1	3318	+	HiC_scaffold_15		
chr16	falcon	000527F	1	60244		HiC_scaffold_15	84575007	
chr16	gap		1	10000	+	HiC_scaffold_15		
chr16	falcon	000193F	2001	1124064	+	HiC_scaffold_15	84643598	85680182
chr16	gap		1	6900	+	HiC_scaffold_15		
chr16	falcon	000571F	338380	396102	-	HiC_scaffold_15	85687083	85744741
chr16	gap		1	4671	+	HiC_scaffold_15		
chr16	falcon	000305F	8	1887383	+	HiC_scaffold_15	85749413	87603965
chr17	falcon	000075F	1	9373204	+	HiC_scaffold_11	1	9549632
chr17	gap		1	500	+	HiC_scaffold_11		
chr17	falcon	000097F	1	8030563	+	HiC_scaffold_11	9550133	17728789
chr17	gap		1	4465	+	HiC_scaffold_11		
chr17	falcon	000092F	1	8388593	+	HiC_scaffold_11	17733255	26342953
chr17	falcon	000200F	49	3843161	+	HiC_scaffold_11	26342954	30238504
chr17	gap		1	31719	+	HiC_scaffold_11		
chr17	falcon	000268F	1	2335460	+	HiC_scaffold_11	30270224	32519346
chr17	gap		1	8308	+	HiC_scaffold_11		
chr17	falcon	000667F	18	271158	+	HiC_scaffold_11	32527655	32798879
chr17	gap		1	2334	+	HiC_scaffold_11		
chr17	falcon	000028F	1	14186338	+	HiC_scaffold_11	32801214	47211624
chr17	gap		1	1769	+	HiC_scaffold_11		
chr17	falcon	000129F	1	6059729	+	HiC_scaffold_11	47213394	53336630
chr17	gap		1	8085	+	HiC_scaffold_11		
chr17	falcon	000414F	1	834482	+	HiC_scaffold_11	53344716	54215145

chr17	gap		1	6603	+	HiC_scaffold_11		
chr17	falcon	000269F	1	2348110	+	HiC_scaffold_11	54221749	56513556
chr17	falcon	000168F	1	4044123	+	HiC_scaffold_11	56513557	60771325
chr17	falcon	000033F	1	14414957	+	HiC_scaffold_11	60771326	75652573
chr17	gap		1	2074	+	HiC_scaffold_11		
chr17	falcon	000353F	220728	1358395	+	HiC_scaffold_11	75654648	76852229
chr17	gap		1	6166	+	HiC_scaffold_11		
chr17	falcon	000274F	1	2289710	+	HiC_scaffold_11	76858396	
chr17	gap		1	10000	+	HiC_scaffold_11		
chr17	falcon	000365F	5	1240879	+	HiC_scaffold_11	79327626	80635772
chr17	gap		1	793	+	HiC_scaffold_11		
chr17	falcon	000156F	1	4949819	+	HiC_scaffold_11	80636566	85505749
chr18	falcon	000346F	1	1414850	+	HiC_scaffold_21	1	1421566
chr18	gap		1	8288	+	HiC_scaffold_21		
chr18	falcon	000128F	4172	6109759	+	HiC_scaffold_21	1429855	7723864
chr18	gap		1	7576	+	HiC_scaffold_21		
chr18	falcon	000046F	10652622	12267313	+	HiC_scaffold_21	7731441	
chr18	gap		1	10000	+	HiC_scaffold_21		
chr18	falcon	000633F	286253	310020	+	HiC_scaffold_21	9388052	9411677
chr18	subsequence of a corrected read	CAAGAAGGATGTCCTTTTATTCTT GAAAGTACTCCAAATAAACTAACA CCATAATTTGAATAATAATAGAGG GGTTGACAGAGACATAATGCATT ATGATGAGATGATTA				HiC_scaffold_21	9411678	9412259
chr18	falcon	000118F	14	1939510	+	HiC_scaffold_21	9412260	11443382
chr18	gap		1	10675	+	HiC_scaffold_21		
chr18	falcon	000278F	1	2261313	+	HiC_scaffold_21	11454058	13783278
chr18	gap		1	7903	+	HiC_scaffold_21		

chr18	falcon	000266F	1	2203920	+	HiC_scaffold_21	13791182	16116307
chr18	falcon	000125F	1	5767593	+	HiC_scaffold_21	16116308	22124047
chr18	gap		1	6739	+	HiC_scaffold_21		
chr18	falcon	000236F	1	3099382	+	HiC_scaffold_21	22130787	
chr18	gap		1	10000	+	HiC_scaffold_21		
chr18	falcon	000237F	1	3058734	+	HiC_scaffold_21	25374881	28649162
chr18	falcon	000080F	6309684	9251274	+	HiC_scaffold_21	28649163	31599800
chr18	gap		1	7190	+	HiC_scaffold_21		
chr18	falcon	000257F	134747	2568028	+	HiC_scaffold_21	31606991	34012903
chr18	gap		1	7162	+	HiC_scaffold_21		
chr18	falcon	000167F	1	4731064	+	HiC_scaffold_21	34020066	38918547
chr18	falcon	000300F	1	1912895	+	HiC_scaffold_21	38918548	40896171
chr18	gap		1	8167	+	HiC_scaffold_21		
chr18	falcon	000548F	11959	428203	+	HiC_scaffold_21	40904339	
chr18	gap		1	10000	+	HiC_scaffold_21		
chr18	falcon	000050F	1	11322188	+	HiC_scaffold_21	41277065	52889165
chr18	gap		1	74	+	HiC_scaffold_21		
chr18	falcon	000356F	1	1310547	+	HiC_scaffold_21	52889240	54026093
chr18	gap		1	1581	+	HiC_scaffold_21		
chr18	falcon	000201F	1	3593464	+	HiC_scaffold_21	54027675	57592295
chr18	gap		1	7852	+	HiC_scaffold_21		
chr18	falcon	000178F	25108	4389721	+	HiC_scaffold_21	57600148	62057817
chr18	gap		1	5145	+	HiC_scaffold_21		
chr18	falcon	000180F	1	4301594	+	HiC_scaffold_21	62062963	66353987
chr18	gap		1	2411	+	HiC_scaffold_21		
chr18	falcon	000248F	106477	2546317	+	HiC_scaffold_21	66356399	
chr18	gap		1	10000	+	HiC_scaffold_21		
chr18	falcon	000021F	248683	587061	+	HiC_scaffold_21	69024828	69118911

chr18	gap		1	500	+	HiC_scaffold_21		
chr18	falcon	000434F	145799	754792	+	HiC_scaffold_21	69119412	69611568
chr18	gap		1	500	+	HiC_scaffold_21		
chr18	falcon	000265F	661491	2432977	+	HiC_scaffold_21	69612069	71193379
chr18	gap		1	500	+	HiC_scaffold_21		
chr18	falcon	000384F	237755	1079048	+	HiC_scaffold_21	71193880	71955936
chr18	gap		1	500	+	HiC_scaffold_21		
chr18	falcon	000360F	1	1278487	+	HiC_scaffold_21	71956437	73106746
chr18	gap		1	7572	+	HiC_scaffold_21		
chr18	falcon	000354F	1	1282377	+	HiC_scaffold_21	73114319	74439525
chr18	gap		1	500	+	HiC_scaffold_21		
chr18	falcon	000263F	82651	2452372	+	HiC_scaffold_21	74440026	76795703
chr18	gap		1	500	+	HiC_scaffold_21		
chr19	falcon	000173F	1	4487210	+	HiC_scaffold_19	1	4571520
chr19	subsequence of a corrected read	ACCCATGAGTCACGAAATAGTTTGCATGTACTGAGATGTCCCGC				HiC_scaffold_19	4571521	4571550
chr19	falcon	000205F	1	3750909	+	HiC_scaffold_19	4571551	8480559
chr19	gap		1	8185	+	HiC_scaffold_19		
chr19	falcon	000038F	1	13229099	+	HiC_scaffold_19	8488745	22125684
chr19	gap		1	4445	+	HiC_scaffold_19		
chr19	falcon	000139F	1	5656796	+	HiC_scaffold_19	22130130	27912283
chr19	falcon	000101F	504	7493717	+	HiC_scaffold_19	27912284	35614478
chr19	falcon	000217F	1	3446513	+	HiC_scaffold_19	35614479	39253106
chr19	gap		1	8303	+	HiC_scaffold_19		
chr19	falcon	000055F	1	10236176	+	HiC_scaffold_19	39261410	49908744
chr19	gap		1	499	+	HiC_scaffold_19		
chr19	falcon	000194F	1	3845754	+	HiC_scaffold_19	49909244	53818770
chr19	gap		1	501	+	HiC_scaffold_19		

chr19	falcon	001469F	1	80018	+	HiC_scaffold_19	53819272	53895950
chr19	gap		1	6889	+	HiC_scaffold_19		
chr19	falcon	000227F	1	3171452	+	HiC_scaffold_19	53902840	57137851
chr19	gap		1	4115	+	HiC_scaffold_19		
chr19	falcon	000358F	4	1286090	+	HiC_scaffold_19	57141967	58492560
chr19	gap		1	32737	+	HiC_scaffold_19		
chr19	falcon	000210F	1	3612248	+	HiC_scaffold_19	58525298	62237451
chr19	gap		1	8307	+	HiC_scaffold_19		
chr19	falcon	000087F	1	8408638	+	HiC_scaffold_19	62245759	70909541
chr19	gap		1	8911	+	HiC_scaffold_19		
chr19	falcon	000287F	959700	2157314	-	HiC_scaffold_19	70918453	72157535
chr19	falcon	000503F	1	534605	+	HiC_scaffold_19	72157536	72719326
chr19	gap		1	7854	+	HiC_scaffold_19		
chr19	falcon	000254F	1	2584086	+	HiC_scaffold_19	72727181	75330604
chr20	falcon	000113F	1	6776902	+	HiC_scaffold_2	1	7027770
chr20	gap		1	33635	+	HiC_scaffold_2		
chr20	falcon	001714F	6298	8068		HiC_scaffold_2	7061406	7071200
chr20	falcon	000073F	8	9632707	+	HiC_scaffold_2	7071201	17027067
chr20	falcon	000042F	3846	2450347	-	HiC_scaffold_2	17027068	19639428
chr20	falcon	000380F	111112	1088176	+	HiC_scaffold_2	19639429	20612275
chr20	subsequence of a corrected read	TTTGTTATTTTCCCTCGCCCCTCT AAGAAATACGCCTTTCCTTTTCTG TTCCAGGTAGGGCTTGACGGGTA CACAGCTCTAGCCAATCAGACTGC CCAGTCTTTTGTCCTTGGTGGGA GAAAAGGTTGTTCAGGGAGTAGT				HiC_scaffold_2	20612276	20612430
chr20	falcon	000226F	1	1171280	+	HiC_scaffold_2	20612431	21827471
chr20	gap		1	8370	+	HiC_scaffold_2		

chr20	falcon	000071F	2001	9391647	+	HiC_scaffold_2	21835842	31465450
chr20	gap		1	6163	+	HiC_scaffold_2		
chr20	falcon	000226F	1208067	3287616	+	HiC_scaffold_2	31471614	33651870
chr21	falcon	000342F	1	1448643	+	HiC_scaffold_7	1	1195858
chr21	gap		1	499	+	HiC_scaffold_7		
chr21	falcon	000413F	131874	921538	+	HiC_scaffold_7	1196358	
chr21	gap		1	10000	+	HiC_scaffold_7		
chr21	falcon	000859F	1	98645	+	HiC_scaffold_7	1770476	
chr21	gap		1	10000	+	HiC_scaffold_7		
chr21	falcon	000761F	90280	167392	-	HiC_scaffold_7	1725798	
chr21	gap		1	10000	+	HiC_scaffold_7		
chr21	falcon	000482F	221725	577784	+	HiC_scaffold_7	2137830	
chr21	gap		1	10000	+	HiC_scaffold_7		
chr21	falcon	000270F	1	2339343	+	HiC_scaffold_7	2536657	4880612
chr21	gap		1	7512	+	HiC_scaffold_7		
chr21	falcon	000600F	1	371710	+	HiC_scaffold_7	4888125	5392120
chr21	gap		1	16768	+	HiC_scaffold_7		
chr21	falcon	000614F	1	324522	+	HiC_scaffold_7	5408889	5541837
chr21	gap		1	9497	+	HiC_scaffold_7		
chr21	falcon	000423F	13	810289	+	HiC_scaffold_7	5551335	6390469
chr21	gap		1	8770	+	HiC_scaffold_7		
chr21	falcon	000333F	1	1565677	+	HiC_scaffold_7	6399240	8007117
chr21	gap		1	16786	+	HiC_scaffold_7		
chr21	falcon	000377F	1	1116375	+	HiC_scaffold_7	8023904	9310891
chr21	gap		1	9663	+	HiC_scaffold_7		
chr21	falcon	000386F	1	1060639	+	HiC_scaffold_7	9320555	10266284
chr21	gap		1	23203	+	HiC_scaffold_7		
chr21	falcon	000290F	1	2127523	+	HiC_scaffold_7	10289488	12130971

chr21	gap		1	9840	+	HiC_scaffold_7		
chr21	falcon	000573F	1	318121	+	HiC_scaffold_7	12140812	12482733
chr21	gap		1	593	+	HiC_scaffold_7		
chr21	falcon	000325F	1	1602360	+	HiC_scaffold_7	12483327	13947281
chr21	gap		1	1999	+	HiC_scaffold_7		
chr21	falcon	000184F	1	4254682	+	HiC_scaffold_7	13949281	18327795
chr21	gap		1	8562	+	HiC_scaffold_7		
chr21	falcon	000854F	1	174872	+	HiC_scaffold_7	18336358	18509513
chr21	gap		1	8150	+	HiC_scaffold_7		
chr21	falcon	000253F	1	2569911	+	HiC_scaffold_7	18517664	
chr21	gap		1	10000	+	HiC_scaffold_7		
chr21	falcon	000887F	1	162358	+	HiC_scaffold_7	21151519	21303521
chr21	gap		1	500	+	HiC_scaffold_7		
chr21	falcon	000175F	1	4434222	+	HiC_scaffold_7	21304022	25772566
chr21	falcon	000295F	1	1733073	+	HiC_scaffold_7	25772567	27601711
chr21	gap		1	17728	+	HiC_scaffold_7		
chr21	falcon	000303F	1	1915825	+	HiC_scaffold_7	27619440	29446437
chr18	falcon	000163F	1	4754744	+	HiC_scaffold_21	76796204	81383262
chr22	falcon	000499F	1	550546	+	HiC_scaffold_22	1	514575
chr22	gap		1	323	+	HiC_scaffold_22		
chr22	falcon	000526F	1	437339	+	HiC_scaffold_22	514899	938167
chr22	gap		1	8020	+	HiC_scaffold_22		
chr22	falcon	001766F	1	48825	+	HiC_scaffold_22	946188	988753
chr22	gap		1	20430	+	HiC_scaffold_22		
chr22	falcon	000574F	953	401690	+	HiC_scaffold_22	1009184	1336039
chr22	gap		1	1179	+	HiC_scaffold_22		
chr22	falcon	001327F	1	94112	+	HiC_scaffold_22	1337219	1429198
chr22	gap		1	10803	+	HiC_scaffold_22		

chr22	falcon	000694F	1	268418	+	HiC_scaffold_22	1440002	1708790
chr22	gap		1	6634	+	HiC_scaffold_22		
chr22	falcon	000490F	1	578505	+	HiC_scaffold_22	1715425	2241860
chr22	gap		1	501	+	HiC_scaffold_22		
chr22	falcon	000590F	1	383315	+	HiC_scaffold_22	2242362	2567726
chr22	gap		1	5435	+	HiC_scaffold_22		
chr22	falcon	002393F	1	31361	+	HiC_scaffold_22	2573162	2594209
chr22	gap		1	5299	+	HiC_scaffold_22		
chr22	falcon	000559F	1	220933	+	HiC_scaffold_22	2599509	2838980
chr22	gap		1	26173	+	HiC_scaffold_22		
chr22	falcon	000535F	1	450222	+	HiC_scaffold_22	2865154	3343878
chr22	gap		1	7956	+	HiC_scaffold_22		
chr22	falcon	000374F	1	1156391	+	HiC_scaffold_22	3351835	
chr22	gap		1	10000	+	HiC_scaffold_22		
chr22	falcon	000901F	1	159535	+	HiC_scaffold_22	4520825	4670819
chr22	gap		1	9449	+	HiC_scaffold_22		
chr22	falcon	000555F	1	152232	+	HiC_scaffold_22	4680269	4822307
chr22	gap		1	2518	+	HiC_scaffold_22		
chr22	falcon	000669F	1	314455	+	HiC_scaffold_22	4824826	5105144
chr22	gap		1	12830	+	HiC_scaffold_22		
chr22	falcon	001328F	1	87543	+	HiC_scaffold_22	5117975	
chr22	gap		1	10000	+	HiC_scaffold_22		
chr22	falcon	000396F	1	996930	+	HiC_scaffold_22	5204357	6203873
chr22	gap		1	7375	+	HiC_scaffold_22		
chr22	falcon	000454F	1	683989	+	HiC_scaffold_22	6211249	6969173
chr22	gap		1	4616	+	HiC_scaffold_22		
chr22	falcon	001159F	1	104334	+	HiC_scaffold_22	6973790	7067392
chr22	gap		1	2000	+	HiC_scaffold_22		

chr22	falcon	000586F	1	310830	+	HiC_scaffold_22	7069393	7432630
chr22	gap		1	32312	+	HiC_scaffold_22		
chr22	falcon	000749F	74060	250616	-	HiC_scaffold_22	7464943	
chr22	gap		1	10000	+	HiC_scaffold_22		
chr22	falcon	000488F	1	503513	+	HiC_scaffold_22	7656780	8198952
chr22	gap		1	8077	+	HiC_scaffold_22		
chr22	falcon	000656F	1	276050	+	HiC_scaffold_22	8207030	8518391
chr22	gap		1	10462	+	HiC_scaffold_22		
chr22	falcon	000569F	1	410135	+	HiC_scaffold_22	8528854	
chr22	gap		1	10000	+	HiC_scaffold_22		
chr22	falcon	000539F	502	437162	+	HiC_scaffold_22	9020698	
chr22	gap		1	10000	+	HiC_scaffold_22		
chr22	falcon	000383F	1	971759	+	HiC_scaffold_22	9336240	
chr22	gap		1	10000	+	HiC_scaffold_22		
chr22	falcon	000602F	1277	327137	+	HiC_scaffold_22	9576676	
chr22	gap		1	10000	+	HiC_scaffold_22		
chr22	falcon	000857F	1	107818	+	HiC_scaffold_22	9846168	
chr22	gap		1	10000	+	HiC_scaffold_22		
chr22	falcon	000758F	1	184766	+	HiC_scaffold_22	10692837	10880477
chr22	gap		1	100	+	HiC_scaffold_22		
chr22	falcon	000562F	1	403794	+	HiC_scaffold_22	10880578	11240285
chr22	gap		1	208	+	HiC_scaffold_22		
chr22	falcon	000425F	1	801643	+	HiC_scaffold_22	11240494	12081051
chr22	gap		1	6485	+	HiC_scaffold_22		
chr22	falcon	000534F	1	460813	+	HiC_scaffold_22	12087537	12538300
chr22	gap		1	7469	+	HiC_scaffold_22		
chr22	falcon	000419F	1	770112	+	HiC_scaffold_22	12545770	
chr22	gap		1	10000	+	HiC_scaffold_22		

chr22	falcon	000335F	2581	1517104	+	HiC_scaffold_22	13283088	
chr22	gap		1	10000	+	HiC_scaffold_22		
chr22	falcon	000389F	1	1035836	+	HiC_scaffold_22	14890775	15857511
chr22	gap		1	1741	+	HiC_scaffold_22		
chr22	falcon	000415F	1	624122	+	HiC_scaffold_22	15859253	16596344
chr22	gap		1	3369	+	HiC_scaffold_22		
chr22	falcon	000477F	1	600482	+	HiC_scaffold_22	16599714	17143784
chr22	falcon	000907F	986	158273	+	HiC_scaffold_22	17143785	17273960
chr22	gap		1	8096	+	HiC_scaffold_22		
chr22	falcon	001076F	1	116927	+	HiC_scaffold_22	17282057	17401248
chr22	gap		1	35938	+	HiC_scaffold_22		
chr22	falcon	000410F	1	937905	+	HiC_scaffold_22	17437187	18375906
chr22	gap		1	15825	+	HiC_scaffold_22		
chr22	falcon	000370F	1	1157215	+	HiC_scaffold_22	18391732	
chr22	gap		1	10000	+	HiC_scaffold_22		
chr22	falcon	001012F	1	126079	+	HiC_scaffold_22	19692225	19817102
chr22	gap		1	23663	+	HiC_scaffold_22		
chr22	falcon	000661F	1	276525	+	HiC_scaffold_22	19840766	20129999
chr22	gap		1	15529	+	HiC_scaffold_22		
chr22	falcon	000443F	1	765998	+	HiC_scaffold_22	20145529	20817464
chr22	gap		1	6242	+	HiC_scaffold_22		
chr22	falcon	001511F	1	73583	+	HiC_scaffold_22	20823707	20888495
chr22	gap		1	14272	+	HiC_scaffold_22		
chr22	falcon	000401F	1	990256	+	HiC_scaffold_22	20902768	21911217
chr22	gap		1	8716	+	HiC_scaffold_22		
chr22	falcon	000314F	1	1714028	+	HiC_scaffold_22	21919934	23724306
chr22	gap		1	2849	+	HiC_scaffold_22		
chr22	falcon	000605F	1	345413	+	HiC_scaffold_22	23727156	24081003

chr22	gap		1	7322	+	HiC_scaffold_22		
chr22	falcon	001552F	1	64048	+	HiC_scaffold_22	24088326	24147216
chr22	gap		1	9264	+	HiC_scaffold_22		
chr22	falcon	000411F	1	912270	+	HiC_scaffold_22	24156481	25129277
chr22	gap		1	7670	+	HiC_scaffold_22		
chr22	falcon	000469F	1	674710	+	HiC_scaffold_22	25136948	25776063
chr22	gap		1	6170	+	HiC_scaffold_22		
chr22	falcon	000851F	1	196899	+	HiC_scaffold_22	25782234	25976583
chr22	gap		1	6175	+	HiC_scaffold_22		
chr22	falcon	000426F	1	801970	+	HiC_scaffold_22	25982759	26805218
chr22	gap		1	6156	+	HiC_scaffold_22		
chr22	falcon	000361F	1	1268488	+	HiC_scaffold_22	26811375	28109687
chr22	gap		1	5241	+	HiC_scaffold_22		
chr22	falcon	002389F	1	28151	+	HiC_scaffold_22	28114929	28141152
chr22	gap		1	31893	+	HiC_scaffold_22		
chr22	falcon	002793F	1	20090	+	HiC_scaffold_22	28173046	28192762
chr22	gap		1	280	+	HiC_scaffold_22		
chr22	falcon	002560F	1	22116	+	HiC_scaffold_22	28193043	28215091
chr22	gap		1	568	+	HiC_scaffold_22		
chr22	falcon	001341F	1	79755	+	HiC_scaffold_22	28215660	28301696
chr22	gap		1	3663	+	HiC_scaffold_22		
chr22	falcon	000687F	1	251135	+	HiC_scaffold_22	28305360	28552808
chr22	gap		1	5072	+	HiC_scaffold_22		
chr22	falcon	001517F	1	62448	+	HiC_scaffold_22	28557881	28629837
chr22	gap		1	6849	+	HiC_scaffold_22		
chr22	falcon	001575F	1	61166	+	HiC_scaffold_22	28636687	28696775
chr22	gap		1	12617	+	HiC_scaffold_22		
chr22	falcon	000476F	231576	604442	+	HiC_scaffold_22	28709393	29091948

chr22	gap		1	6708	+	HiC_scaffold_22		
chr22	falcon	000674F	1	266822	+	HiC_scaffold_22	29098657	29360209
chr22	gap		1	3248	+	HiC_scaffold_22		
chr22	falcon	000453F	1	693180	+	HiC_scaffold_22	29363458	30106952
chr22	gap		1	6462	+	HiC_scaffold_22		
chr22	falcon	000537F	1	444853	+	HiC_scaffold_22	30113415	30600682
chr22	gap		1	20726	+	HiC_scaffold_22		
chr22	falcon	001397F	1	76022	+	HiC_scaffold_22	30621409	30696938
chr22	gap		1	11446	+	HiC_scaffold_22		
chr22	falcon	000297F	1	1992451	+	HiC_scaffold_22	30708385	32779716
chr22	gap		1	7451	+	HiC_scaffold_22		
chr22	falcon	001576F	1	40812	+	HiC_scaffold_22	32787168	32822692
chr22	falcon	000705F	1	252007	+	HiC_scaffold_22	32822693	33064883
chr22	gap		1	9935	+	HiC_scaffold_22		
chr22	falcon	001096F	1	119006	+	HiC_scaffold_22	33074819	33198299
chr22	gap		1	500	+	HiC_scaffold_22		
chr22	falcon	000287F	1	894242	+	HiC_scaffold_22	33198800	34093675
chr22	gap		1	501	+	HiC_scaffold_22		
chr22	falcon	000493F	1	572190	+	HiC_scaffold_22	34094177	
chr22	gap		1	10000	+	HiC_scaffold_22		
chr22	falcon	000902F	1	158135	+	HiC_scaffold_22	34537171	34702798
chr22	gap		1	8458	+	HiC_scaffold_22		
chr22	falcon	000676F	1	264156	+	HiC_scaffold_22	34711257	34989190
chr22	gap		1	6306	+	HiC_scaffold_22		
chr22	falcon	001313F	1	84231	+	HiC_scaffold_22	34995497	35074646
chr22	gap		1	10054	+	HiC_scaffold_22		
chr22	falcon	000399F	1	1002678	+	HiC_scaffold_22	35084701	36113472
chr22	gap		1	5621	+	HiC_scaffold_22		

chr22	falcon	000556F	1	417370	+	HiC_scaffold_22	36119094	36553695
chr22	gap		1	869	+	HiC_scaffold_22		
chr22	falcon	000515F	1	495855	+	HiC_scaffold_22	36554565	37066976
chr22	gap		1	7166	+	HiC_scaffold_22		
chr22	falcon	000456F	1	673538	+	HiC_scaffold_22	37074143	37781822
chr22	gap		1	6111	+	HiC_scaffold_22		
chr22	falcon	003200F	1	18103	+	HiC_scaffold_22	37787934	37800521
chr22	gap		1	36937	+	HiC_scaffold_22		
chr22	falcon	000295F	1851372	1994414	-	HiC_scaffold_22	37837459	
chr22	gap		1	10000	+	HiC_scaffold_22		
chr22	falcon	001150F	1	107332	+	HiC_scaffold_22	38129900	38234251
chr22	gap		1	3749	+	HiC_scaffold_22		
chr22	falcon	000564F	1	409057	+	HiC_scaffold_22	38238001	38660579
chr22	gap		1	7952	+	HiC_scaffold_22		
chr22	falcon	000472F	1	646332	+	HiC_scaffold_22	38668532	39267813
chr22	gap		1	3837	+	HiC_scaffold_22		
chr22	falcon	002567F	1	10752	+	HiC_scaffold_22	39271651	39282234
chr22	falcon	000267F	5475	2375305	+	HiC_scaffold_22	39282235	41667580
chr22	gap		1	9644	+	HiC_scaffold_22		
chr22	falcon	000304F	825537	1896565	+	HiC_scaffold_22	41677225	42832912
chr22	falcon	000471F	14627	625425	+	HiC_scaffold_22	42832913	43468647
chr22	gap		1	6439	+	HiC_scaffold_22		
chr22	falcon	001582F	1	65384	+	HiC_scaffold_22	43475087	43540174
chr22	gap		1	5027	+	HiC_scaffold_22		
chr22	falcon	000422F	680936	826398	-	HiC_scaffold_22	43545202	
chr22	gap		1	10000	+	HiC_scaffold_22		
chr22	falcon	000603F	1	352982	+	HiC_scaffold_22	43672255	44030628
chr22	gap		1	32241	+	HiC_scaffold_22		

chr22	falcon	000355F	1	1322473	+	HiC_scaffold_22	44062870	45432795
chr22	gap		1	2225	+	HiC_scaffold_22		
chr22	falcon	000785F	1	215686	+	HiC_scaffold_22	45435021	45662965
chr22	gap		1	20269	+	HiC_scaffold_22		
chr22	falcon	001031F	1	139750	+	HiC_scaffold_22	45683235	45832093
chr22	gap		1	18821	+	HiC_scaffold_22		
chr22	falcon	000403F	1	958173	+	HiC_scaffold_22	45850915	46814539
chr22	gap		1	6350	+	HiC_scaffold_22		
chr22	falcon	000666F	1	272627	+	HiC_scaffold_22	46820890	47089989
chr22	gap		1	21158	+	HiC_scaffold_22		
chr22	falcon	000125F	5774006	6150690	-	HiC_scaffold_22	47111148	47515033
chr22	falcon	000688F	18321	263793	+	HiC_scaffold_22	47515034	47762591
chr22	gap		1	10626	+	HiC_scaffold_22		
chr22	falcon	001056F	1	123398	+	HiC_scaffold_22	47773218	47911839
chr22	gap		1	101	+	HiC_scaffold_22		
chr22	falcon	000560F	1	419459	+	HiC_scaffold_22	47911941	48374562
chr22	gap		1	11351	+	HiC_scaffold_22		
chr22	falcon	000502F	1	528368	+	HiC_scaffold_22	48385914	48933787
chr22	gap		1	5014	+	HiC_scaffold_22		
chr22	falcon	000104F	7072279	7365078	-	HiC_scaffold_22	48938802	49233093
chr22	gap		1	6514	+	HiC_scaffold_22		
chr22	falcon	000334F	1	1538222	+	HiC_scaffold_22	49239608	50694918
chr22	gap		1	7774	+	HiC_scaffold_22		
chr22	falcon	002950F	1	44557	+	HiC_scaffold_22	50702693	50747224
chr22	gap		1	8254	+	HiC_scaffold_22		
chr22	falcon	000675F	1	259835	+	HiC_scaffold_22	50755479	51032160
chr22	gap		1	17012	+	HiC_scaffold_22		
chr22	falcon	003251F	1	6384	+	HiC_scaffold_22	51049173	51055548

chr22	gap		1	2175	+	HiC_scaffold_22		
chr22	falcon	000903F	19597	159894	+	HiC_scaffold_22	51057724	51202947
chr22	gap		1	12786	+	HiC_scaffold_22		
chr22	falcon	000409F	1	950525	+	HiC_scaffold_22	51215734	52255347
chr22	gap		1	24970	+	HiC_scaffold_22		
chr22	falcon	000506F	72	518855	+	HiC_scaffold_22	52280318	52892079
chr22	gap		1	25500	+	HiC_scaffold_22		
chr22	falcon	000201F	3600255	3780435	-	HiC_scaffold_22	52917580	53104114
chr22	gap		1	6851	+	HiC_scaffold_22		
chr22	falcon	000344F	1	1424292	+	HiC_scaffold_22	53110966	54682035
chr22	gap		1	6190	+	HiC_scaffold_22		
chr22	falcon	000279F	1	2238764	+	HiC_scaffold_22	54688226	57045629
chr22	gap		1	17280	+	HiC_scaffold_22		
chr22	falcon	000228F	1	624806	+	HiC_scaffold_22	57062910	57638897
chr22	gap		1	6665	+	HiC_scaffold_22		
chr22	falcon	000657F	1	274075	+	HiC_scaffold_22	57645563	57896939
chr22	gap		1	16314	+	HiC_scaffold_22		
chr22	falcon	000327F	1	1593242	+	HiC_scaffold_22	57913254	59516274
chr22	gap		1	8019	+	HiC_scaffold_22		
chr22	falcon	000448F	1	723483	+	HiC_scaffold_22	59524294	60271098
chr22	gap		1	11428	+	HiC_scaffold_22		
chr22	falcon	000589F	6	378424	+	HiC_scaffold_22	60282527	60645441
chr22	gap		1	24121	+	HiC_scaffold_22		
chr22	falcon	000286F	1	2170354	+	HiC_scaffold_22	60669563	62907549
chr22	gap		1	3782	+	HiC_scaffold_22		
chr22	falcon	000712F	6097	238893	+	HiC_scaffold_22	62911332	63146850
chr22	gap		1	6168	+	HiC_scaffold_22		
chr22	falcon	000880F	1	167053	+	HiC_scaffold_22	63153019	63326103

chr22	gap		1	6899	+	HiC_scaffold_22		
chr22	falcon	000381F	4	1087473	+	HiC_scaffold_22	63333003	64470054
chr22	gap		1	1740	+	HiC_scaffold_22		
chr22	falcon	000428F	1	797111	+	HiC_scaffold_22	64471795	65204434
chr22	gap		1	11248	+	HiC_scaffold_22		
chr22	falcon	000186F	1	4168152	+	HiC_scaffold_22	65215683	69317897
chr22	gap		1	1836	+	HiC_scaffold_22		
chr22	falcon	001345F	1	82344	+	HiC_scaffold_22	69319734	69429746
chr22	gap		1	10676	+	HiC_scaffold_22		
chr22	falcon	001285F	1	116157	+	HiC_scaffold_22	69440423	
chr22	gap		1	10000	+	HiC_scaffold_22		
chr22	falcon	000391F	1	1034891	+	HiC_scaffold_22	69457555	70456348
chr22	gap		1	7802	+	HiC_scaffold_22		
chr22	falcon	000366F	433546	1189206	+	HiC_scaffold_22	70464151	71263568
chr22	gap		1	4741	+	HiC_scaffold_22		
chr22	falcon	000397F	1	999685	+	HiC_scaffold_22	71268310	72325291
chr22	gap		1	20749	+	HiC_scaffold_22		
chr22	falcon	000420F	1	859219	+	HiC_scaffold_22	72346041	73236367
chr22	gap		1	36609	+	HiC_scaffold_22		
chr22	falcon	000455F	1	682586	+	HiC_scaffold_22	73272977	74062868
chr22	gap		1	19184	+	HiC_scaffold_22		
chr22	falcon	000444F	1	740881	+	HiC_scaffold_22	74082053	74895601
chr22	gap		1	7799	+	HiC_scaffold_22		
chr22	falcon	002117F	1	36213	+	HiC_scaffold_22	74903401	74927998
chr22	gap		1	27300	+	HiC_scaffold_22		
chr22	falcon	001607F	1	59279	+	HiC_scaffold_22	74955299	75002638

chr22	subsequence of a corrected read	GACATAATTAAAAATCTGTAATCCACAAAATTGGAAAATATAAAAATGAATGTTTTATA				HiC_scaffold_22	75002639	75002699
chr22	falcon	000458F	1	683236	+	HiC_scaffold_22	75002700	75747842
chr22	gap		1	8104	+	HiC_scaffold_22		
chr22	falcon	000501F	1	526454	+	HiC_scaffold_22	75755947	76302719
chr22	gap		1	5240	+	HiC_scaffold_22		
chr22	falcon	000460F	1	678938	+	HiC_scaffold_22	76307960	77035839
chr22	gap		1	9669	+	HiC_scaffold_22		
chr22	falcon	000352F	1	1377536	+	HiC_scaffold_22	77045509	78412549
chr22	gap		1	3971	+	HiC_scaffold_22		
chr22	falcon	002242F	1	33508	+	HiC_scaffold_22	78416521	78449948
chr22	gap		1	8545	+	HiC_scaffold_22		
chr22	falcon	000407F	1	955247	+	HiC_scaffold_22	78458494	79354898
chr22	gap		1	14063	+	HiC_scaffold_22		
chr22	falcon	000348F	1	1426264	+	HiC_scaffold_22	79368962	80875221
chr22	gap		1	6244	+	HiC_scaffold_22		
chr22	falcon	000101F	7516036	7674230	+	HiC_scaffold_22	80881466	81029015
chr22	gap		1	499	+	HiC_scaffold_22		
chr22	falcon	000479F	1	615463	+	HiC_scaffold_22	81029515	81667876
chr22	gap		1	3602	+	HiC_scaffold_22		
chr22	falcon	000457F	309071	688259	+	HiC_scaffold_22	81671479	82128179
chr22	gap		1	25132	+	HiC_scaffold_22		
chr22	falcon	001419F	1	67471	+	HiC_scaffold_22	82153312	82222469
chr22	gap		1	3281	+	HiC_scaffold_22		
chr22	falcon	000650F	1	288885	+	HiC_scaffold_22	82225751	82517186
chr22	gap		1	19874	+	HiC_scaffold_22		
chr22	falcon	001953F	1	33136	+	HiC_scaffold_22	82537061	82569528

chr22	gap		1	27933	+	HiC_scaffold_22		
chr22	falcon	000340F	1	1487052	+	HiC_scaffold_22	82597462	84111306
chr22	gap		1	8480	+	HiC_scaffold_22		
chr22	falcon	000191F	1	4069210	+	HiC_scaffold_22	84119787	88263978
chr22	gap		1	5145	+	HiC_scaffold_22		
chr22	falcon	000726F	1	228310	+	HiC_scaffold_22	88269124	
chr22	gap		1	10000	+	HiC_scaffold_22		
chr22	falcon	000126F	1	601577	-	HiC_scaffold_22	88498724	89147060
chr22	gap		1	28861	+	HiC_scaffold_22		
chr22	falcon	000679F	1	270391	+	HiC_scaffold_22	89175922	89484265
chr22	falcon	000485F	1	585900	+	HiC_scaffold_22	89484266	90054233
chr22	gap		1	500	+	HiC_scaffold_22		
chr22	falcon	000146F	1	659480	+	HiC_scaffold_22	90054734	90596195
chr22	gap		1	3820	+	HiC_scaffold_22		
chr22	falcon	001440F	1	79250	+	HiC_scaffold_22	90600016	90618336
chr22	gap		1	499	+	HiC_scaffold_22		
chr22	falcon	000711F	2218	243254	+	HiC_scaffold_22	90618836	90852442
chr22	gap		1	7512	+	HiC_scaffold_22		
chr22	falcon	000743F	1	221518	+	HiC_scaffold_22	90859955	91094667
chr22	gap		1	7856	+	HiC_scaffold_22		
chr22	falcon	001319F	502	92811	+	HiC_scaffold_22	91102524	91220196
chr22	gap		1	8635	+	HiC_scaffold_22		
chr22	falcon	000447F	1	752336	+	HiC_scaffold_22	91228832	
chr22	gap		1	10000	+	HiC_scaffold_22		
chr22	falcon	001296F	1	88118	+	HiC_scaffold_22	91938698	92039036
chr22	gap		1	3540	+	HiC_scaffold_22		
chr22	falcon	000609F	1	334728	+	HiC_scaffold_22	92042577	92368287
chr22	gap		1	9591	+	HiC_scaffold_22		

chr22	falcon	000461F	1	305068	+	HiC_scaffold_22	92377879	92701403
chr22	gap		1	6602	+	HiC_scaffold_22		
chr22	falcon	001880F	1	42131	+	HiC_scaffold_22	92708006	92736835
chr22	gap		1	23810	+	HiC_scaffold_22		
chr22	falcon	003520F	1	5838	+	HiC_scaffold_22	92760646	92766485
chr22	gap		1	6204	+	HiC_scaffold_22		
chr22	falcon	000441F	366509	753627	+	HiC_scaffold_22	92772690	93192252
chr22	gap		1	14043	+	HiC_scaffold_22		
chr22	falcon	001503F	1	68389	+	HiC_scaffold_22	93206296	93271874
chr22	gap		1	6465	+	HiC_scaffold_22		
chr22	falcon	001518F	1	65216	+	HiC_scaffold_22	93278340	
chr22	gap		1	10000	+	HiC_scaffold_22		
chr22	falcon	000446F	1	742010	+	HiC_scaffold_22	93384705	94177760
chr22	falcon	001034F	1	123263	+	HiC_scaffold_22	94177761	94309346
chr22	gap		1	836	+	HiC_scaffold_22		
chr22	falcon	000612F	1	341532	+	HiC_scaffold_22	94310183	94681581
chr22	gap		1	7161	+	HiC_scaffold_22		
chr22	falcon	000049F	11153015	11446512	+	HiC_scaffold_22	94688743	94989670
chr22	gap		1	16422	+	HiC_scaffold_22		
chr22	falcon	000571F	1	331733	+	HiC_scaffold_22	95006093	95371960
chr22	gap		1	8021	+	HiC_scaffold_22		
chr22	falcon	000373F	1	1171030	+	HiC_scaffold_22	95379982	96578969
chr22	gap		1	8707	+	HiC_scaffold_22		
chr22	falcon	002894F	1	9898	+	HiC_scaffold_22	96587677	96597561
chr22	gap		1	23189	+	HiC_scaffold_22		
chr22	falcon	000283F	1	2207306	+	HiC_scaffold_22	96620751	98873354
chr22	gap		1	10962	+	HiC_scaffold_22		
chr22	falcon	000362F	1	1253583	+	HiC_scaffold_22	98884317	100163244

chr22	gap		1	7950	+	HiC_scaffold_22		
chr22	falcon	000400F	194	977512	+	HiC_scaffold_22	100171195	101137421
chr22	gap		1	12653	+	HiC_scaffold_22		
chr22	falcon	000558F	1	410069	+	HiC_scaffold_22	101150075	101473621
chr22	gap		1	1715	+	HiC_scaffold_22		
chr22	falcon	000566F	259419	418459	+	HiC_scaffold_22	101475337	101640464
chr22	gap		1	5987	+	HiC_scaffold_22		
chr22	falcon	000507F	1	528416	+	HiC_scaffold_22	101646452	102201074
chr22	gap		1	886	+	HiC_scaffold_22		
chr22	falcon	001409F	1	69209	+	HiC_scaffold_22	102201961	102266868
chr22	falcon	000429F	1764	796832	+	HiC_scaffold_22	102266869	103109277
chr22	gap		1	10467	+	HiC_scaffold_22		
chr22	falcon	000339F	1	1485709	+	HiC_scaffold_22	103119745	104702156
chr22	gap		1	6157	+	HiC_scaffold_22		
chr22	falcon	000442F	1	756769	+	HiC_scaffold_22	104708314	105479775
chr22	gap		1	4149	+	HiC_scaffold_22		
chr22	falcon	000496F	1	549640	+	HiC_scaffold_22	105483925	106037837
chr22	gap		1	17548	+	HiC_scaffold_22		
chr22	falcon	000466F	1	657815	+	HiC_scaffold_22	106055386	106729281
chr22	gap		1	26693	+	HiC_scaffold_22		
chr22	falcon	000310F	1	1765768	+	HiC_scaffold_22	106755975	108574440
chr22	gap		1	6354	+	HiC_scaffold_22		
chr22	falcon	000427F	1	649821	+	HiC_scaffold_22	108580795	109094394
chr22	gap		1	500	+	HiC_scaffold_22		
chr22	falcon	000865F	139397	164814	+	HiC_scaffold_22	109094895	109114256
chr22	gap		1	26274	+	HiC_scaffold_22		
chr22	falcon	000494F	1	561631	+	HiC_scaffold_22	109140531	
chr22	gap		1	10000	+	HiC_scaffold_22		

chr22	falcon	001193F	1	51613	-	HiC_scaffold_22	109575325	109634063
chr22	gap		1	19377	+	HiC_scaffold_22		
chr22	falcon	000709F	1	229866	+	HiC_scaffold_22	109653441	109932899
chr22	falcon	002009F	1	37248	+	HiC_scaffold_22	109932900	109973200
chr22	gap		1	24858	+	HiC_scaffold_22		
chr22	falcon	000462F	1	683492	+	HiC_scaffold_22	109998059	110651025
chr22	gap		1	24928	+	HiC_scaffold_22		
chr22	falcon	000686F	1	263374	+	HiC_scaffold_22	110675954	110924085
chr22	gap		1	15457	+	HiC_scaffold_22		
chr22	falcon	000439F	1	811045	+	HiC_scaffold_22	110939543	111744728
chr22	gap		1	33257	+	HiC_scaffold_22		
chr22	falcon	000864F	11247	51054	+	HiC_scaffold_22	111777986	111822495
chr22	gap		1	500	+	HiC_scaffold_22		
chr22	falcon	001609F	25816	46086		HiC_scaffold_22	111822996	111843937
chr22	gap		1	1558	+	HiC_scaffold_22		
chr22	falcon	000689F	77054	271150	+	HiC_scaffold_22	111845496	111994495
chr22	gap		1	500	+	HiC_scaffold_22		
chr22	falcon	000663F	1	295324	+	HiC_scaffold_22	111994996	112258288
chr22	gap		1	18964	+	HiC_scaffold_22		
chr22	falcon	000627F	1	313363	+	HiC_scaffold_22	112277253	112593924
chr22	gap		1	22874	+	HiC_scaffold_22		
chr22	falcon	003051F	1	16695	+	HiC_scaffold_22	112616799	112633097
chr22	gap		1	9464	+	HiC_scaffold_22		
chr22	falcon	001007F	1	137828	+	HiC_scaffold_22	112642562	112722379
chr22	gap		1	6910	+	HiC_scaffold_22		
chr22	falcon	000791F	1	196795	+	HiC_scaffold_22	112729290	112946981
chr22	gap		1	101	+	HiC_scaffold_22		
chr22	falcon	001649F	1	54764	+	HiC_scaffold_22	112947083	112989017

chr22	gap		1	19014	+	HiC_scaffold_22		
chr22	falcon	001240F	1	71223	+	HiC_scaffold_22	113008032	113085394
chr22	gap		1	3671	+	HiC_scaffold_22		
chr22	falcon	001349F	1	91895	+	HiC_scaffold_22	113089066	113212100
chr22	gap		1	23137	+	HiC_scaffold_22		
chr22	falcon	000714F	1	241206	+	HiC_scaffold_22	113235238	
chr22	gap		1	10000	+	HiC_scaffold_22		
chr22	falcon	002450F	1	31204	+	HiC_scaffold_22	113579187	113610296
chr22	gap		1	29431	+	HiC_scaffold_22		
chr22	falcon	002249F	1	40653	+	HiC_scaffold_22	113639728	113680327
chr22	gap		1	20347	+	HiC_scaffold_22		
chr22	falcon	000369F	1	983562	+	HiC_scaffold_22	113700675	114659321
chr22	gap		1	500	+	HiC_scaffold_22		
chr22	falcon	000532F	41259	484027	+	HiC_scaffold_22	114659822	114996528
chr22	gap		1	500	+	HiC_scaffold_22		
chr22	falcon	000622F	40060	248399	-	HiC_scaffold_22	114997029	115136170
chr22	gap		1	6185	+	HiC_scaffold_22		
chr22	falcon	000197F	20595	71119	-	HiC_scaffold_22	115142356	115193736
chr22	gap		1	14422	+	HiC_scaffold_22		
chr22	falcon	000623F	1	327629	+	HiC_scaffold_22	115208159	
chr22	gap		1	10000	+	HiC_scaffold_22		
chr22	falcon	000379F	1	1130356	+	HiC_scaffold_22	115566667	116712002
chr22	gap		1	16437	+	HiC_scaffold_22		
chr22	falcon	000301F	1	1693218	+	HiC_scaffold_22	116728440	118470252
chr22	gap		1	25705	+	HiC_scaffold_22		
chr22	falcon	000385F	95496	1061943	+	HiC_scaffold_22	118495958	119411788
chr22	gap		1	8982	+	HiC_scaffold_22		
chr22	falcon	002565F	1	21058	+	HiC_scaffold_22	119420771	119441817

chr22	gap		1	12880	+	HiC_scaffold_22		
chr22	falcon	000320F	1	1665709	+	HiC_scaffold_22	119454698	121170123
chr22	gap		1	48181	+	HiC_scaffold_22		
chr22	falcon	002470F	1	28216	+	HiC_scaffold_22	121218305	121239156
chr22	gap		1	38010	+	HiC_scaffold_22		
chr22	falcon	000881F	1	169552	+	HiC_scaffold_22	121277167	121455960
chr22	gap		1	13295	+	HiC_scaffold_22		
chr22	falcon	001222F	1	105595	+	HiC_scaffold_22	121469256	121575117
chr22	gap		1	8950	+	HiC_scaffold_22		
chr22	falcon	000302F	1	1896581	+	HiC_scaffold_22	121584068	123508609
chr22	gap		1	4904	+	HiC_scaffold_22		
chr22	falcon	000773F	1	205983	+	HiC_scaffold_22	123513514	123712534
chr22	gap		1	16322	+	HiC_scaffold_22		
chr22	falcon	000387F	1	1055255	+	HiC_scaffold_22	123728857	124856593
chr22	falcon	000879F	92	171046	+	HiC_scaffold_22	124856594	125033496
chr22	gap		1	21668	+	HiC_scaffold_22		
chr22	falcon	001030F	1	126719	+	HiC_scaffold_22	125055165	125174978
chr22	gap		1	10408	+	HiC_scaffold_22		
chr22	falcon	000072F	1	1183582	+	HiC_scaffold_22	125185387	126404863
chr22	gap		1	6723	+	HiC_scaffold_22		
chr22	falcon	000491F	1	596347	+	HiC_scaffold_22	126411587	127053517
chr22	gap		1	4220	+	HiC_scaffold_22		
chr22	falcon	001680F	1	52652	+	HiC_scaffold_22	127057738	
chr22	gap		1	10000	+	HiC_scaffold_22		
chr22	falcon	000218F	42855	50476	-	HiC_scaffold_22	127105610	127113167
chr22	gap		1	500	+	HiC_scaffold_22		
chr22	falcon	000281F	2106457	2240828	-	HiC_scaffold_22	127113668	127238467
chr22	gap		1	6546	+	HiC_scaffold_22		

chr22	falcon	000776F	1	210714	+	HiC_scaffold_22	127245014	127452302
chr22	gap		1	16555	+	HiC_scaffold_22		
chr22	falcon	000583F	1	385001	+	HiC_scaffold_22	127468858	127874175
chr22	gap		1	12296	+	HiC_scaffold_22		
chr22	falcon	002918F	1	14634	+	HiC_scaffold_22	127886472	127895859
chr22	gap		1	4011	+	HiC_scaffold_22		
chr22	falcon	000474F	1	618876	+	HiC_scaffold_22	127899871	128667055
chr22	gap		1	17900	+	HiC_scaffold_22		
chr22	falcon	000637F	1	306690	+	HiC_scaffold_22	128684956	129003077
chr22	gap		1	6003	+	HiC_scaffold_22		
chr22	falcon	000856F	1	169450	+	HiC_scaffold_22	129009081	129174069
chr22	gap		1	8801	+	HiC_scaffold_22		
chr22	falcon	000449F	1	710772	+	HiC_scaffold_22	129182871	129906732
chr22	gap		1	6315	+	HiC_scaffold_22		
chr22	falcon	002954F	1	20142	+	HiC_scaffold_22	129913048	
chr22	gap		1	10000	+	HiC_scaffold_22		
chr22	falcon	001995F	1	51186	+	HiC_scaffold_22	129968830	130017243
chr22	gap		1	5082	+	HiC_scaffold_22		
chr22	falcon	003020F	1	16163	-	HiC_scaffold_22	130022326	130039065

Effect of polishing our golden hamster genome assembly by Arrow

	Before polishing with Arrow ratio (%)	After polishing with Arrow ratio (%)
mismatch ratio	0.12068%	0.11216%
insertion/deletion ratio	0.07203%	0.02774%
mismatch and indel ratio	0.19271%	0.13990%
nucleotide identity	99.80729%	99.86010%

Class	Clade/Superfamily	MesAur1.0_HiC
SINE	B1	2.71
	B2	1.69
	B4	2.27
	ID	0.30
	MIR	0.64
	other SINE	0.21
LINE	L1	11.83
	L2	0.50
	other LINE	0.11
LTR	ERV1	0.51
	ERVK	3.18
	ERVL	4.89
	other LTR	0.69
DNA	hAT	0.86
	TcMar	0.24
	other DNA	0.03
Other TE		0.33
Unknown TE		0.08
Total		**31.07**